UNIVERSITY OF SOUTHAMPTON
FACULTY OF ENGINEERING, SCIENCE AND MATHEMATICS
SCHOOL OF ELECTRONICS AND COMPUTER SCIENCE

High Speed Planar Electrical Data Transmission Structure Modelling using VHDL-AMS with Skew and EMI Management

by

Mark R. Burford

A thesis submitted for the
degree of Doctor of Engineering

April 2008

UNIVERSITY OF SOUTHAMPTON, FACULTY OF ENGINEERING, SCIENCE AND MATHEMATICS, SCHOOL OF ELECTRONICS AND COMPUTER SCIENCE

ABSTRACT

Doctor of Engineering

High Speed Planar Data Transmission Structure Modelling using VHDL-AMS with Skew and EMI Management

by Mark R. Burford

Signal integrity constraints in modern high speed data communication protocols are becoming increasingly stringent. Consumers are demanding faster, more powerful systems with lower power requirements that require faster internal data transfers over longer distances. These two statements are not mutually compatible because as frequency increases there are increased losses and increased abberations to the data signal from a variety of sources. It, therefore, becomes increasingly difficult to guarantee a receiver will be able to recover the signal.

Large system level time domain simulations have been possible for a while, however, the inclusion of an efficient, compatible and accurate time domain transmission line model that responds to the signal in real time has not as yet been possible. Additionally, as the frequency increases, any difference in transmission time between each component of a differential signal will also increase linearly as the period decreases. This signal skew has not as yet presented a problem to signal integrity or loss. However, as the frequency increases there will be increased signal skew which increases mode conversion so less of the signal will be available for recovery using existing skew compensation methodologies. Mode conversion is the process where the energy in a signal is converted from one mode to another, with a variety of possible causes. The primary cause of mode conversion in this research is signal skew, which causes a potential gradient between the traces forming a differential pair. This allows energy to be coupled and transferred between the copper traces, causing signal asymmetries.

This thesis examines high speed planar copper data transmission structures through the use of time and frequency domain modelling. Models for physical loss, reflection and signal skew are created in the time domain using the hardware description language VHDL-AMS while physical loss, reflection, mode conversion and losses to electromagnetic radiation are modelled in the frequency domain using Agilent's Genesys®.

There are three main contributions presented in this thesis. The first of which is a signal dependent time domain methodology of calculating skin depths and dielectric conductances in high speed planar data transmission structures.

The second contribution is a platform independent time domain model of the main loss mechanisms, including signal dependent skin effect and dielectric conductances for implementation in almost any system level mixed signal simulation up to 7 GHz.

The third major contribution is a new methodology of approaching and compensating for losses due to mode conversion and EM loss as caused by signal skew in differential microstrip line pairs up to 15 GHz. These methodologies are to be named as skew and EMI management collectively.

Finally, there is a set of guidelines for skew management for layout engineers to take into consideration and combine with their existing in depth knowledge of the theory and practice of signal routing at high speed. This will enable high speed planar data transmission structures to transmit signals over longer distances and at higher frequencies whilst preserving signal integrity, thus permitting the continued use of copper for the next generations of products.

Contents

List of Figures

Acknowledgements

Many thanks to my supervisor, Dr. T. Kazmierski who's vast academic experience and industrial contacts have managed to bring academia and industry a little closer through this collaboration.

Special thanks to Stuart Taylor, formerly of Xyratex Technology Ltd. and Paul Levin of Xyratex Technology Ltd, for their help, guidance and mentoring throughout this project without which I would surely have struggled.

Dave Milward of Xyratex Technology Ltd was the man that made things happen and networked me around the company on many an occasion performing new introductions on an almost weekly basis. A close liaison between Dave Milward and Dr. Kazmierski ensured the EngD moved along as smoothly as possible.

I must also express my gratitude and affection to my partner Emily Blanshard for her constant support and understanding in times of work and stress that I could not be with her.

Abbreviations

°	degrees
”	inches
ω	2*PI*frequency
Ω	omega (Ohms)
AMS	Analogue and Mixed Signal extensions
C	Capacitance in Farads
c_0	Speed of light
CAD	Computer Aided Design
cm	centimetre
dB	decibel
EM	ElectroMagnetic
ε	permittivity
G	Conductance in Siemens
GHz	Gigahertz
HDL	Hardware Description Language
ISI	Inter-Symbol Interference
L	Inductance in Henrys
mA	milliamps
MHz	Megahertz
mil	thousandths of an inch
MPA	Microstrip Patch Antenna
nA	nanoAmps
ns	nanoseconds
nW	nanoWatts

PCB	Printed Circuit Board
PCIe	Peripheral Computer Interface express
ps	picoseconds
PWL	PieceWise Linear
R	Resistance in Ohms
S_{11}	Input reflection coefficient
S_{21}	Forward transmission loss
SI	Signal Integrity
TDR	Time Domain Reflectometry
μm	micro metres (microns)
μs	microseconds
VHDL	Very High Speed Integrated Circuit Hardware Description Language
VNA	Vector Network Analyser

Chapter 1

Introduction

This thesis is supported by Xyratex Technology Ltd, a network and storage solutions company, and the University of Southampton. Both parties are concerned with modelling transmission lines in the time domain and refining high speed layout guidelines to maximise signal integrity and minimise loss. If signal integrity is allowed to degrade, or losses allowed become to great, there is an increased chance of errors and a higher probability that digital data in the signal will not be received correctly by the receiver, causing the system or product to fail. The three main types of transmission structure considered in this thesis are single microstrip line, coupled microstrip line and buried coupled microstrip line. Single microstrip line is a single piece of copper on top of a dielectric material above a ground plane used to deliver a signal. Coupled microstrip line comprises two copper traces on top of a dielectric material above a ground plane where the signal transmitted is derived from the signals on each copper trace. Buried coupled microstrip line is the same as coupled microstrip line, however, the pair are located within the dielectric material above a ground plane. Stripline, that is, two metal strips in a dielectric medium between two ground planes is not investigated in this thesis because it suffers far less from skew and also designers at the sponsoring company prefer to use system boards with fewer layers to minimise costs, meaning most routing is done on the face of the boards

1.1 Aim

The aim of this thesis is to produce a time domain signal dependent electrical model of planar digital data microstrip transmission lines that can be easily incorporated into any mixed signal system level simulator. Specifically, in this instance for use in a high speed digital switch fabric containing around a thousand transmission lines from 0.02 m up to almost 1 m. The focus of this thesis is not to extend an existing modelling or mixed signal hardware description language, but to use an existing and mature language with an equally mature and stable simulator environment. The model would need to be computationally efficient and react to the signal or data that was sent along it, capturing he major types of loss. As a result of this research being industry led and sponsored, the research focus was shifted shortly after a successfully validated model was achieved before it could be fully integrated into a wider system level simulation as per it's original purpose. It is the intention to validate the model against a physical experiment.

Following the truncation of the research at this stage the sponsor, to their credit, rapidly found a related area of research they required that would build on knowledge gained thus far. The sponsor required research on skew in electrical digital data transmission lines and it's effect on signal integrity (SI) and electro magnetic (EM) losses. Also required were the best methods of mitigating any harmful effects caused by skew or EM losses should they pose a problem when higher data-rates are used in future product road maps. A set of guidelines that layout and electronic design engineers can refer to and use in combination with their existing knowledge and experience is to be produced to aid in electrical signal routing in copper at frequencies up to 15GHz. This will allow the continued use of low cost existing electronics design and manufacturing methods and processes.

1.2 Motivation

The miniaturisation of modern electronics has led to faster clock speeds and hence faster requirements to get data on and off of a processing unit. Data is coming from further away in the system and over more complicated routes then ever before with advancements such as system on chip. Signals must be routed through connectors, pin fields, different types of vias and in close proximity to other signal aggressors to name a few

obstacles to the successful transmission of a recoverable digital signal. The limiting factor in most cases is the interconnection between processing unit and input output (IO) ports in the system. This is mainly because there can be anything from a fraction of a wavelength to many wavelengths travelling between two ports along an interconnect, depending on the frequency of the signal. As data travels along the transmission line it is subject to distortion from various mechanisms. This in itself is a problem, because the protocols governing how the signal is sent and received at both ends of the interconnect generally have highly stringent conditions on the integrity of the signal. If these protocols are invalidated, correct resolution of a '1' or '0' cannot be guaranteed by the receiving electronics and errors then follow [1,2,3,4,5].

Engineers are always looking to model entire systems as much as possible in the shortest time and at the least cost. By using Hardware Description Languages (HDLs) such as VHDL-AMS [6,7], efficient and cheap models can be created that can not only model the electronic system itself but also, as this thesis will describe, can capture effects that are dependent on what the signal itself is doing at any instant in time. Such effects, on which most industry standard circuit simulators allocate a fixed value, dependent on the given frequency of operation and geometry, are skin effect [8] and dielectric absorption [9].

By allocating a fixed value for frequency of operation to the entire transmission network in a system, and having existing models allocate fixed losses and distortions that components or electrical transmission lines impart on the signal, this always assumes the signal is a pure sinusoid. Real data depending on the encoding used, can have several 1's or 0's in a row which would of course appear as a much lower frequency or data-rate. As a result of this, the losses based on a fixed frequency of operation would be potentially over estimated. Also, effects such as skin effect do not give a new loss from a higher or lower resistance instantaneously, but are instead tended towards, taking time to establish themselves, also affecting the signal shape and certainly the first few bits sent. During longer periods of 1's or 0's the effects abate somewhat as the transmission line will tend towards a resistance nearer a DC value.

Other motivations for producing a signal dependent model as opposed to purchasing an expensive industry standard piece of software are that the algorithm will be highly portable and so can be used by research institutions and individuals without the resources to afford expensive software licenses. The portability will allow many programming or hardware description languages to be used to model transmission lines in a variety of applications. Most industrial software also requires a fixed frequency

to be given on which it bases all signal distortions, by reacting to the signal itself, the model can more accurately calculate effects in real time and the time it takes the effects establish themselves.

Motivation for the research into skew and EM loss and their inter-relation / dependence and respective effects on the quality of a signal comes from future product road maps of the sponsor. Future products are expected to operate at higher data rates. It is well documented that higher frequencies produce more radiation (EM loss), however quite how this is related to skew and how this will affect signal quality and loss in differential transmission lines has not been addressed since 2000 [10] where the relationship between skew and EM loss was only addressed up to 1GHz. Skew was not looked at or indeed is still not considered to be an important mechanism for loss in copper differential transmission lines.

1.3 Outcomes

This thesis has three major contributions, the first is a new methodology for modelling high frequency electrical conductor effects in the time domain which determines the skin depths and dielectric conductances based on what the signal is doing at a specific point on the transmission line. The methodology enables on the fly skin depths and dielectric conductances to be calculated. More signal changes present more loss so this would enable designs that had long runs of 1's and 0's, approaching a DC scenario, to use a routing strategy that would perhaps not have been suitable for a clock signal. Although not as accurate as using significantly more processing power to compute the exact skin depth, this approach presents a means for a cost effective, computationally efficient, portable and excellent approximation to 0.1 dB (0.5% based on a 1 V signal) up to 7 GHz of high frequency electrical transmission line effects. This offers designers who cannot perhaps afford specialised industry simulation tools an opportunity to calculate loss in a time domain situation based on what the signal is doing, not a predetermined loss per transmission structure section.

The second contribution takes the novel methodology for calculating skin depths and dielectric conductances and incorporates it into a platform independent time domain model for implementation in almost any system level mixed signal simulation. This allows modelling of high speed planar lossy microstrip structures in the time domain offering better than 0.1 dB (0.5%) error when compared to experimental measurements

from near DC up to 7 GHz. The salient feature of the model is the use of signal variation rate, present value and amplitude of the signal instead of frequency to determine the non-linear effects of skin depths and dielectric conductance as well as the linear signal skew effects for loss calculation. A highly efficient, customisable and scalable model is implemented in VHDL-AMS for use in system level high speed time-domain mixed-signal simulations, especially for applications involving very high speed digital switch fabrics.

The third major contribution from this research explores the use of current methods of length matching in differential microstrip and buried microstrip transmission lines when used with data-rates of up to 15 GHz. Length matching or 'de-skewing' is used to mitigate the effects of skew as caused by unequal metal trace lengths in the pair caused by non-direct routing strategies. It is shown that using current methods of length matching could worsen mode conversion and EM loss than with no length matching at all. A new methodology is suggested whereby interconnect geometry can be engineered to exactly negate skew at a specific frequency instead of matching the length of a pair, whilst also minimising other signal distortions such as reflections. This is achieved through appropriate engineering of de-skew wiglets (skew compensation / de-skew geometry) achieved by variation of their positioning, exact geometry and number. Skew is de-skewed instead of length matched because the amount of de-skew a de-skew wiglet provides is frequency dependent and so merely matching length would not provide the best solution across a broad frequency range.

It is also shown that EM loss is related to the amount of skew. This thesis looked at how EM loss can be minimised by considering how antennas optimise their efficiency, then constructing highly inefficient antennas. From this third contribution of research, it is shown that signal skew, the associated mode conversion and EM loss are facts of life that cannot be totally avoided and as frequency increases, become increasingly problematic. Therefore "skew and EMI management" should be employed as opposed to the common conception of 'length matching' currently widely in use.

From the modelling work carried out in this thesis, it was possible to create a set of guidelines which high speed design engineers may choose to use in conjunction with their already vast knowledge of signal integrity (SI). The guidelines should be applied in the order they are presented with the first guideline having the greatest impact on signal integrity and loss and subsequent guidelines having less and less impact.

1.4 Thesis outline

This thesis is split into two inter-related areas of research. The first area is the development of novel methodologies for the determination of skin depth and dielectric conductance in the time domain based on signal variation rate. Also included in this area is the modelling of high speed electrical transmission lines or similar structures with VHDL-AMS, incorporating the new methodologies of determining the signal dependent effects. As previously stated, the research had to be truncated by the industrial sponsor for business reasons. The sponsor provided another related area of research for investigation that they had a need for that could use the knowledge already gained from previous research. The latter part of this thesis validates and uses some field solving software to research the management of signal skew and electro-magnetic loss in coupled high speed microstrip and buried microstrip transmission lines in the frequency domain.

Chapter 2 details the state of the art in transmission line modelling techniques, a comparison of system design languages with reasons why VHDL-AMS was chosen and also gives background and recent research on EM loss and skew management.

Chapter 3 describes the novel approach to determining skin depth and dielectric conductances based on the signal behaviour and not frequency.

Chapter 4 describes how to model a lossy transmission line in VHDL-AMS in the time domain and also shows how frequency dependent effects such as skin effect and dielectric conductance can be included in the model in the time domain. Results are compared between assuming a fixed frequency, which is how the majority of circuit simulators consider loss, and our signal dependent method. Signal skew is also discussed and modelled.

Chapter 5 validates the EM planar structure field solving software and also contains simulations of various skew reducing structures. The simulations are of new methodologies for skew and EM loss management in various transmission structure types, researching various de-skew (intentional skew) schemes and their impact on system performance including electro-magnetic radiation losses, mode conversion losses and reflections.

Chapter 6 presents a summary of the research outcomes along with a set of guidelines for industry on how best to manage skew and EM loss to preserve signal integrity and enable interconnect speeds to keep up with electronic systems' increasing demand for

higher IO bandwidth whilst still using current manufacturing processes. Some possible extensions to this work are also suggested in this chapter, namely experimental validation of the skew management methodology, further exploration of buried differential microstrip geometries and the possibility of a software based time domain reflectometer (TDR).

Appendix A lists published work from this thesis.

Appendix B lists the VHDL-AMS code used in the first part of this thesis to create the signal dependent model for microstrip transmission lines.

Chapter 2

Transmission Line Effects and Modelling Approaches

As stated in the introduction, there are three main planar transmission structures under investigation in this thesis, the single microstrip line, coupled microstrip line and buried coupled microstrip line. Figures 2.1, 2.2 and 2.3 show the three types of line considered in this thesis as they are the most common types of communication in modern high speed board layout.

There exist many transmission line effects and models which attempt to capture these effects that are based in the frequency domain giving fixed line parameters at a given frequency. These models are in many circuit simulators and general purpose description languages but none have been found in VHDL-AMS as yet. Real data has no frequency so therefore the rate of change of the signal, signal amplitude and the signal's shape will define the severity of the skin effect dielectric conductance. Here follows a discussion on two major effects to be modelled and work carried out to date on the methods associated with the modelling of these effects in transmission lines.

2.1 Key effects to be modelled

2.1.1 Skin effect

Skin depth with frequency is commonly given by Equation 2.1 as described in [11]:

$$\delta = \sqrt{\frac{2\rho}{2\pi f \mu_0 \mu r}} \tag{2.1}$$

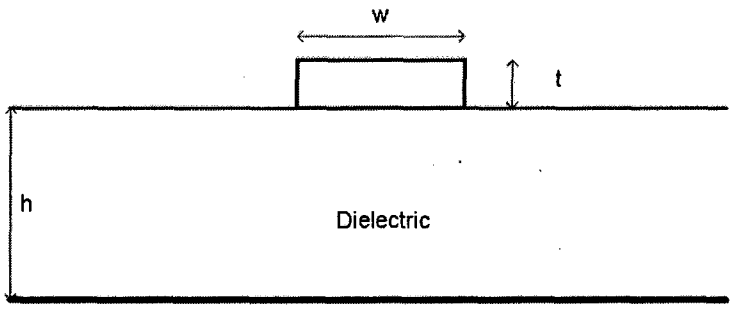

FIGURE 2.1: Lossy microstrip transmission line on a dielectric above ground

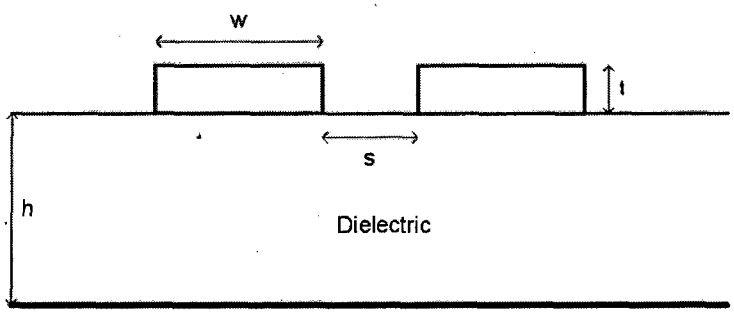

FIGURE 2.2: Edge coupled lossy microstrip transmission line on a dielectric above ground

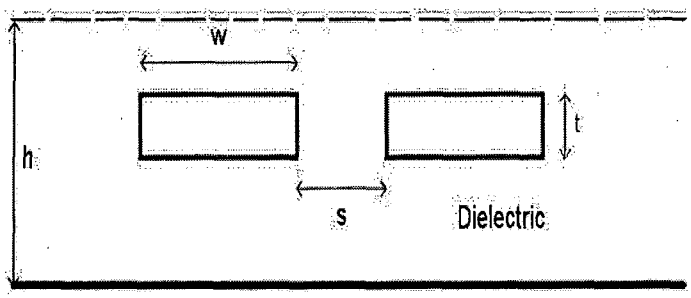

FIGURE 2.3: Buried Edge coupled lossy microstrip transmission line within a dielectric above ground

where ρ is the resistivity of copper and f is the maximum frequency of operation, μ_0 and and μ_r are the permeability of free space and the relative permeability of the material respectively. Relative permeability describes how well a material can concentrate magnetic flux. This formula is used to obtain an instantaneous value of skin depth for a given frequency and is how most models use it. A skin depth is achieved by the driving electric field penetrating further into the copper conductor as time progresses. As the field initially establishes itself, it causes a relatively low number of electrons to be swept along with it [12] so a relatively high resistance is experienced by the signal as the majority of the current is confined to a relatively small area near the surface, the skin depth. Over time the electric field will penetrate further into the conductor, sweeping more and more electrons and thus lowering resistance. The electric field strength is not uniform as it permeates the conductor however for modelling purposes it is assumed to be uniform. A DC condition is where the e-field has penetrated so far that nearly all electrons are swept along with the field and the whole cross sectional area is used for resistance calculation as in Equation 2.2

$$R_{DC} = \frac{\rho L}{A} \tag{2.2}$$

where L is the length of the transmission line, A is the cross sectional area the current travels in an ρ is resistivity of the metal trace. If the field switches direction, the field collapses and the current recedes back towards the surface nearest the reference place before the field establishes itself in the opposite orientation. The field again starts penetrating the conductor sweeping electrons along in the other direction. The faster the signal switches, the less distance the field and hence moving electrons can penetrate into the conductor giving higher resistances for higher frequencies. The surface we are talking about is the surface closest to the medium that carries the EM wave. In reference to Figure 2.2 this medium would be the regions under the microstrip conductor and the sides of the microstrip conductor above the ground plane which is filled with dielectric material. There would be very little current on top of the conductor because the electric field, or signal, is mostly confined between the metal trace and the reference plane.

Skin depth is a measure of the skin effect. A single skin depth is the distance into the conductor where the electric field intensity has fallen off and hence current density has fallen off by 1/e or to about 37 percent of it's value at the surface. The number of skin depths is largely irrelevant and is just a measure. We are only interested in the depth a signal (e-field) penetrates into the conductor. It should be noted immediately that the e-field does not penetrate into the conductor to the skin depth that Equation 2.1 would give

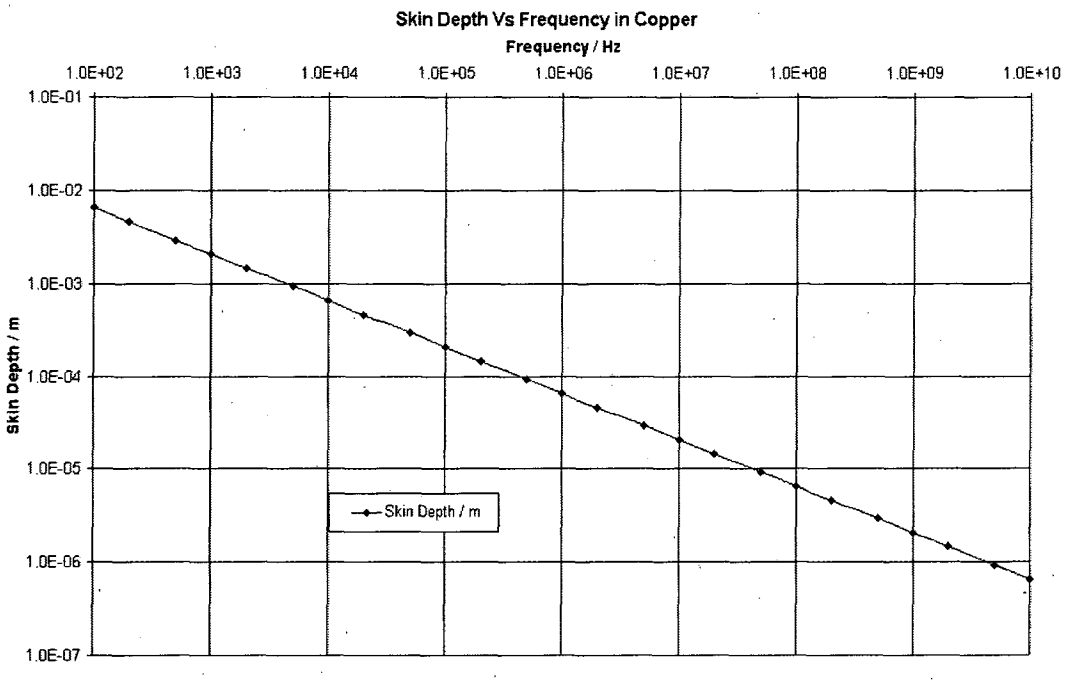

FIGURE 2.4: Skin depth in copper of signal vs. frequency. Both skin depth and frequency are logarithmic scales.

in zero time, should the frequency of the signal suddenly change. It takes a finite time for a certain field strength to be achieved at a certain depth into the conductor. Figure 2.4 shows the skin depths for copper for frequencies from 100 MHz to 10 GHz and it is clearly shown that at 100 Hz the skin depth is given as approximately 8 mm which is much thicker than most wires in common use for transporting signals at that frequency. Metal traces in high speed digital circuits have thickness of he order of approximately 25 microns (μm). The frequency giving this as a skin depth is approximately 10 MHz so it is expected to begin to see the effects of the electric field penetration times at around this frequency in modern microstrip transmission lines. The figure also shows skin effect to be a non-linear effect in that a two fold increase in frequency does not give a correspondingly proportionate increase in resistance.

2.1.2 Dielectric conductance

The loss mechanisms in a dielectric comprise four main types, all of which are a result of the impinging electric field interacting with either charge carriers or ionic molecules. There is an entire field of study devoted to the research of dielectric materials which

is sophisticated and is an area dominated by physicists studying quantum phenomena. Here only a brief overview is required.

When an electric field is applied to a dielectric material, the material becomes polarised. This arises from several mechanisms. If the molecules are polar (have a built in polarisation) they will normally have random alignment, but in an electric field they will tend to line up giving a net polarisation. This is not usually very important in solid dielectrics and is only significant at low frequency. The applied electric field may also induce a polarisation by stretching or distorting the bonds between atoms or distorting the distribution of electronic charge around the positive nuclei. This induced ionic or electronic polarisation will be significant to frequencies above those of interest here.

The polarisation of the material stores energy, which may be returned to the electric field as the field decreases. However, the process of creating the polarisation also leads to the dissipation of energy by non-reversible mechanisms. This energy is lost as heat.

The relative permittivity, ε_r, of a dielectric is a direct measure of the degree to which a material can be polarised. This governs and describes both the phase variation and attenuation of the impinging field on the dielectric. The dielectric constant is therefore a complex quantity with the real part, ε', referred to as the dielectric constant and the complex part, ε'', referred to as the imaginary part. The real part describes the amount of electrostatic charge that can be stored per unit volume for a given applied field, such as in a capacitor. The imaginary part is the tangent of the loss angle, $\tan(\delta)$, or dissipation factor, or loss factor. This describes the lag in polarisation upon application of the applied field and the energy dissipated as heat associated with the polarisation process. The relative dielectric constant can be summarised by Equation 2.3

$$\varepsilon_r = \varepsilon' - j\varepsilon'' = \varepsilon'(1 - j\tan(\delta)) \tag{2.3}$$

Because the relative dielectric constant is so closely related to polarisation, it can be strongly frequency dependent, with higher frequencies imparting more energy to the dielectric medium as the free charge carriers and dipoles are moved in the higher frequency field. This increased energy loss continues to increase with frequency until the ionic polarisation cannot respond fast enough to the field and so the dielectric constant will decrease somewhat. Such frequencies are much higher than those studied in this research [13].

Every dielectric will have a relative dielectric constant associated with it, from 1 up to three orders of magnitude higher in some cases. We are concerned with numbers between 2 and 4 in this research, air has a relative dielectric constant of 1. A lower number generally means there will be less energy dissipated as the material is not very susceptible to the polarisation effects of an impinging field. The real part of the relative dielectric constant describes how the material will increase capacitance between two boundaries and slow the speed of the signal:

$$\varepsilon_r = \frac{C_{filled}}{C_{empty}} \tag{2.4}$$

where C_{filled} and C_{empty} are the capacitances between the materials both with and without a dielectric material present. The dielectric constant slows the speed of light in the medium according to Equation 2.5:

$$c_r = \frac{c_0}{\sqrt{\varepsilon_r}} \tag{2.5}$$

where c_r is the speed of light when the relative dielectric constant is considered and c_0 is the speed of light in a vacuum. This also shrinks the wavelength as frequency has to remain constant. The effective dielectric constant k_{eff} is used when the electric field of the signal experiences two homogenous dielectrics simultaneously, each with their own ε_r. The resulting effective dielectric constant the signal experiences will be between the values of ε_r of each of the materials. The exact number depends on the portion of the signal's electric field in each of the dielectric mediums. A first order approximation of the effective dielectric constant is to take an average, however, exact calculation of k_{eff} requires at least a 2D field solver.

In order to model the 'resistive' or dissipative effects of the complex part of the relative dielectric constant, Equation 2.6 links resistive loss (a conductance) to frequency, dissipation factor and capacitance and is derived from Equation 2.3:

$$G_{AC} = 2\pi f \tan(\delta) C \tag{2.6}$$

here, G_{AC} is conductance and C is line capacitance. The exact physics of how a dielectric behaves under different conditions (dielectric spectroscopy) is beyond the scope of this text. All we need understand is that small dissipation factors give less loss and small dielectric constants yield faster signal propagation and smaller per unit length

capacitances. Smaller capacitances are associated with lower dielectric conductances according to Equation 2.6 which in turn present less losses.

2.2 Signal skew

Signal skew is any difference between two signals travelling in a pair of traces used to convey a single signal using such standards of physical transmission as the PCIe [14] or the more recent 10GHz ethernet standards [15]. Skew is caused by any difference in the transmission path between one of the two traces comprising a pair but not the other from such things as connector pads, bends or manufacturing anomalies as Bianco showed recently in 2006 [16]. These cause an impedance change in one or both traces which causes the signal to behave differently in the traces. The main focus on skew in this thesis is to look at skew in time, (temporal skew) which is mainly caused by transmission line paths that are unequal in length or by driver output skew as investigated by Hubing in 2001, [17] giving an unbalanced differential pair as described by Smith in 2006 [18]. The skew creates a common mode signal. A common signal is given by the average of the signals in each trace in the differential pair, that is:

$$V_{CM} = \frac{1}{2}(V_1 + V_2) \tag{2.7}$$

Where V_{CM} is the common signal, and $V_{1,2}$ are the signals in each trace in the pair.

A purely differential signal would give zero common component, this is backed up by experimental research conducted by Bucker and Gerling in 2002 [19].

Driver output skew was first discovered as a problem and researched by Braxton in 1988 [20] where the skew between the outputs of the driver of a differential transmission line system was found to cause common mode currents which then subsequently added to radiated emissions and caused the product to fail emission tests. The problem was resolved by simply replacing the drivers with ones that had less skew. The issue of skew has never gone away but drivers have become more reliable and can give outputs with very small amounts of skew. Data sheets hardly ever quantify this though. It has been found by Hoeft in 1998 that differences in driver slew rate and differences in the drivers rise time in general are the lesser of the two sources of skew in time [21]. These two sources of skew are again driver output skew and differences in the path length (delay skew) each signal sees in each trace. In 2000, Knighten et al [10] furthered Hoeft's

work by creating a test board where the path length could be manually altered and radiated emissions detected. Their findings suggested that delay skew would become an increasingly important design consideration when faced with products where radiated emissions had to be kept low. In 2001, Hubing et al. [17] used formulas to investigate how the odd and even harmonics of the common mode signal that was generated when a differential signal was skewed by 1 and 10% compared to a single ended signal. They found that with just 1% skew at the 50th harmonic the amplitudes of the common signal and single ended signal were the same whereas with 10% skew, most harmonics of the common mode signal were of the same amplitude as the single ended signal. As this thesis is concerned mainly with signal integrity and the modelling thereof, the EMI emissions are important because if the energy leaves the transmission line it does not arrive at the receiver and constitutes added loss in the system and must, therefore, be considered. Methods of reducing EM loss resultant from delay skew will be considered towards the end of this thesis that reduce common mode signals without compromising signal integrity.

2.2.1 Odd and even mode, differential and common drive

A clear distinction needs to be made to enable the reader to follow exactly what is intended when the four distinctions in the title of this section are used throughout this text. In the simplest terms, differential and common signals describe how a signal is launched and indeed how it is intended to be interpreted or received. Modes define how a signal is travelling along a pair of copper traces. A differential signal is expected to travel in the odd mode and a common signal is expected to travel therefore in the even mode. Odd mode is where the signal on one of a coupled pair of traces is 180° (degrees) out of phase with the other and both signals are of equal magnitude. Even mode occurs when two signals travel in phase with identical magnitude on a pair of coupled traces. The odd mode, in microstrip line, travels with greater velocity than the even mode. Velocity of the mode is governed only by the effective dielectric constant, k_{eff}, of the material through which the signal propagates. The differences in velocity between the modes occur because the dielectric medium slows the speed of light. In microstrip line in both modes the electric field permeates the dielectric and the air above. In the even mode there are more field lines in the dielectric than in the odd mode and since the dielectric slows the speed of light, even mode signals will travel more slowly than odd ones. Figure 2.5 illustrates the odd and even mode of propagation showing the electric

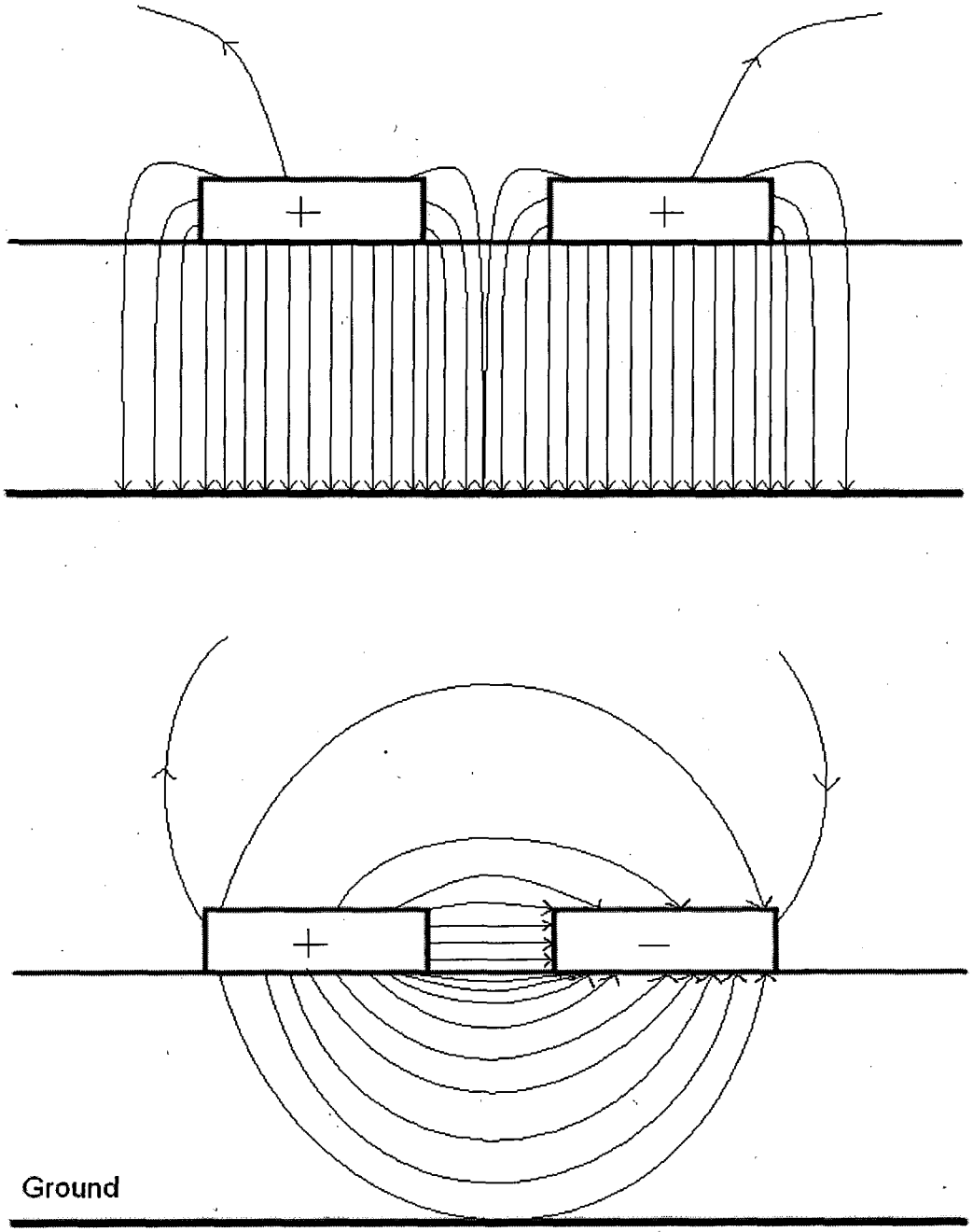

FIGURE 2.5: Diagram showing the even (top) and odd (bottom) modes of propagation for a coupled pair of microstrip transmission lines with the associated electric field lines in a dielectric above a ground plane

field lines in air and in the dielectric, the field lines in the dielectric are closer together signifying the dielectric's ability to increase capacitance and slow the signal.

When a signal is launched in the odd mode and for some reason one of the signals encounters some difference in the metal track it is travelling along compared to the other trace, the impedance will change. Impedance is a ratio of voltage and current at any one point along the pair. If the signal becomes distorted in any way whether through being delayed or encountering different geometry, the impedance will change. Whenever the signal on one trace behaves differently to that of the other track, the mode will not be purely odd any longer. The signal can be divided into portions travelling in the odd mode and portions travelling in the even mode. In this case, the odd mode portion is reduced and the even mode starts to exist, travelling at slower velocity. This process is called mode conversion and constitutes another loss in the system. In 2006, Kirk et al [22] showed skew to cause mode conversion as many others have and they also gave the usual method of skew compensation. Skew compensation is usually achieved by adding length to the shorter of the two metal tracks in the pair. Kirk et al considered common mode as it passed through a connector that had good common mode rejection. They did not, as this thesis does, look in detail at the best methodology of compensating for temporal skew. At frequencies below 6 to 7 GHz according to this research, mode conversion from delay can be easily dealt with by matching the lengths of the traces in a pair at or near termination. Past 6 to 7 GHz, more thought is required. When the even mode is created, portions of the signal are in common to each track in the pair. We can say in fact that there are portions of the signal moving in-phase on each trace. This can lead to electro-magnetic phenomena as discussed briefly in the next section.

Other modes, that are not the odd and even mode as these simply describe how the signal is propagating, that can be excited in a transmission line are observed when a multiple of the exact wavelength of the signal fits precisely inside the transmission structure. This can cause a resonance between the ends of the line and also between the metal microstrip conductor and the ground plane. Resonances cause severe signal integrity issues. These modes are usually only apparent at very high frequencies, usually past those of interest in high speed digital signalling applications. High valued dielectric constant materials shrink the wavelength down, thus pushing these imposed upper frequency limits, defined by where resonance first occurs, further up the frequency scale. Also, decreasing the conductor to ground spacings will mean that even smaller wavelengths caused by much higher frequencies could allow resonance, or the excitation of higher modes, to occur.

Other sources of higher modes that could be a potential problem when modelling a transmission line are the inductors and capacitors in each transmission line section.

FIGURE 2.6: Diagram showing a common method of increasing the length of one side of a differential pair of transmission lines using 45 degree wiglets (skew compensation geometry).

These could begin to resonate if their values are sufficiently large, this will be avoided by using a large number of transmission line sections, thus making each L and C component in each section as small as possible. Again, this will push the point at which resonance occurs far up the frequency scale, and away from where this research is concentrated in the 0.1 to 15 GHz range.

2.2.2 Skew and skew compensation

It is important at this point to make a declaration pertinent to this work. Skew is examined and defined in this work as unavoidable interconnect geometry resulting in a differential signal becoming skewed in time, meaning a portion of the differential signal is no longer 180° out of phase. This portion is defined to be the common signal, as it is common to both traces. De-skew is defined as intentional interconnect geometry attempting to realign in time the signals and thus convert the common mode back to differential mode. Current methods of 'de-skewing' a differential pair involve elongating the shorter trace by adding 'wiglets' such as those found in Figure 2.6, much like the ones used in Figure 2.10, at some point on the shorter trace in the pair, often far from the skew next to termination is a common practice. At low frequencies this is not a problem as any realistic skew, 12 ps for example, which is a good estimate of the amount of skew generated as a differential pair turns a 180° bend, would not constitute a significant portion of the signal period. At higher frequencies however the problem worsens. Figures 2.7, 2.8 and 2.9 produced in MS Excel® show 12 ps of skew between differential signals at 0.1 GHz, 1 GHz and 10 GHz, all frequencies in common use today. Also shown are the amounts of common mode the skew has created. If a common mode signal was created, then this is the portion of the signal lost through mode conversion. In all three figures, differential signals are on the left axis and common signals are on the right axis. Differential signals are defined as the difference between the signals on the pair and common signals are defined as the average of the signals between the pair.

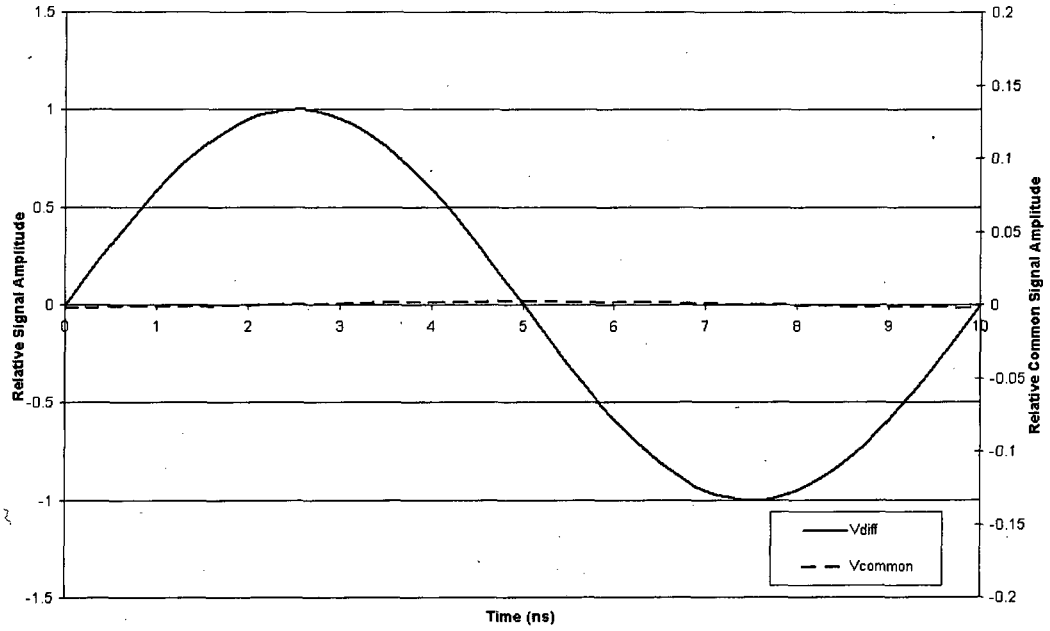

FIGURE 2.7: Illustration showing effect of 12 ps of skew on the differential and common mode signals at 100 MHz

The signals were off set by adding a value for phase to one of the signals. It is clear that as frequency is increased, the same 12 ps becomes a greater portion of a period and contributes more to mode conversion giving greater common mode signals at the expense of the differential signals.

Higher frequencies give smaller periods so the 12 ps is a relatively larger portion of the period with each order of magnitude jump in frequency in these examples. From Figures 2.7 through 2.9, the differential signal is clearly seen to be shifting by greater amounts as the frequency is increased. This gives evidence that as the frequency is increased, the 12 ps of skew becomes a greater portion of the period.

2.2.3 Existing skew compensation methodology

As previously stated in this section, wiglets such as those in Figures 2.10 and 2.6 are used to negate the length mismatch in a differential microstrip pair caused primarily by routing around obstacles on the printed circuit board (PCB). The wiglets are traditionally placed near termination for reasons including ease of routing and the presence of no publication or formal guide to compensating for temporal skew in a differential pair.

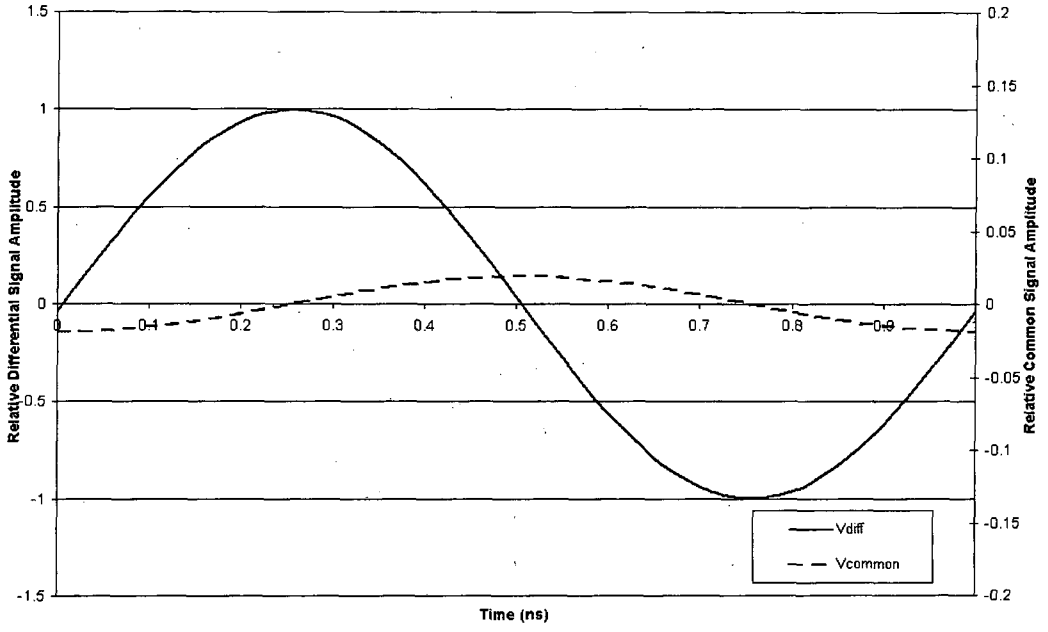

FIGURE 2.8: Illustration showing effect of 12 ps of skew on the differential and common mode signals at 1 GHz

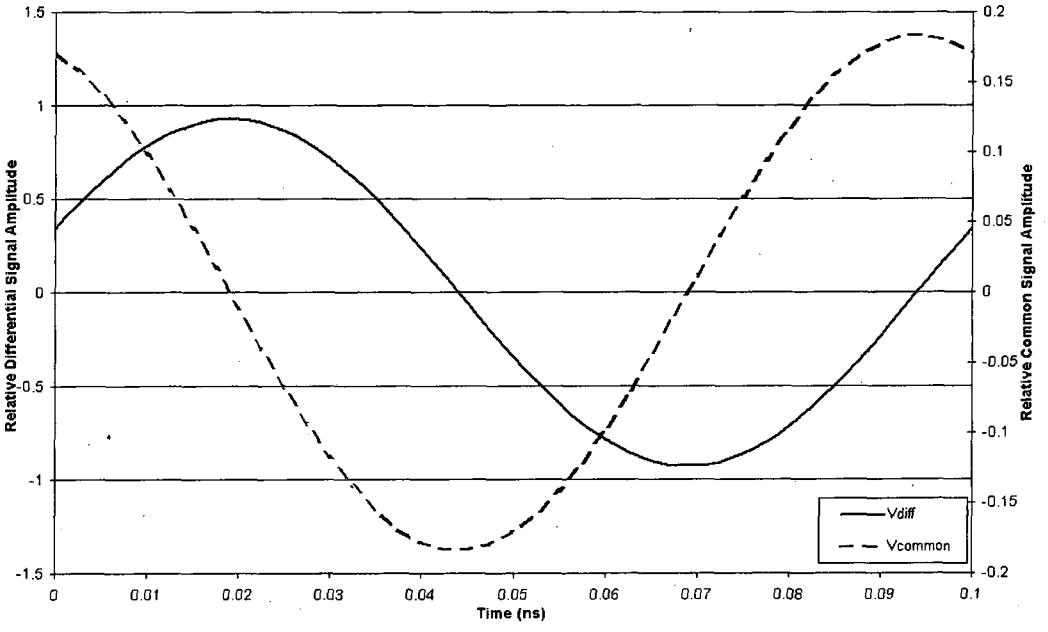

FIGURE 2.9: Illustration showing effect of 12 ps of skew on the differential and common mode signals at 10 GHz

Having questioned several PCB layout engineers they all agreed unanimously that unless otherwise directed they would all have used these same '45 degree snaking' wiglets to match length. Length matching is viewed as just that, the length of the traces in the

pair (the distance along the centre line of each metal trace) is matched, not the time it takes a signal to pass through them. These are two different things due to field interactions within the wiglets themselves. If the signal fields do not behave as they do in uniform differential microstrip lines in the length matching wiglets, then matching length alone may not sufficiently ensure the two signals in the pair arrive concurrently. It is the field orientations that enable the odd mode and the even mode to travel with different velocities. This is a generic solution that is applied, no matter the geometry, frequency or amount of skew. Tolerances are also provided by system designers that describe by how many thousandths of an inch (mils) the traces in the pair must fall within to be accepted as being of the same length. A commonly accepted tolerance here is 10 mils (25.4 μm), a number obtained again by inspecting existing layout CAD tool constraint defaults and asking PCB layout engineers. The number does vary but 10 mils is commonplace because it is far easier to match the lengths to a looser tolerance. If this is taken as an example, at 1 GHz, in a dielectric that has an odd mode relative dielectric constant of 2.411, it will take an odd mode signal 394.4 ps to travel 3" (inches). An extra 10 mils will take another 1.2 ps which is a negligible portion of a period at 1 GHz. At 10 GHz, however, this constitutes 1.2% of a period or 4.3° of signal mismatch.

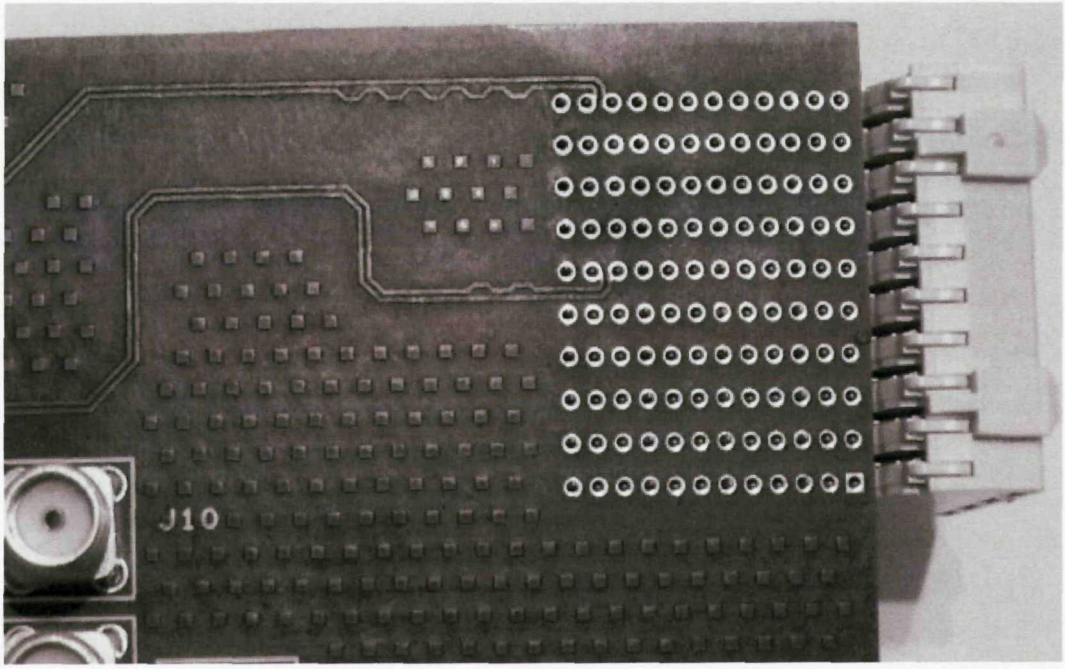

FIGURE 2.10: A differential pair of transmission lines are forced to make turns around PCB components and skew results which requires 'de-skew' wiglets just before the connector at the top right of the figure.

2.3 Electro-magnetic radiation

Printed structures are commonly used to create planar antennas designed specifically to radiate electro-magnetic waves. Differential pairs are designed specifically to keep electrical energy contained between the planar structure and the ground plane. Electro-Magnetic fields are cancelled due to the opposing currents in each half of the pair. Producing differential pairs can be thought of as attempting to produce a very inefficient planar antenna. Radiation is a form of energy transference and in the case of planar structures the electrical energy is transferred from the circuit driver to the surrounding medium, which in this case is air, via the planar structure. The electric potential creates a field that sweeps electrons along with it. Moving electrons constitute a current and currents generate a magnetic field. An accelerating electron in either direction creates a time varying magnetic field. Time varying magnetic fields also create time varying electric fields and the process can become almost self sustaining depending on the propagation medium. This process occurs most efficiently, according to literature [23, 24], by having an antenna (planar structure) to ground distance that approaches similar dimensions to the signal wavelength. Using lower dielectric constant substrates, having currents and hence fields that are in-phase with each other, high frequency time varying currents, open current loops and not enclosing the antenna in an EM impenetrable material all increase EM loss also. Hence with these general rules on how to improve radiation efficiency, by doing the opposite of the rules we can hope to minimise radiation.

EM radiation in the context of electronic design is of most significance when the amount of energy radiated reaches such a level that it could potentially interfere with other electronic devices as the energy attempts to return to its source. The acceptable levels of EM radiation or electro-magnetic interference (EMI) are governed by international standards which vary depending on the intended environment and use of the product.

2.4 High speed transmission line modelling

Based on the fact that the aim of this project is to produce a model that can be incorporated into a large system level time domain simulation and based largely on comprehensive review of frequency domain transmission line modelling techniques by Achar and Nakhla [25], only time domain techniques shall be reviewed in this section. It has

been attempted to model stripline structures such as those in Figure 2.1 and Figure 2.2 since the early works of Cohn [26] where it was attempted to model the characteristic impedance of such electrical transmission lines. The closed form and empirical equations for the line parameters have been refined over the years with enhancements for varying geometries catering for different width to thickness and line spacing to height above ground ratios [27]. These models for characteristic impedance, capacitance, inductance, resistance and conductance have been added into various computer languages such as C [28] and MathCAD [29]. Electronic engineering specific pieces of software such as HSPICE [30] now come with built in models of transmission lines for customisation by the end user. These models are a little too generic and often fail to capture fully the transmission line behaviour and high frequency effects. A 2D field solver is a commonly used tool in industry by many high speed circuit designers which allows fields to be examined in 2 dimensions for structures that are uniform along their z axis when considered end-on. This offers very accurate calculation of all parameters associated with a particular type of transmission line but is restricted to simple structures in two dimensions only, usually looking end-on into a transmission line. The best modern day tools for analysing any 3D structure which will have high frequency currents propagating are 3D field solvers which rely on Maxwell's Equations to calculate electric and magnetic fields and their effects on signals travelling at different velocities through the structure. These tools are often too expensive for many companies, or for that matter many interested persons, to afford. These 3D field solvers also rely on a constant frequency of operation to be given them, hence part of the motivation for this work. Real data could potentially be simulated propagating along an arbitrary length of transmission line where reflections, crosstalk, ringing, over and undershoot and delay could all be examined and the high frequency effects could also be included as differential equations representing most linear and non- linear effects present.

The rest of this state of the art chapter will discuss line parameter extraction and various transmission line models. It will finish with a description of signal skew and its causes followed by a brief, high level explanation of electro-magnetic radiation and it's causes.

2.4.1 Line parameter extraction

Line parameters are classically taken to be electrical properties of a transmission line that allow it to be described in a way that can be understood by all. This is achieved by describing the line as having some series resistance (R), series inductance (L) and some

conductance (G) and capacitance (C) to ground. A transmission line is simply a piece of metal that will have measurable electrical properties like any other, the difference being tat a transmission line implies the length of the metal trace is longer than the spatial extent of the signal rise time. It is therefore the signal itself that defines whether a transmission media is a transmission line or not. These RLGC values define how current and a signal will move along the line and what losses there will be. Differential lines also have capacitance and inductance between the pair referred to as Cm and Lm respectively where the 'm' signifies a mutual value that is shared between both lines in the pair. In order to model a line or pair of lines, these parameters need to be known, as modelling electrical systems can only be achieved in terms of what is understood, which is the electrical properties RLGC. Any circuit theory book such as Hayt and Kemmerly [31] will give details of why RLGC are used and where they come from. Due to the time element involved in high speed lines where the electrical signal is varying along the line, it is not sufficient when modelling to have one lumped value for each parameter of RLCG for the line. These parameters must be distributed equally along the line, that is, the parameter value divided into smaller values that are allocated to smaller sections making up the length of the line. This is because if a signal is varying along the line, a single lumped resistor, for example, can only give a single value for current when we know current to be varying along the length of the line, having multiple values at different points at the same instant in time.

The first paper found on the extraction of parameters for a transmission line was from Cohn [26] where simple formulas were given for the characteristic impedance of single ended shielded strip transmission line. A formula was also given for fringing capacitance. However, both formulas became inaccurate when the fringing fields of coplanar stripline interacted such as with narrow stripline. A paper was released soon after this by Barrett in 1955 [32] which describes the first use of stripline and microstrip by V. H. Rumsey and H. W. Jamieson during World War II as a power division network. Cohn published again [33] in 1955 but this time with formulas for parameter extraction of shielded coupled strip transmission lines which are metal traces suspended between two return planes in odd and even modes. These are much like the traces found in Figure 2.3 but with another reference or ground plane above them. Rigorous formulas for zero-thickness strips and approximate formulas for finite thickness strips are given for characteristic impedance. Approximations for fringing capacitances are also given for these two line types. In 1957, Horgan [34] published a paper which gave by using the numerical method of finding complete elliptic integrals, an approximation of total line capacitance to better than 2 % accuracy. Unfortunately finding elliptic integrals

is computationally expensive and the computing power overhead was deemed unjustified in this work. Also finding elliptic integrals is beyond the capabilities of most line simulators of today. Cohn produced his first paper on broadside coupled transmission lines in 1960 [35] which gave formulas for their characteristic impedance in odd and even modes. Broadside coupled lines are lines that are again between two return planes but are stacked on top of each other so their widest dimensions are facing each other. The problem with formulas produced thus far had been accuracy which worsened the further the lines deviated from the rigorous zero line thickness formulas available. To remedy this Cohn, in the same year as his previous paper, published thickness corrections [27]. The corrections were implemented by the addition of two terms, one for mutual coplanar capacitance and one for parallel plate capacitance to existing capacitance formulas. Getsinger in 1962 [36] produced more accurate fringing capacitance formulas for varying thicknesses of rectangular bars between parallel plates (coplanar transmission lines), claiming accuracy to more than 1.24 percent for bars whose width is greater than 35 percent of the difference between plate spacing and line thickness which compares well to today's transmission line dimensions and ratios. This method again however used elliptic integrals. One of the final words for a time on parameter extraction was by Gupta in 1969 [37] who added to Getsinger's work by creating an expanded scale for the fringing capacitance curves allowing, it was claimed, more accurate fringing capacitance to be found for tightly coupled lines using 2D Laplace equations with appropriate boundary conditions.

From this point on, much more attention was focussed on microstrip as it became ever more important in the field of VLSI and printed circuit boards. Bianco 1978 [38] explores various methods developed for finding the characteristic impedance of microstrip lines based on known values such as voltage, current or power in the line. He highlights the fact the the different definitions can and do give varying characteristic impedances with varying frequency. These are non-geometrical based methods for determination of characteristic impedance. Most geometrical methods thus far had assumed a DC condition however Bianco's work shows that up to near 20 GHz, the characteristic impedance varies by plus or minus ten percent [39]. This is understood to be about the same fluctuation inherent in today's modern processes, which is why this research uses one characteristic impedance value to save computing power across for all frequencies under test.

In 1988 Birchak [40] published with yet more geometry based equations for finding transmission line parameters for microstrip and stripline configurations. This work is

validated with multilayered experimental boards with emphases on gigahertz signalling, capacitive and inductive coupling. The work also describes measurements conducted to validate their model as well as a SPICE sub-circuit lumped element model using the work's methods for parameter calculation. This was possibly the first modified SPICE model to cope specifically with transmission lines, however no losses were considered.

In the same year Bogatin [41] summarised most known capacitance formulas for microstrip line and compared them with measured capacitances generating an error fraction. The best fitting models for line capacitance per length (including parallel plate and fringe) appeared to be Schneider [42] and Wheeler [43]. These models and formulas appeared to be sufficient for engineering design purposes until frequencies and transmission line became higher and denser respectively so mutual capacitance and mutual inductance became much more important to get right. More recently Young-Sooo [44] took a test board of various coupled microstrip and created formulas for self and mutual capacitance and inductance for homogenous and inhomogeneous dielectric media. The formulas were compared to a known field solver [45] and agreement was found to be always better than 10 percent.

2.4.2 Transmission line models

Modelling is essentially the prediction of something's behaviour under a set of conditions based on a theory. The predicted behaviour will only be as good as the model itself. Models are described by equations which can be very simple or highly complicated, generally more complicated equations give higher accuracy models. More complicated (accurate) equations also generally mean more computational power or tighter conditions imposed on their use. There also comes a point in modelling where increasing complexity will not give a sufficiently large increase in accuracy to justify the extra time or cost.

One of the first papers to mention and attempt calculation of dispersion, the process where separate frequency components are attenuated by different amounts, was by Elliot in 1957 [46] where he concluded that by assuming that phase velocity in a waveguide is a quadratic function of frequency, it is possible to derive a formula for pulse degradation due to dispersion. From the formula, effects of line length, pulse width, and dispersion on the pulse shape could be explored.

Before computers were applied to the modelling of transmission lines, Nahman in 1962 [47] produced graphs predicting (modelling) the step response of coaxial flexible cables in various sheathing. This method would have been exceedingly time consuming and had many calculations at every new point plotted. The model did, however, take into account skin effect [48] and dielectric losses [49]. Relatively little activity on transmission line modelling in the time domain occurred until 1971 when Smith [50] wrote a computer program to calculate elliptic integrals and, hence, find fringing capacitance accurately. The code did not model transient behaviour of a transmission line but calculated the capacitance between regular structures of lines. In 1971 the Transmission Line Matrix (TLM) method was initially brought to light by Johns and Beurle [51] who were inspired by Whinnery, Kron and Ramo all in 1944 [52, 53, 54]. The method basically employs a cartesian mesh of open two wire transmission lines to simulate 2D propagation of delta function impulses. This method is memory and computationally expensive as it uses wave theory. The TLM algorithm itself uses a discretised version of Huygens's wave model suitable for computer implementation. A detailed description of this model can be found in work by Johns [55]. Hoefer [56] gives an excellent summary of many limitations, additions and applications for the TLM method. TLM allows modelling of reflections, dispersion, losses and basic anomalous structures to be explored. Many languages could implement the TLM method. Bernard in 1972 [57] came up with a transmission line model for transient Computer Aided Circuit Design (CACD) programs. The model was implemented with CIRC-TR [58] and Fortran IV coding and simulates a distortion free lossless transmission line with the option of basic losses to be incorporated by entering attenuation coefficients. The first record of a C program written to simulate transmission lines was by Messerschmitt in 1984 called LINEMOD [59]. This program was limited to low frequency. It works by calculating ABCD matrices [60] containing complex valued elements of input and output voltage and current at a given frequency. LINEMOD cascades a series of ABCD matrices and hence calculates the ABCD matrix of the line. ABCD for a uniform line was calculated from polynomial approximations of the primary parameters for any line of resistance, inductance, capacitance and conductance. The line is 'coded' into an input file which is read by LINEMOD where the frequency and impulse response are calculated. LINEMOD was used in conjunction with a known simulator of the time, BLOSIM, where many BLOSIM simulations was performed for a given transmission line configuration. The method used recursive techniques thus saving memory. No consideration of high frequency or signal dependent effects was given.

Much discussion was given to modelling the distortion of DC and RF pulses in all

forms of transmission line and as an example microstrip was considered by Veghte [61] in 1986. This was accomplished by using dispersion models and numerical integration, Taylor series expansion or segmenting methods which were analysed against computing time for the analysis of various pulses in microstrip media. DC and arbitrary shaped pulses required numerical methods, however RF pulse shapes could be evaluated much faster with either Taylor series or segmenting method at the expense of accuracy. All models considered used discrete frequencies to evaluate phase constants and associated distortion of pulses.

Additionally in 1986 Brews [62] gives a framework for developing a transmission line model for interconnect at high frequencies where the waveguide nature of transmission lines becomes evident. This framework differed from the conventional analogy between transmission lines and waveguides because it extended to cases where losses were too large to be treated as perturbation. Formulas for the required R, L, G, and C line parameters were provided. Equivalent formulas in terms of the electric field 'E' and magnetic field 'F' variables were also given. These parameters differed from the static values when the longitudinal field components are considered important, or when losses are severe. A complication in the use of the equivalent transmission line is that the low-frequency concepts of voltage and current lose their intuitive appeal at higher frequencies where 'voltage' and 'current' are related in an abstract manner to the transverse electric and magnetic field of the waveguide. An example of the analogy between a lossy waveguide structure in an inhomogeneous medium and its equivalent transmission line was provided. By using the analysis of this paper one could determine whether any proposed R, L, G, and C line is adequate to model a given interconnection.

In 1987 Brews [63] added to and clarified Bianco's work [38] by showing it feasible to impose the usual current voltage relation for complex power for the case when one mode propagates, even if this mode is a hybrid mode of a non-TEM (Transverse Electro-Magnetic) structure. Once imposed, the complex power condition forced all the definitions of characteristic impedance based on voltage, current and power to agree. With this complex power condition imposed, current, voltage, and magnitude of the characteristic impedance all became interdependent. It was showed that one was free to choose only one of the magnitudes of current, voltage or characteristic impedance and also to choose the phase of either I or V (but not their relative phase). As the requirement for complex power agreed with ordinary circuit theory, and was useful in applying any equivalent circuit, it was argued reasonable to adopt it. This allowed simplification of circuits through the choice of current, voltage, or magnitude of characteristic

impedance.

Zhang argued in 1988 [64] that when modelling in the time domain, a sharp gGaussian pulse should be used as opposed to a pure tone sinusoidal one when frequency domain design data are required of transmission media. This was due to the increased computational expense of running in this case, a finite difference method for a sine wave than for a pulse, however, for most methods a transient analysis and subsequent fast Fourier transform (FFT) of the result into the frequency domain is much faster.

In the same year a paper was published by Djordjevic [65] which describes techniques used and known to date for calculating the time domain transient response of multiconductor transmission lines (MTLs). These included the time stepping method which is akin to the method of finite differences, which involves the discretisation of the telegraphers equations [66] in space and time. This method is the simplest to implement and understand in terms of programming. However, it is also one of the least efficient methods due to large circuit node count resultant from the large number of sections the paper describes that are required to accurately model, in a lumped element sense, the line parameters and cross talk. Djordjevic states this method cannot be used for frequency dependent parameters such as skin effect and dielectric losses. Djordjevic's statement provides a partial motivation for this work which aims to show frequency dependent parameters can in fact be simulated in the time domain using a distributed element or similar method. Modal analysis in the time and frequency domain is discussed and is claimed to use less storage and be more efficient than lumped elements methods. Modal analysis uses the eigenvalue equation derived from the wave equation. The line eigenmodes propagate along the (lossless) line without dispersion (assuming the quasi-TEM mode of propagation only). In the frequency domain, frequency dependent parameters could be explored at a given frequency and with the fast Fourier transform, conversion between the time and frequency domain was possible. This method was at the time found to be less efficient than the time domain modal approach but still better than the time stepping method. Djordevic finally looks at a convolution technique which uses Green's functions [67]. This technique can be far more general although it is implied that it would not cope well with multiple reflections. These reflections would be resultant from a non-linear termination to a line which could be common in MTL analysis and would generate large equation sets and be less efficient no doubt than the time stepping method in this instance. Experiments were carried out where MTLs were made on a PCB and the response measured and computed, all results agreed well it was claimed.

The first model the author encountered for microstrip which included conductive losses from both the conductor, dielectric and dispersive distortion was by Leung [68] in 1988. The underlying theory of dispersion and modelling thereof remain largely the same for stripline and microstrip. Various pulse shapes and transmission line geometries were explored and all distortion factors were influenced by geometrical changes in the line. The author hopes to implement all the above losses in this work. In 1991 Pramanick and Mansour [69] investigated uniform, tapered and coupled microstrip when stimulated with a non-ideal square pulse and found the less ideal the pulse, the less distortion was experienced. It was also concluded that rapid impedance changes along any transmission line would lead to larger distortions and reflections.

As speeds of signalling increased and wavelengths approached the order of now 'on chip' wiring, attention was turned to transmission lines on a VLSI chip. To this end, Matthaei in 1990 [70] gave a discussion concerning the on- and off-chip high-speed digital situation, where small cross sectional area transmission lines are highly lossy. It was shown that the quasi-TEM approximation is still useful even when very small conductor areas are used in spite of the large loss. Charge was shown to be confined to the surface of the conductors so that static capacitance calculations such as are commonly used for TEM-mode analysis are still relevant, even though propagating fields and current penetrate deeply into the conductor. It was seen that the total internal current in a conductor can always be computed from the surface charge density as long as the conductor is homogeneous. These sentiments were taken on board and used to enable the author to use common TEM-mode approximations for his work.

In Fache's paper of 1990 [71] a new high-frequency model for N coupled lossless and lossy waveguides was presented. A coupled transmission line model of such structures, for both the non-dispersive and dispersive case, was found based on a power-current formulation of the impedances. The full-wave eigenmode problem for the transmission lines under consideration required solving. It was required to determine the propagation constants and power distribution over the cross sectional area of the line for each eigenmode. This approach agreed with others' of the period, however, at higher frequencies, different equivalent circuit models were produced.

Dhaene in 1992 [72] draws on many previous works to produce a time domain lumped element model for coupled and uncoupled transmission lines. The work uses existing techniques such as those used by Djordjevic in his 1988 paper [65] for calculating the appropriate number of sections to divide the line into but adds his own methods for finding the accuracy of the lumped element model at major steps in the calculations.

Dhaene also uses 3 normalised parameters which could be used in other models and applications allowing ease of comparison. More focus is given to crosstalk (coupled) evaluation.

In the same year Hayes et al. [73] produced a paper focussing more on thin wire and packaging considerations for high speed multi-conductor interconnect modelling. He examined three methods, those of Boundary- and Finite-Element Methods, (BEM) and (FEM) respectively and also the Partial Element Equivalent Circuit (PEEC) method. A description and history was given of the evolution of these techniques and finally comment was given on Hayes' own MICAP program [74] which was written in C and used the BEM and handles systems of arbitrary geometry with or without an infinite ground plane. All methods discussed in the paper only considered lossless lines, that is only gave consideration to inductance and capacitance calculation using the methods mentioned. It was considered that the BEM was more efficient for many common problems however FEM was more efficient for complex problems such as irregular structures. All methods used considerable computing resources.

Mesa et al. in 1992 [75] discussed when quasi-TEM and full wave analysis could be used. It was found that unless a high conductivity substrate was used, quasi-TEM analysis was sufficient for phase constant, characteristic impedance and attenuation constant prediction, else full wave analysis was required. Both techniques are suitable for lossless and lossy lines.

Skin effect has been analysed over the years by many people and is a well understood phenomenon. Its effect was always known on the attenuation factor commonly known as alpha α but its affect on the phase constant commonly known as beta β was always up until this point considered a small perturbation. He et al. [76] in 1993 showed that by including the skin effect in the phase constant, attenuation constant and characteristic impedance for low loss conductors, the skin effect's influence on the phase constant in particular could not be ignored as it contributed to a relatively significant phase shift. This was shown by using a step and ramp like input to a model. The author of this work however will be using a signal dependent model and fixed frequency model for calculation of skin effect resistance.

Gordon's paper in 1992 [77] addressed the frequency dependence of dielectric and conductive losses in the time domain by using the dependence on frequency of the dielectric constant and on the material's tan(δ) [78]. Skin effect was modelled using a perturbation to the boundary element solution. All frequency dependent parameters assumed a

constant frequency of operation in each calculation and did not take into account the highly variable rate of change of the incident wavefront which this research aims to do.

Yu and Wing in 1994 [79] proposed ladder networks of RL and RC elements to model skin effect and line delay respectively as part of an equivalent transmission line circuit. They also proposed similar networks for frequency dependent dielectric loss. The advantages are clear in that no convolution or FFT is required for the time domain results and also it lends itself to incorporation into many circuit simulators such as SPICE [80].

Stubbs et al. in 1995 [81] used VNA (Vector Network Analyser) S-Parameters S_{21} (insertion loss) and S_{11} (return loss) of a single shortened (to ground) test structure to optimise a frequency dependent transmission line model.

Gupta in the following year shows again that a uniform transmission line can be modelled by the method of characteristics, that is it can be defined in terms of lumped elements of its characteristics such as its per unit length resistance, (R') [82]. Gupta goes on to produce an error function drawing on theory from work by Ghausi [83] that can be used as a matrix operation to give the number of 'lumps' for a desired modelling error when using lumped element methods. His next paper [84] summarises the method of characteristics, a lumped modelling approach and the state based convolution technique. A method is produced to automatically select a model dependent on the type of line, efficiency or accuracy required. It was found that the state based convolution method worked most efficiently for long lossy lines, however, this did not take into account the pre-characterisation of the line.

Hwangkhunnatham [85] in the same year devised a 2 level lumped element modelling method where the simulation is split into two parts. These are the circuit level and transmission line level, each dealing with its own variables. The reason for this is that the system as a whole would make standard sparse matrix evaluation techniques [86] inefficient. This allowed matrix size reduction and hence more efficient simulation. No comment was given as to the characterisation of the line or the model's accuracy. The transmission line simulation part was reported to use standard numerical integration techniques such as backward Euler or trapezoidal methods [87].

Chiprout [88] covers many models in his paper and summarises with comment that switching time, resistance of the line, resistance of the load, accuracy requirements, engineering experience, measurements and CPU usage determine their usage'. The specific comment stating engineering experience is a key factor in model choice had not as yet been made. This is very much true in today's world of circuit simulation

where the engineer must always draw on experience to make the right choices about models or whether to model at all.

There was a flurry of papers during the mid 1990's where authors were attempting to produce SPICE type models [89, 90, 91, 92, 93] which would suit all types of transmission line. Each one had a downfall of some sort but most compared well in accuracy to 'exact' solutions. Many of the possible modelling techniques are summarised by Jithesh [94] with tabulations of their respective merits and downfalls.

Coperich argued in 2001 [95] that *"a physically consistent model for the frequency dependent behaviour of the per-unit-length (p.u.l.) conductance matrix of interconnects in lossy dielectrics must be based on a mathematical representation of the complex permittivity that is consistent with causality"* [96]. It was claimed the Debye [8] model could be used for this purpose and such a model could be obtained from measured values of the complex permittivity at several frequencies over the bandwidth of interest. The analysis showed that the wide-band permittivity model is needed in order to prevent both over- and under-estimation of the p.u.l. conductance. The downfall here of course is that measured data must be used and all individual boards made from even the same material such as FR4 will have different measured permittivities.

Mei [97] drew on works by Silvester and Kim [98, 99] to produce a model of the skin and proximity effect by considering the creation of RL ladders and mutual inductances respectively. Methods are given for calculation of the values of the lumped components in these structures based on geometrical data of the lines in question. Also in 2004 a work was published by Seungyong et al. [100] where a method of using additional voltage and current sources in a differential transmission line model was used. This was achieved by finding mixed-mode S-parameters by measuring open and short patterned differential lines, and extracting equivalent circuit model parameters from a subsequent de-embedding and fitting process. The model was verified using time domain measurement to 3GHz. The problem obviously lies here with the model being developed by measurement first and the measurements would have to be redone for each new geometry. Shizhong et al. [101] claims their model works up to on chip wiring dimensions and not necessarily board level interconnect, possibly due to computational expense.

2.5 Choice of modelling languages and environments

In considering the correct modelling language and tool for the task of capturing signal dependent effects in high speed transmission lines, it is prudent to give a very brief history of the evolution of mixed signal simulators such as SystemVision from Mentor Graphics® [102] and Genesys from Agilent® [103].

The first mention in the literature of mixed signal simulation, defined from here on in as analogue and digital signal modelling within the same simulation run, is by Ko in 1990 [104]. Before this, any mixed signal design relied upon using at least two simulators, one for analogue hardware and one for digital hardware. This also of course meant more than two modelling languages were also required. This was time consuming, inefficient and the two distinct simulations allowed very little insight into how the mixed signal physical design would actually behave when analogue and digital signals were combined in the real world. Coupling and timing issues for example were difficult to model in mixed signal designs. A number of analogue and digital modelling languages, tools and simulators were developed at the time. The AMP (Analog Modeling Package) for example was created as an add-on to, at the time, commercially available logic simulation packages. The first efforts at truly mixed signal simulation came from the combination of using Saber, a more generalised SPICE-like simulation engine [105] and MAST, an analogue hardware description language [106]. Slightly later in 1994, analogue hardware description languages were beginning to be combined with digital hardware description languages such as VHDL and Verilog-HDL [107, 108]. This brought about more general acceptance of the real possibility of system level modelling. The benefits of system level modelling are multifaceted. Models may be described behaviourally and entered into tools relatively quickly presenting a speed up immediately in model creation time. A general significant speed up in simulation time is achieved through the combination of behavioural and mixed signal modelling within the same environment. Also, early verification of system level concepts before more detailed models are developed [109] is possible with system level modelling as Dumlugol shows. This approach enables the top down hierarchical development of systems with varying degrees of abstraction in each level as the designer requires. Designers have been using customised code and creating customised models to suit their purposes for varying levels of abstraction for many years using generic programming and modelling languages such as the C programming language [28] and MATLAB/SIMULINK® [110, 111]. These type of approaches can give excellent results however, they do often require a lot more effort on the designer's part such as writing special conversion algorithms to

interface custom models with existing HDLs such as VHDL-AMS. They also usually involve more than two programming languages and environments as Mu highlighted in 2005 [112]. The problems and issues that arose from using different languages within a single simulator included designers needing to learn and familiarise themselves with multiple languages. Also there were and still are incompatibilities between the languages and the simulator in terms of suspension points. Other difficulties included there being similar statements or concepts in different languages which offered different functionality. A common problem was found with the initialisation of signals in different modelling languages which can lead to problems when different languages are used within the same simulator. Finally, each language will promote or lend itself to certain modelling approaches and so attempting to use multiple languages may be incongruent with using a single modelling approach according to Goldgeisser [113]. A far better solution that is being adopted more commonly is to use a single language within a single simulator and to only use multiple languages where absolutely necessary.

There is as ever more than one choice when choosing a modelling language and simulator. Most mixed signal simulators allow the designer to enter models in a variety of languages, however the problems mentioned previously do still exist. Research and development work is continually being done to extend and modify existing programming / modelling languages to accommodate mixed signal designers.

There have been recent developments using SystemC [114, 115, 116] and SystemC-AMS with the SEAMS [117, 118, 119] simulator for the development of mixed signal modelling methodology, however, this sort of work was in its infancy when the choice over language and simulator had to be made and lacked the technical support that would have been required.

There have been two main standards in hardware description languages that have been used for many years. These standards have been used with a variety of simulators which have offered the designer many options for modelling including the use of multiple modelling languages and design entry techniques. These standards are Verilog [120] and VHDL [121]. These modelling language standards have both been extended and standardised to include analogue and mixed signal extensions. The result was the creation of the two standards of Verilog-AMS [122, 123] and VHDL-AMS [6, 124]. There exist standards committees for both languages and a vast amount of technical support and experience has been built up around them also. Both standards provide much the same functionality and are both highly suitable for the task of modelling signal dependent effects in high speed transmission lines. They would both allow analogue signals

comprising the input, output and all signal interactions in between, to be combined with an established modelling language standard. Previous experience by the author with VHDL-AMS and the SystemVision simulation environment tool meant a more efficient use of time could be made through a greater initial familiarity with the language and environment. It was this fact that meant that these were chosen to perform the signal dependent transmission line effect portion of this research.

Concerning the exploration of losses from skew and electro-magnetic effects, a frequency domain modelling tool and simulator was required. All structures within the scope of this research would experience a non-changing medium comprising air and dielectric for the duration of their signal path in the z-direction (from launch to termination). This is also true in the x and y-directions. It is because of this that a full 3D EM modelling tool, at significant cost, would be quite unnecessary. Instead, a 2.5D planar EM modelling tool would suffice at a much reduced cost. 2.5D planar means the signal paths are built up in layers where each layer is identical apart from the signal path itself which may have any geometry within it's plane. The 3D design space is a 3D box where each layer has the same properties and can be subdivided into a mesh for analysis. The tool selected was Agilent's® Genesys as it was able to fulfil the remit for this research.

This concludes the peer review section where the author hopes to have given an historical account of the progress of transmission line modelling and future problems we may face with the many methods given. The author intends to show that new ground is broken by developing a new methodology for calculating the skin depth and dielectric conductance developing a signal dependent model to model these effects. In order to save CPU time and to take advantage of modern software, no equations will be used to determine the p.u.l. parameters of the line. Instead, a 2D field solver will be used [125] because it takes an engineer less than 30 seconds to input the line geometry and less for the software to produce the answer. These values will be input directly into the model. This should make for a fast and efficient way of working by having a geometrically configurable distributed parameter model to insert in a large time domain system level simulation. It is also intended to show through this research, and prove that delay skew poses a threat as yet not fully explored in the literature to signal integrity and not just EMI issues. The threat will increase as frequencies of operation increase to 10 GHz and a small tolerable amount of delay skew that is historically corrected just before the receiver to within a tolerance may not be sufficient in the future. Higher frequencies mean the same amount of delay skew becomes an ever increasing percentage of the

signal wavelength and again adds to common mode currents but also challenges the tolerance receivers have to skew between differential signals.

Frequency dependent effects were of first concern to those in the radio communications (analogue / frequency domain) community so a large portion of the literature has been from a communications person's point of view. This research is from a digital (time domain) data transmission person's point of view, and as such will remain largely in the time domain and will keep relating points made back to real data that does not have a frequency associated with it.

Chapter 3

New Method for Time Domain Analysis of Signal Dependent Effects

In time domain modelling of real data, there is no concept of frequency in that there are no cyclic continuous patterns that a period can be ascertained from. In terms of modelling data transmission paths or 'transmission lines', using a distributed lumped element approach, this means there is no frequency from which fixed values for frequency dependent components such as the resistive and conductive elements can be calculated. This is true unless the signal is a pure tone sine wave of constant frequency which conveys zero useful data, unless used as a clock. Some new method was required in order to be able to more efficiently and accurately model frequency dependent effects such as skin effect and dielectric conductance in the time domain. Long sequences of 1's or 0's, the exact number of each will be dependent on the signalling scheme which, can lead to apparent 'frequency' being a lot less than the value the designer has allocated to the model. Less signal activity presents lower losses hence using a constant frequency for loss modelling can lead to the over-estimation of average loss in a transmission line. Some method other than using the existing formula for skin depth in Equation 2.1 or for the amount of dielectric conductance in Equation 2.6 which both give fixed losses in the time domain when given a fixed frequency was required. It was conjectured that by using the existing accurate formulas for frequency dependent effects and manipulating them to be reliant on signal rate of change, amplitude and present value of the signal, they could still be used to provide an accurate amount of loss in a time domain computer model [126].

3.1 Signal dependent skin depth

As stated in the previous section, the following is the manipulation of formulas so that the frequency term, 'f' can be defined in terms of signal amplitude, rate of change of signal and signal value at an instant in time. The skin depth equation and the dielectric conductance equation can then be evaluated based on these parameters also with no explicit need to define frequency, 'f'. This was accomplished by using a method of trigonometric identities and back substitution:

$$\begin{aligned} V &= A\sin(2\pi f t) \\ \frac{dV}{dt} &= A2\pi f\cos(\omega t) \end{aligned} \tag{3.1}$$

where V is the signal value, or voltage, A is the signal amplitude, f is frequency and t is time.

Using identity:

$$\begin{aligned} \cos^2\alpha + \sin^2\alpha &= 1 \\ \cos\alpha &= \sqrt{1-\sin^2\alpha} \end{aligned} \tag{3.2}$$

And:

$$\begin{aligned} V &= A\sin\alpha \\ \sin\alpha &= \frac{V}{A} \end{aligned} \tag{3.3}$$

The following estimate for the signal rate is obtained by substituting Equation 3.2 into Equation 3.1 where α means ωt:

$$\frac{dV}{dt} = A\omega\sqrt{1-\sin^2(\omega t)} \tag{3.4}$$

Then by substituting Equation 3.3 into Equation 3.4 and re-arranging for ω :

$$\begin{aligned} \frac{dV}{dt} &= A\omega\sqrt{1-\left(\frac{V}{A}\right)^2} \\ \frac{dV}{dt} &= \omega\sqrt{|A^2-V^2|} \\ \omega &= \frac{dV}{dt}\cdot\frac{1}{\sqrt{|A^2-V^2|}} \end{aligned} \tag{3.5}$$

With ω isolated it is possible to eliminate it from the original skin depth equation shown again here for convenience:

$$\delta = \sqrt{\frac{2\rho}{2\pi f\mu_0\mu_r}} \tag{3.6}$$

where ρ is the resistivity of copper and f is the maximum frequency of operation, μ_0 and μ_r are the permeability of free space and the relative permeability of the material respectively. Equation 3.5 is substituted in to Equation 3.6. This finally gives an equation for skin depth that does not depend on frequency, but instead on the signal maximum amplitude 'A', the present amplitude 'V' and the rate of change of amplitude as the continuously changing variables.

$$\delta = \sqrt{\frac{2\rho\sqrt{|A^2-V^2|}}{\mu_0\mu_r dV/dt}} \tag{3.7}$$

With the effective skin depth now calculable in a time-domain situation, it could be incorporated into a resistance equation where the area term is replaced by the skin depth and multiplied by width giving the approximate area that the current flows in for a rectangular cross section line:

$$R_{AC} = \frac{\rho L}{\delta(w+2t-2\delta)} \tag{3.8}$$

where w is width, t is thickness and L is the length of the metal track. Equation 3.8 makes an assumption about the distribution of the fields around the conductor in that it assumes the fields and currents will be confined to the skin depth around the conductor edge nearest the reference plane and the sides of the conductor, but not the surface farthest from the reference plane. The signal (fields) will be guided and mostly confined between the reference plane and the interface between the conductor and the dielectric.

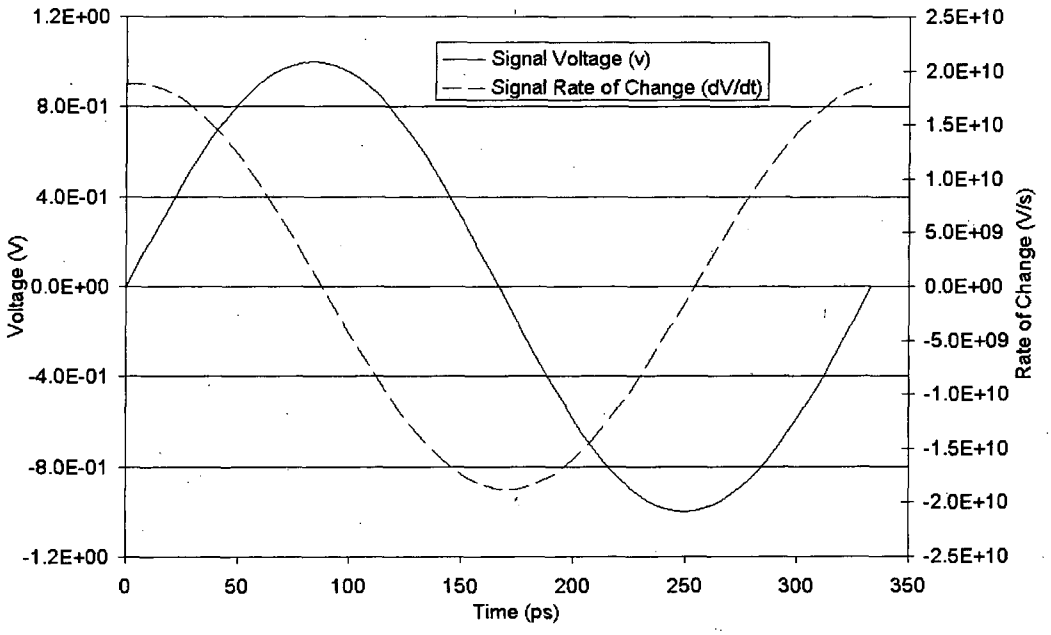

FIGURE 3.1: An ideal sinusoidal voltage source (solid line) accompanied by its respective rate of change (dashed line)

Equation 3.8 is now highly suitable for incorporation into any time domain model of a high speed lossy transmission line.

In order to ensure that the equation gave a reasonable approximation of the skin depth, the Equation 3.7 was presented with an ideal voltage source as created in MS Excel®. The voltage source was a 3 GHz sinusoidal waveform, this and its derivative became the 'V' and 'dV/dt' component in the equation. The amplitude was fixed at 1 V. The constant skin depth equation that uses the constant frequency of 3 GHz was also used and plotted. At 3 GHz the skin depth in copper is 1.19 μm according to Equation 3.6. Figure 3.1 shows the input waveform and its derivative. Figure 3.2 shows the fixed skin depth and the skin depth that depends on the signal. As expected, in Figure 3.1, the derivative is at a peak when the signal is at it's highest rate of change, or where it passes through 0 V. The signal dependent skin depth in Figure 3.2 fluctuates closely either side of 1.19 μm with an average value of 1.19 μm. The average error, calculated by taking the average of the differences between the fixed frequency and signal dependent plots in Figure 3.2, is given as 0.131% presenting minimal error. The signal dependent skin depth becomes asymptotical periodically when the $A^2 - V^2$ part of the equation approaches zero. This could be a potential problem for modelling as it could cause the equation set, when incorporated into a resistance equation, to go to near infinity.

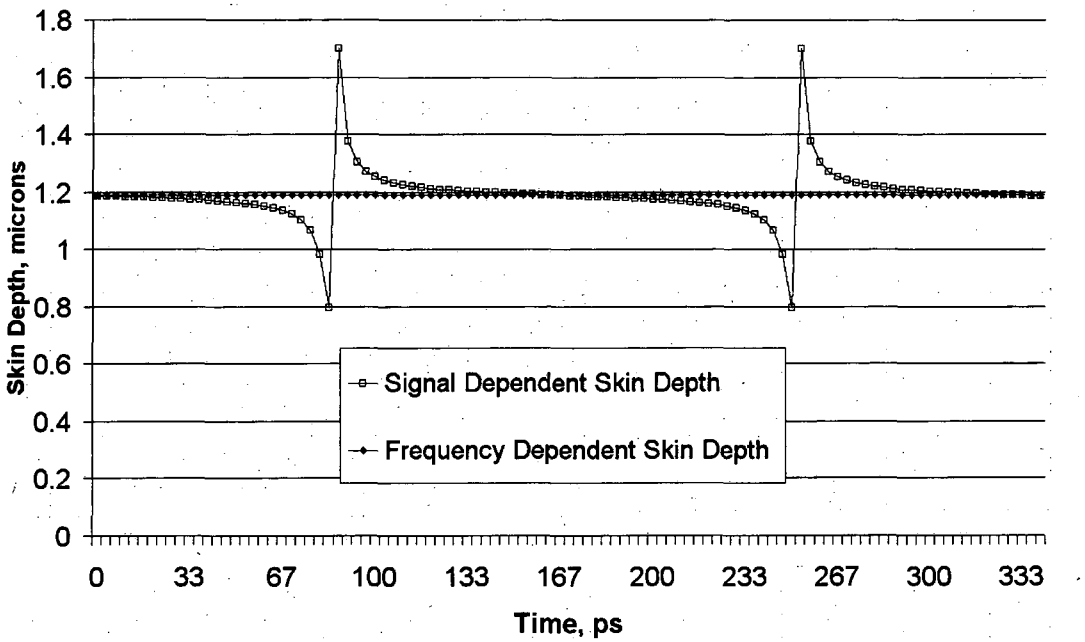

FIGURE 3.2: Skin depth for a constant frequency of 3 GHz given by the constant frequency skin depth equation. Also shown is the skin depth as calculated by the signal dependent method

Another potential issue is what the algorithm should use for an amplitude value, and how to arrive at an appropriate value for amplitude. If amplitude is defined as the peak to peak measurement of the signal then as the signal propagates the amplitude will diminish, however, there is no obvious method of finding and incorporating the amplitude into the equation set as it changes value.

If these and other as yet unknown issues can be resolved, it appears the signal dependent skin depth equation would be very suitable for use in a high speed digital simulation package as it would allow very efficient and accurate determination of the skin depth due to the signal itself [126]. This would cater for long sequences of 1's and 0's where the signal would appear DC and the skin depth would increase considerably, thus minimising loss and also potentially allowing inter symbol interference to be reduced. Using a fixed frequency and hence fixed loss would potentially over-estimate the amount of loss and may result in extra design time to minimise losses where the existing design may have been suitable for the desired use.

3.2 Signal dependent dielectric conductance

The same approach was applied to the equation for determining the amount of dielectric conductance in a transmission line. Again for convenience the equation for dielectric conductance is included with the frequency (ω) term included:

$$G_{AC} = 2\pi f tan(\delta)C \tag{3.9}$$

where G_{AC} is conductance and C is line capacitance.

Substituting Equation 3.5 in to Equation 3.9 leaves an equation for dielectric conductance, again with the frequency component eliminated:

$$G_{SD} = \frac{|dV/dt|}{\sqrt{|A^2 - V^2|}} \tan(\delta)C \tag{3.10}$$

where G_{SD} is the signal dependent dielectric conductance.

The dielectric conductance is now dependent on the maximum signal amplitude, rate of change of signal and the present value of signal, just as for the skin depth. All these variables are readily available for access in most time domain computer simulation packages so this approach could lend itself well to incorporation into these packages.

3.3 Benefits of calculating signal dependent effects in the time domain

Here follow some simple arguments promoting the use of the previously discussed methods of calculating effects that are dependent on what the signal is doing at that time when present in high speed transmission media.

The frequency is never known exactly, nor can i be defined when real data present unless there is a pure sinusoidal signal being transmitted so another method of determining losses should be used.

Real data has no frequency and so losses will either be greater or less than assuming a fixed frequency of operation.

Components that have frequency dependent losses in models generally have some form of look up table where the loss for the given frequency is used or an equation is used when given the frequency of operation. These look up tables can be far too coarse to give accurate loss estimates, and also the models are not available to everyone in the design world due to prohibitively expensive modelling tools and industry standardisation. Where an equation is used, or set of equations, these rely on being given a frequency in the first place also so although an exact frequency may be known, it is, as previously stated, rare that a pure sine wave will actually be used.

If real data is used, there can be long periods of either inactivity if the transmission line is a control line or long periods of 1's or 0's. In either case the line tends towards a DC condition where losses are very low. Use of a frequency domain approach may lead to large over-estimation of losses in the transmission media which may cause wasted design time and extra unnecessary expense. This would be because losses may be assumed to be too high when really the small amount of data sent would experience relatively little loss.

The method from the 'idealised' graphs presented appears to give a good approximation to the signal dependent effect of skin effect, varying by less than 0.1 μm for most of the time.

Everyone from student to small electronics design house could benefit from this novel method of calculating signal dependent effects in the time domain as it appears easily portable to many circuit simulation tools, including ones available on student license.

No vast amount of computing power would be necessary either it seems as all calculations can be transformed to ordinary differential equations with potentially minimal memory storage required.

Some methods use domain conversion techniques where conversions are made from the time domain to the frequency domain and perhaps back again. This requires a lot of extra computing power and normally time also. The approach mentioned here is completely based in the time domain.

Chapter 4

Time Domain Modelling of Signal Dependent Effects in High Speed Transmission Media with VHDL-AMS

As stated in Chapter 2, from the a search of the literature no one has yet created a mixed signal hardware description language based model of a transmission line for implementation in a full system level simulation. The model was produced in VHDL-AMS and is a longitudinally distributed lumped section coupled and uncoupled microstrip transmission line over a ground plane, which consists of a generation module (top-level module) and the netlist module (section module). The generate module contains minimally three instances of the netlist with the first connecting to the source resistor (Rs) and the last connecting to the load (Rl). This module automatically calculates the number of sections (n), such that sectional delay is less than $1/20^{th}$ of signal rise time [39]. The middle instantiations of the netlist are replicated n times using a VHDL-AMS 'generate' statement with the VHDL-AMS 'electrical_vector' nature to link the sections together. The code excerpt in Figure 4.1 shows the generate statement used.

The netlist module contains all lumped components for a single section which comprises a series resistor (R'), conductance (G') to ground, a capacitor to ground (C'), a mutual capacitor (Cm') and a series inductor (L') as shown in Figure 4.2, where the prime (') indicates a per unit length parameter. The values for the lumped components R', G', L', C', Cm' and Lm' for any microstrip transmission line structure to be modelled were obtained from a known 2D field solver [125]. The VHDL-AMS model can be driven

```
- -Create number held in 'total_sections' sections
sections: for i in 1 to (total_sections) generate
- -Each section referenced as 's_rest' and uses standard 'netlist' module for each
  s_rest: entity work.netlist
    - -Used to pass definable values to common parameters in the generated modules
    generic map(
      generics => values
      ...
      )
    port map( - -Used to connect or 'map' the generated module inputs and outputs
      ports => ports
      ...
      );
  end generate;
```

FIGURE 4.1: VHDL-AMS '*generate*' statement in the generation module.

by any two VHDL-AMS sources. For test purposes two single frequency sources in anti-phase were employed to give a differential signal. The line propagates the signals through Rs along each coupled section and the output is measured across Rl. Crosstalk is taken into account through Cm and also through a mutual inductance which, because the lines are being driven in the odd mode, is taken away from L' due to magnetic field orientations.

Initially only fixed frequency resistive and fixed frequency conductive losses were considered. The resistive loss is given by Equation 2.2 but the area term is calculated using Equation 2.1 at a fixed frequency. DC conductive losses were obtained from a data sheet for whichever dielectric was considered and again Equation 2.6 was used to give a fixed frequency conductive loss for the dielectric. These losses were constant and the exiting signal can be seen in Figure 4.3, closely resembled that which was launched and thus showed that the model propagated a signal, giving a loss and a delay. Resistive and conductive losses are dependent on signal shape as discussed in Section 2.1.1, so the next section describes the time domain Signal Dependent Resistor (SDR).

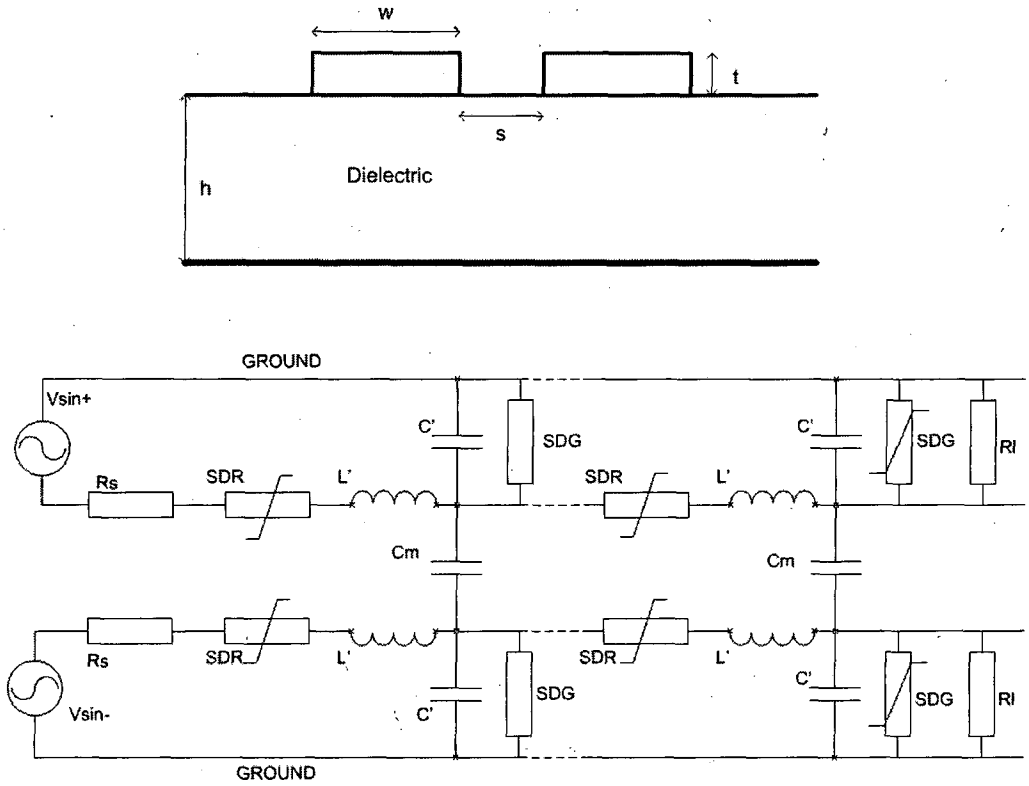

FIGURE 4.2: Edge coupled lossy microstrip transmission line on a dielectric above ground and the equivalent discretised circuit.

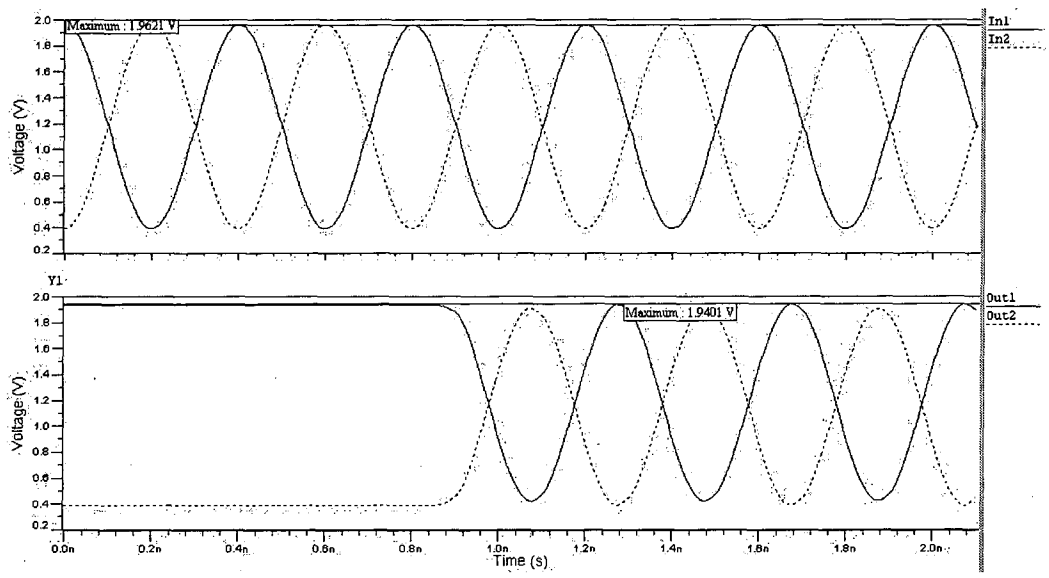

FIGURE 4.3: Differential input and output of an edge coupled microstrip transmission line as modelled in VHDL-AMS with fixed losses at 2.5 GHz.

4.1 Time domain model of a signal dependent resistor in VHDL-AMS

In addition to motivations already presented for the development of a signal dependent resistor, the modelling of real data need also be considered. For long periods of 1's or 0's, the line is effectively at DC, so allocating resistances to all sections for the maximum frequency or data rate of a signal would lead to a large over estimate of loss on the line, unless data was always 101010 ... which conveys zero information. And also if a new frequency is identified the line will not instantaneously jump to the skin depth associated with it, but instead will tend towards the skin depth and associated resistance. The SDR captures these effects.

The SDR is a non-linear device because it depends on signal variation rate for its value. The SDR uses the derived equations from Section 2.1.1 in a VHDL-AMS process which is triggered by breaches in defined resolution thresholds of voltage and rate of change of voltage giving good efficiency. A clocking mechanism was also introduced which uses a period of two fifths of the bandwidth of the signal which is determined from the fastest rise time which is always known from the system specifications or the driver specifications and hence can be given in advance. Several tests were conducted to arrive at a suitable clocking period that would not run the process excessively but would also give good resolution. The clocking signal was used for periods of signal inactivity when neither the change in present value of voltage compared to the last value of voltage nor rate of change of voltage compared to the last value of rate of change of voltage exceeded the defined thresholds to keep the process updated. The process would evaluate itself even if the thresholds were not breached, thus ensuring resistance tended towards DC as opposed to just dropping to a DC condition. It was felt necessary to have two thresholds that would trigger the skin depth calculation process because all simulators have bugs and for some reason it may have been possible for the code to not have triggered a threshold breach resulting in a jump or glitch in output signal on the next evaluation. Also, it is possible for the signal voltage to change over a long period of time but so slowly that it will not trigger the rate of change of voltage threshold so the present value compared to to last value may still be triggered.

```
--include essential libraries allowing required functionality within module
library IEEE_proposed; use IEEE_proposed.electrical_systems.all;
library IEEE; use IEEE.math_real.all; use IEEE.std_logic_1164.all;
entity sdr is -- begin Signal Dependent Resistor top level description
  generic(    -- generic parameters passed to all SDR modules
```

```
    length      : real;  -- Length of the line in metres
    height      : real;  -- Thickness of the line in metres
    width       : real;  -- Width of the line in metres
    abovegnd    : real;  -- Distance to the ground plane below the line in
                         -- metres
    roe         : real;  -- Resistivity
    skin_onset  : real;  -- Frequency at which skin effect begins affecting
                         -- loss in a way that gives a recognisable amount
                         -- of loss
    sr_onset    : real;  -- Frequency at which surface roughness begins
                         -- affecting loss in a way that gives a recognisable
                         -- amount of loss
    surface_rms : real;  -- The root mean squared roughness of the surface
    BW          : real;  -- The bandwidth of the signal under test
    Ur          : real;  -- Relative constant of permeability
    sections    : real := 1.0); -- The number of sections in total
  port( terminal p1, p2,        -- Electrical physical connections of resistor
   psense_in : electrical;      -- Sense input to read voltage at input with
                                -- respect to ground
    a_in :  real := 0.0;        -- Maximum amplitude read in from previous
                                -- section
    a_out : out real := 0.0);   -- Maximum amplitude read out to next section
end entity sdr;

architecture sdr of sdr is
  quantity v across i through p1 to p2; -- define voltage across and
                                        -- current through the module
  quantity vs across psense_in to ELECTRICAL_REF;  -- sense inputs
  -- find a baseline DC resistance:
  constant rdc    : resistance := ((roe*length)/(width*height))/(sections);
  constant U0     : real := 1.2566e-6; -- Constant of permeability
  constant sigma  : real := 5.96e07;   -- Conductivity of copper
  constant dv     : real := 0.005;     -- RESOLUTION = 5mV, the module will
                                       -- only re-evaluate if the sense voltage
                                       -- changes by +/- 5mV or more
  constant d_vdot : real := skin_onset; -- RESOLUTION  in V/s, the module will
                                        -- only re-evaluate if the rate of
                                        -- change of the signal changes by the
                                        -- skin onset rate of change.
```

```
  signal step_check_s : real := 0.0;     -- A check to ensure a minimum time has
                                         -- elapsed before running again, takes
                                         -- the time at the end of the proces
  signal a, Am_int : real := 0.0;        -- Used to record the present and
                                         -- highest signal amplitude in the
                                         -- section
  signal s_depth_old_s : real  := SQRT((roe/(3.141569*BW*U0))); -- the last
                                         -- value of calculated skin depth
  signal r        : resistance :=        -- the present value of resistance
        ((roe*length)/(width*(SQRT((roe/(3.141569*BW*U0))))))/(sections);
  signal start, run_once, clk  : boolean := FALSE; -- Signals ensuring module
                                                   -- runs correctly,
                                                   -- accurately and
                                                   -- efficiently
  signal threshold, vdotthresh : boolean := FALSE; -- Boolean resolution signals
                                                      monitoring for changes which
                                                      activate the module
  signal v_last                : voltage := 0.0;   -- The last value of the
                                                   -- voltage across the
                                                   -- resistor
  signal vdot_last             : real    := 0.0;   -- The last value of the
                                                   -- rate of change of
                                                   -- voltage across the resistor
begin
-- The 'threshold' signal changes value when the present voltage across the
-- resistor differs from the previous value from the previous time the
-- module ran either positively or negatively by the defined resolution
  threshold <= not vs'above(v_last-dv) or vs'above(v_last+dv);
-- The 'vdotthresh' signal changes when the present value of rate of change
-- of signal differs from the previous value either positively or negatively
-- by the defined resolution
  vdotthresh <= not vs'dot'above(vdot_last - d_vdot) or
                        vs'dot'above(vdot_last + d_vdot);
-- The clk signal allows the module to run with no change of signal allowing
-- a DC state after a natural amount of time to preside.
  clk <= not clk after 0.2/BW*1.0e6us;

-- Any changes in the signals 'threshold' , 'vdotthresh' or 'clk' will cause
-- the process to re-evaluate where the new skin depth and resistance are
```

```
-- calculated.

-- New process referred to as 'new_sd' for NEW_SkinDepth'
new_sd : process (threshold, vdotthresh, clk) is
  variable step : real := 0.0; -- Temporary storage to ensure time has
                               -- progressed since last iteration
  variable s_depth_new, newr_v : real := 0.0; -- Holds the newly calculated
                                              -- skin depth and resistance
  variable start_v : boolean := FALSE         -- Checks if process has run
  -- 's_depth_v' provides an initial guess for the skin depth at the
  -- highest frequency or 'BW'
  variable s_depth_v : real := SQRT((roe/(3.141569*BW*U0)));

begin
step := NOW - step_check_s; -- 'NOW' contains the current time, step receives
                            -- the present time minus the time at the end of
                            -- the last iteration
if step > 1.0e-18 then     -- If the result of the previous line is greater than
                           -- the smallest time step possible in the simulator it
                              means some time has passed and the process may
                              re-evaluate else it may evaluate the same
                              parameters twice
if start = true then       -- Check to see if the process has run before, if it
                           -- hasn't there is no point running it as the module
                           -- does not yet have correct values to run
  if (abs(vs) > Am_int) then -- If the present value of the voltage is greater
  Am_int <= abs(vs);         -- than the internally stored one, then the
  end if;                    -- internal one takes that value to pass out to
                             -- the next section
  s_depth_new_v :=  -- Calculate the new value of skin depth
       SQRT((2.0*roe*SQRT(abs((a**2)-((vs**2)))))/(abs(vs'dot+1.0)*U0*Ur));

  -- Check to see if the new skin depth is greater than half of the metal
  -- thickness, much like a DC condition, if yes, allocate the DC resistance
  if (s_depth_new_v > (0.5*height)) then
    newr_v := rdc;

  -- If the new skin depth is less than the DC condition and greater than
  -- the previous value, increase the skin depth at a rate equal to the
```

```
  -- extrapolated linear equation that follows then allocate new resistance
  else if s_depth_new_v > s_depth_old_s then
    s_depth_v := s_depth_old_s + 4000.0*step;
    newr_v :=
    (((roe*length)/(s_depth_v*width))/(sections))*(1.0+(width/(6.0*abovegnd)));

  -- If the skin depth is less than the DC condition and less than the
  -- previous value, decrease the skin depth at a rate equal to the extrapolated
  -- linear equation that follows then allocate new resistance
  else if s_depth_new_v < s_depth_old_s then
    s_depth_v := s_depth_old_s - 4000.0*step;
    newr_v :=
    (((roe*length)/(s_depth_v*width))/(sections))*(1.0+(width/(6.0*abovegnd)));

  -- If the skin depth is less than the DC condition but is no different to
  -- the previous value, keep the old value and use this to calculate
  -- resistance
  else
    s_depth_v := s_depth_old_s; --no change
    newr_v :=
    (((roe*length)/(s_depth_v*width))/(sections))*(1.0+(width/(6.0*abovegnd)));
    end if; end if; end if; -- terminate all 'if' statements
  s_depth_old_s <= s_depth_v; -- The present value of skin depth becomes the
                              -- old value
  r <= newr_v;                -- The value of resistance to be used in the
                              -- governing equation is updated
end if; -- End the 'if start=true' structure

-- If the process did not have the necessary information to begin properly
-- and 'start' was not 'TRUE' this code latches 'start' true.
if abs(vs'dot) > 2.0e6 then   -- Is signal changing fast enough?
  start <= true;
  start_v := true;
end if;

-- Once the process has run once, 'run_once' is set to 'true', this prevents
-- the signal amplitude from changing and having adverse effects on skin
-- depth and observed loss, and hence on the signal shape
if ( (start_v = true) and (run_once = false) ) then
```

```
  if a_in > 0.1 then
    a <= a_in;
    run_once <= TRUE;
  end if;
end if;

v_last <= vs; vdot_last <= vs'dot; -- The signals are updated
end if;  -- End the 'if step' clause
step_check_s <= NOW; -- Update the time elapsed signal with the current time
end process new_sd;  -- End the process

-- The maximum amplitude achieved is passed out to the next section
a_out <= Am_int;
-- The governing equation is evaluated with the new values of resistance
v==(i*rdc)+ (i*r);
end architecture sdr;
```

The SDR process is triggered ether when the clock ticks or when the A'ABOVE(B) attribute becomes true, when A-B $>$ 0, where A in the first instance is the present voltage and B is the last voltage minus a defined (empirically found) threshold of 5 mV. Upon entering the process the only unknown in determining the skin effect resistance at this point is the amplitude of the signal due to the attenuation in each section. This was resolved by using a vector of 'reals'. The maximum amplitude,according to the previous section, is accepted in with 'a_in' from this vector as a port. The maximum amplitude reached in each section is recorded to a signal 'Am_int' and passed to the port 'a_out' after the process completes which connects to the next element in the vector. Next, a skin depth is calculated as discussed which is first compared with the thickness of the line. If it is more than half this thickness, DC resistance is assumed, else the value is compared with the previous value of skin depth. If the new value is greater then a variable is updated using linear Equation 4.1 which is plotted in Figure 4.7

$$\texttt{new\_skin\_depth\_v} = \pm 4000 ms^{-1} \times \texttt{sim\_step} + \texttt{old\_skin\_depth\_s} \qquad (4.1)$$

where 4000 ms^{-1} is a linear approximation of the speed at which an electric field initially penetrates a few microns into the thickness of copper microstrip line, obtained from Equation 4.2 [12]

$$\tau = \mu\sigma a^2 \qquad (4.2)$$

where τ is time in seconds it takes an electric field to penetrate a material with conductivity σ and thickness a. The rate at which the field penetrates the material (copper in this case) is multiplied by the amount of time passed since the process last ran, then added to or taken from the last skin depth making linear Equation 4.1. The opposite is true for a value less than the previous one. If the old and new values for skin depth are the same then the previous value is retained. The process updates the new skin depth and new resistance to signals acting as single element memory cells for the next process run. These single element memory cells are a highly efficient use of memory resources. The algorithm for the SDR is found as a flow diagram in Figure 4.4. Figure 4.5 clearly shows the skin depth and hence the resistance changing with signal in the time domain. As the signal in Figure 4.5 approaches a local maxima or minima, the skin depth increases as the rate of change has slowed somewhat allowing signal dependent effects to abate. As the signal goes through zero, and has the highest rate of change, the skin depth is seen to reduce as expected. An issue encountered was that the maximum amplitude of the signal from the previous section continued to ramp to it's largest value after the next section had begun to use it as the maximum amplitude. This is a result of the rising edge of the signal spanning multiple transmission line sections at once. This meant that each time the amplitude grew larger than its previous value, the vector of reals was updated which was 'seen' by the next section and gave erroneous values of skin depth. These erroneous values manifested as jumps in estimated skin depth and hence jumps in loss and finally, jumps or spikes in output signal. This was resolved by only accepting the previous maximum amplitude into the next section after two conditions are met. The first was if the process has started or not, which is fulfilled when the rate of change of signal increases past a defined level. The second was a boolean signal that recorded if the amplitude had already been accepted or not. If the conditions were correct, a single value of amplitude would be latched into the next section.

As further refinement to the SDR, the effect of losses in the return plane were also accounted for. An assumption that the return current of a microstrip line in the return plane would be spread over approximately six times the distance of the trace to the return plane under the trace was made as Johnson illustrates [1]. This, coupled with the skin depth equation could be manipulated into the multiplier that is seen on the end of the resistance equations in the code. The refinement is slight as there is a relatively large area for current to travel in under the trace hence little extra resistance is added.

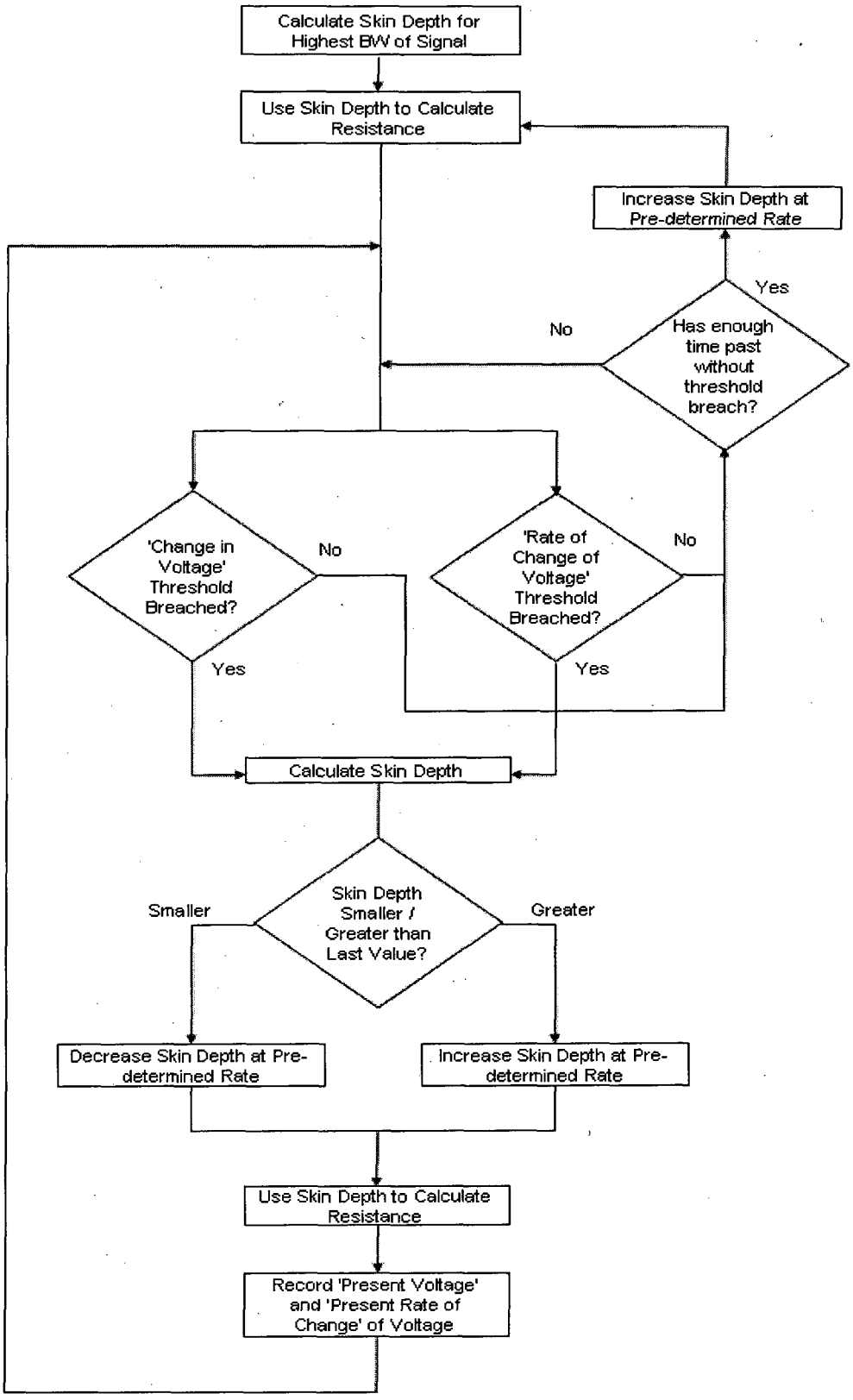

FIGURE 4.4: Simplified algorithm used in the Signal Dependent Resistor to calculate the skin depth

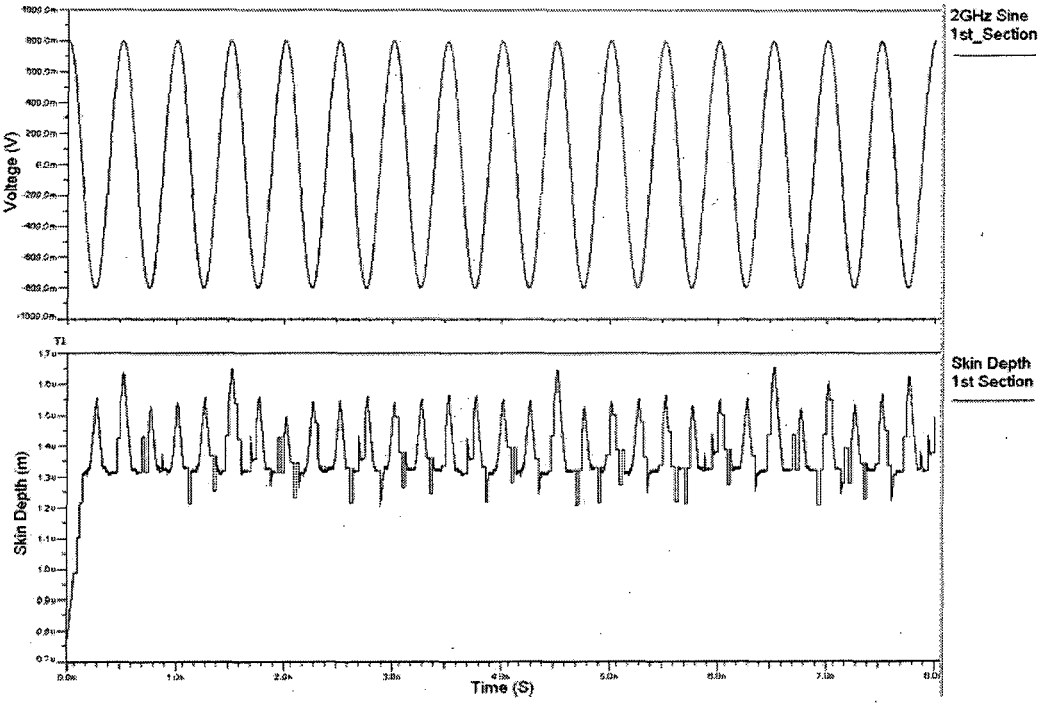

FIGURE 4.5: Skin depth in the first section of a single conductor above ground

4.2 Time domain model of a signal dependent conductance in VHDL-AMS

This model works in an analogous way to the SDR, however, there is no need to record a maximum amplitude in the section as the SDR performs this function. The Signal Dependent Conductance (SDC) just accepts in the amplitude 'a_in' as a port. The SDC is a much simpler implementation than the SDR. This is because the parameters of capacitance C, and tan(δ) from Equation 2.6 are pre-determined and are simply passed with the bandwidth and DC conductance values into the SDC. The process is triggered in exactly the same way as the SDR. Inside the process the conductance is calculated as described in Section 2.1.2 and compared with previous values. It is not compared with the thickness of the conductor as in the SDR. A VHDL-AMS 'quantity' of current to ground is used to model energy lost to the dielectric medium. The current to ground is given by Equation 4.3

$$I = \frac{V}{Con_{dc}} + Con_{ac}V \tag{4.3}$$

where Con_{dc} is the DC leakage resistance and Con_{ac} is the AC dielectric conductances respectively. V and I have their usual meaning.

4.3 Taking account of signal skew in a VHDL-AMS time domain model

As switching speeds are pushed further into the GHz region, any mismatch between either line in a pair will result in some form of signal skew. Signal skew is defined as any difference between the signals in the pair and can be caused by such things as differential driver output skew [20] and discontinuities in only one line of a pair as Braxton shows. This method is able to capture not only differences in the shape of the signals but also in the phase of the two signals. This will be useful in system level design where a pair has to be routed around corners and connectors before having 'wiglets' added to match the length of the pair again and make a connection such as in Figure 2.10.

In order to introduce a phase shift in a real manner, the sources were launched in anti-phase but the model was amended to appear to go around some corners. In doing so, the trace on the outside of the corner will travel further than the one on the inside and hence will lag behind as both signals travel at the same velocity. By lagging behind, the signals are no longer in total anti-phase and will be out by a number of degrees of their wavelength. Instead of the sum of currents in each line cancelling, there will be a residual common mode current, called so because it is common to each trace. If viewed from afar this could be seen as a single trace with a current on it equal to the average of the current on the pair. This then has the potential to radiate [10, 127] but that is beyond the scope of this model. The common mode current is calculated by using the two inductor currents in each of the coupled lines accessible in the netlist. These currents are averaged to give the common current. Two new derivatives of the generate and netlist modules had to be made. The new generate module takes in a bend radius and a bend angle in radians to calculate the length of the inner and outer curves, whereas before a section of transmission line only took in a length.

If a 90° bend is required for instance, it could be approximated by an equivalent 90° curve using the bend radius and bend angle as defined in Figure 4.6. The length the signals travel on the inner and outer bends could be easily found. It is these parameters that are passed to the generate module where the two lengths are calculated and passed to the individual components in the netlist adapted to accommodate bends. The components use the number of sections and the length of their section to find a per unit length parameter for R', L', C', Cm', G' and Lm'. A similar track layout to that in Figure 2.10 was used in the model.

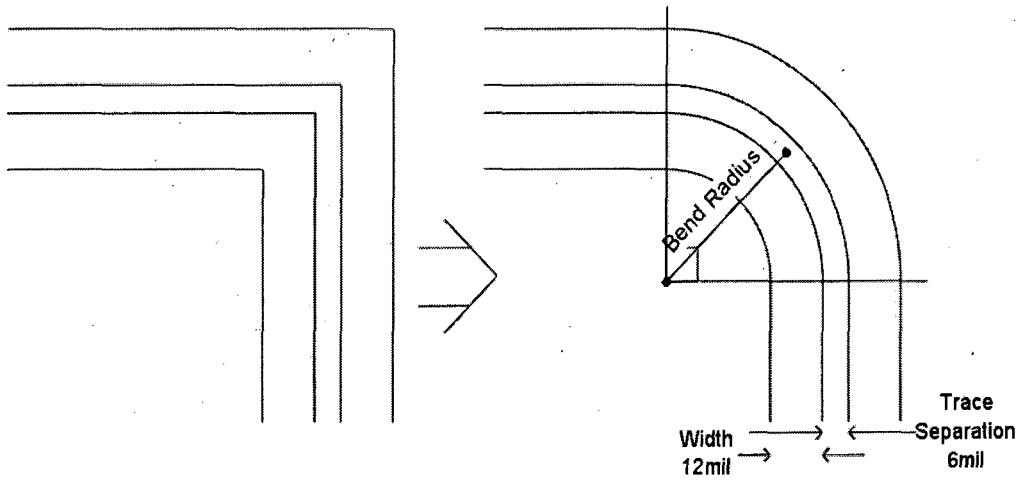

FIGURE 4.6: Equivalent curve for a 90 degree corner

The inductors were replaced by equations in the netlist where it can be clearly seen that the voltage dropped across the inductors given by the fundamental inductance equation is modified for each inductor by the inner and outer bend lengths. Code to calculate the bend lengths is given and is followed by the inductor code where the parameter names are self explanatory.

```
constant innerbendlength : real :=
                    bend_angle*(bend_rad-((0.5*trace_sep)-(0.5*width)));
constant outerbendlength : real :=
                    bend_angle*(bend_rad+((0.5*trace_sep)+(0.5*width)));

 VL1 == (ind1*(innerbendlength/(sections)))*IL1'dot;
 VL2 == (ind2*(outerbendlength/(sections)))*IL2'dot;
 i_com == (IL1+IL2)/2.0; --common current
```

4.4 Sensitivity analysis of the skin depth equation to the amplitude

It was considered prudent to perform a brief sensitivity analysis of the signal dependent skin depth equation to amplitude. This was because the amplitude is the only calculated variable that the simulator will not have available to it in the equation set and so there is

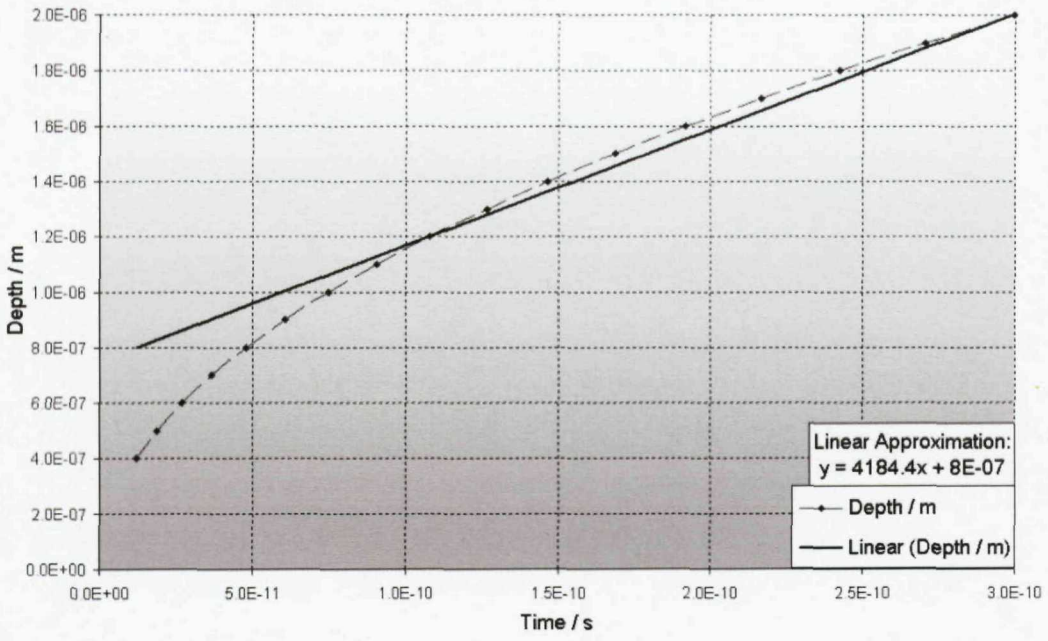

FIGURE 4.7: A linear approximation of the EM field penetration depth into copper as a function of time.

scope for error. When the algorithm and model are considered, it should be remembered that the skin depth, although calculated many times over, is only tended towards at a pre-determined rate from the previous value of skin depth. This would mean that any anomalous or spurious values that resulted from an imprecise amplitude calculation may not show in the values of skin depth when plotted over time. The skin depth was plotted in MS Excel® in the same way as in Figure 3.2 but this time the amplitude was given values of 1, 0.9, 0.8 and 0.7 when used with a signal that had a voltage swing from -1 to +1, and the resultant skin depths were plotted. The signal dependent skin depth equation was given the voltage and rate of change of voltage as well as the various amplitudes considered and graphs were plotted for frequencies of 1 to 5 GHz.

It was found that the closer the amplitude supplied was to the maximum of half the peak to peak voltage value, the closer to the 'ideal' skin depth the signal dependent equation became at that frequency. The signal dependent equation became less susceptible to variations of the amplitude as frequency was increased because the rate of change of voltage became much larger and so dominated the equation much more. The average skin depth calculated for one period of of the signal at each frequency investigated was always within 10% of the ideal skin depth. The actual values of skin depth calculated were off by almost 50% for small portions of the signal period however the skin depth was tended towards in the model so that these values did not become an issue. It was

found that slightly exaggerating the amplitude gave more accurate results as the voltage itself is not of course supposed to exceed the amplitude else the equation set becomes meaningless. The model prohibits this in the way it calculates the amplitude by taking the largest value the signal reaches in the previous section and passing it to the next, thus eliminating this risk. By taking the magnitude of $A^2 - V^2$, this also guards against the voltage exceeding the amplitude.

It was found that although the signal dependent skin depth is sensitive to the value used for amplitude, the model and algorithm are designed to mitigate this risk by tending towards values of skin depth and also in not allowing voltage to exceed amplitude.

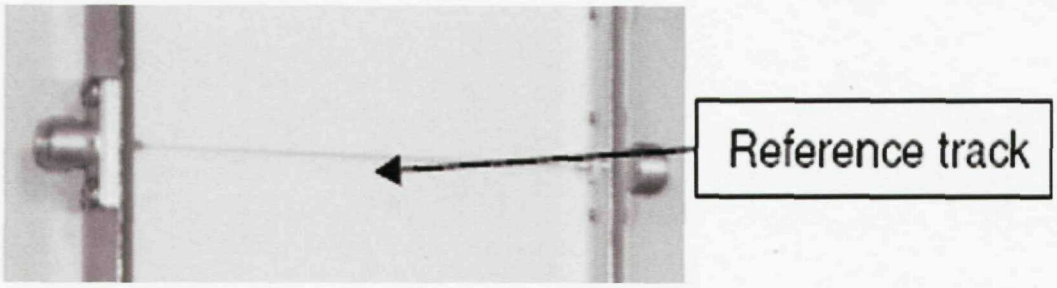

FIGURE 4.8: Photo of test board for a single microstrip with the laminate Rogers 4350.

4.5 Results and experimental validation of the time domain model taking account of signal dependent effects in planar high speed digital transmission media

The new modelling approach was used to create a model of a single microstrip line such as in Figure 4.8 with signal dependent (non-linear) dielectric conductance and resistance. This new model has been validated by comparing simulation results against experimental ones for an equivalent line that was created and measured using the Agilent N5230A PNA-L Network Analyser (VNA). The VHDL-AMS test-bench defines transmission line dimensions, material properties and all R, L, C and G values. The dielectric constant and loss tangent of the substrate were obtained from Rogers Corp. data sheets for dielectric 4350. The fastest launched rise time of the signal was used to estimate model bandwidth. Configurable VHDL-AMS sinusoidal, sigmoidal and piecewise linear (PWL) voltage supply modules were created. Sigmoidal simulation models a driver's 'S' shaped transition characteristic. The PWL results show how a sharp an defined pulse can be distorted over time. Sinusoidal simulation ascertained whether many simulations at single frequencies giving constant losses at those frequencies, gave the same results from 0.1 to 3 GHz as experimental data obtained from the Agilent N5230A PNA-L VNA. The results for the single microstrip line are shown in Figure 4.9 where curve fitting has been applied past 3 GHz to extrapolate the results out to 10 GHz. It is clear to see that this approach offers excellent agreement with the other experiment also featured in the figure up to 7 GHz where the accuracy is within 0.1 dB (approximately 5 mV or 0.5%) of the physical experiment.

Figure 4.10 shows clearly the signal dependent nature of the skin effect which gives a

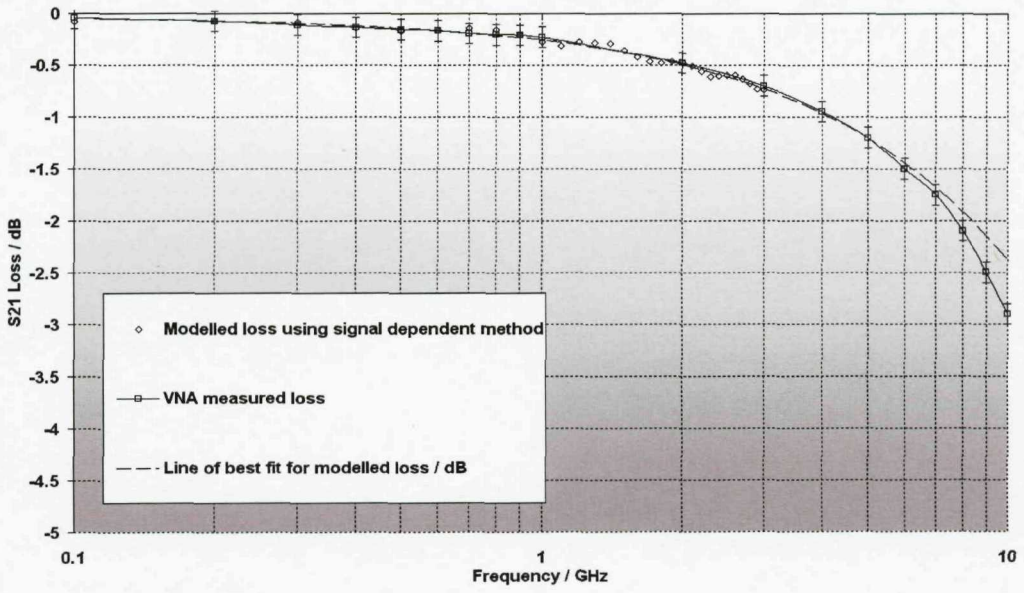

FIGURE 4.9: Losses in dB from individual simulations of single frequency sine waves from 0.1 to 10 GHz at 100 MHz intervals for a VNA measured line and for the same line modelled using the signal dependent algorithm. Line parameters: Width 22 mil, thickness 1.5 μm, dielectric thickness 10 mil, dielectric constant 3.5, loss tangent 0.004

skin depth. The skin depth increases between pulses and decreases during periods of signal change. It should be noted that due to the sigmoidal nature of the pulses, the signal is constantly changing between the rise and fall times hence the skin depth does not get vastly greater in this period. Also, it appears counter intuitive that when there are no pulses, the skin depth gets smaller, implying from statements made thus far that there is a high rate of change when there obviously is not. The skin depth becomes smaller because if there is a very small or no amplitude then there will be less electric field penetration and hence a small skin depth. No signal means no electric field.

According to Equation 2.1 for the 2 GHz sine wave that was used, the skin depth in copper should be 1.46 μm. Figure 4.5 shows that the model has calculated a skin depth that fluctuates around that depth.

Upon examining Figures 4.5 and 4.9 it was decided that the model gave excellent accuracy for the case of a single microstrip line.

Having now ascertained that the signal dependent modelling approach is accurate, the same model was adapted so that it did not use the signal dependent model but instead had a normal resistor inserted in place of the SDR and the same for the SDG. Two simulation runs were conducted, the first used just DC losses, ignoring completely the

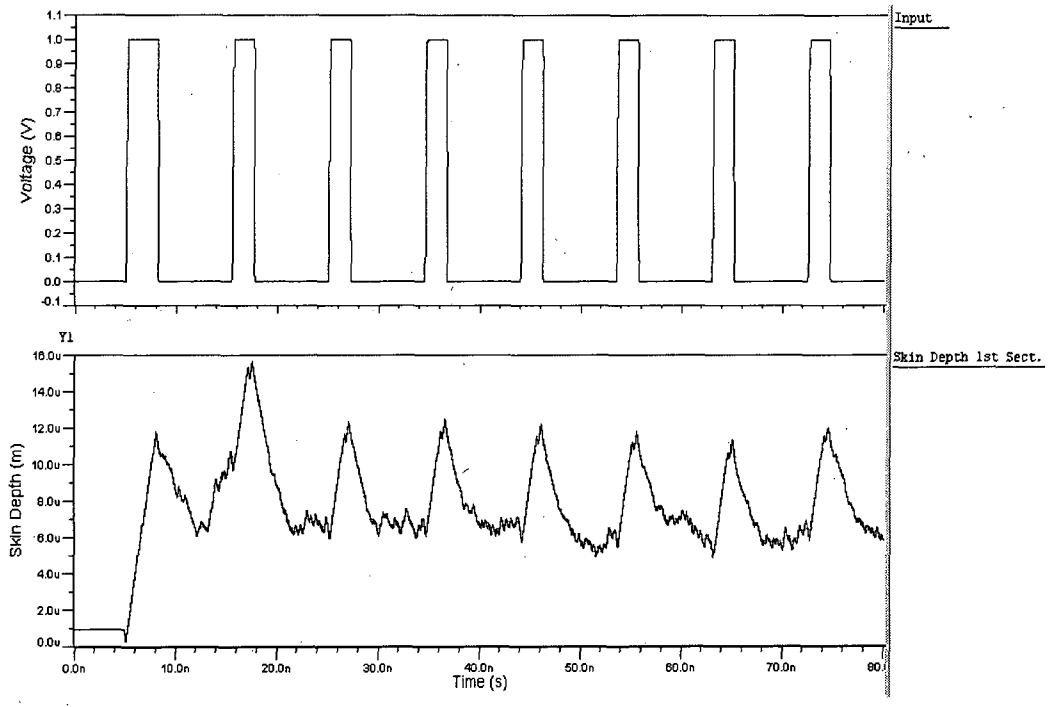

FIGURE 4.10: Pulse train showing signal dependent behaviour of skin depth

frequency / signal dependence of the losses in a transmission line. The second simulation run allocated a fixed value for losses at a frequency of 1.5 GHz to allow both the skin effect and the frequency dependence of the dielectric's absorption of the signal to be seen. Using VHDL-AMS and a hierarchical approach made this task easy as it was as simple as commenting out a line of code that referenced the SDR and SDG and replacing it with a line that referenced a normal resistor. The same losses were simulated with a sinusoidal driver from 100 MHz to 3 GHz in 100 MHz intervals. The results are in Figure 4.11. From examining Figure 4.11, and comparing it to the VNA measured or signal dependent approach in Figure 4.9, we can see that for the DC case, at all frequencies apart from the lowest ones, there is a complete under-estimate of the losses in the line. The perturbations are due to impedance mismatch between the line and the load. This shows that the simple model approach of failing to consider frequency dependent losses is inappropriate for modelling transmission lines and it also shows that the signal dependent model is far superior than using DC losses alone.

Figure 4.11 also shows losses fixed at 1.5 GHz which may occur when a model is required of a data path that will have a wider bandwidth of signals being sent along it. There will be some signals that have faster rates of change and some that have slower so an arbitrary frequency is chosen at which to allocate and fix losses. Comparing again

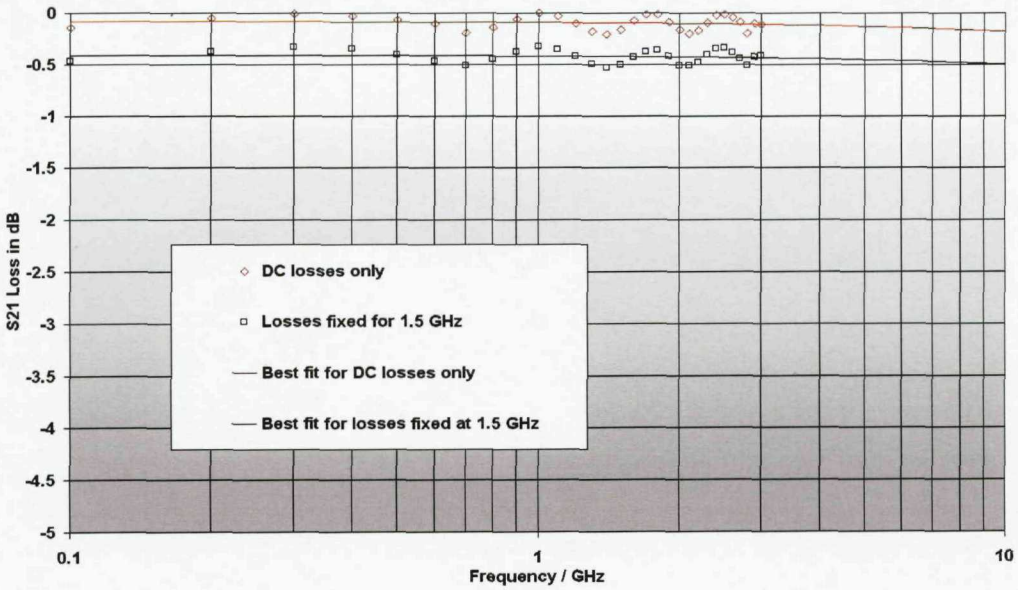

FIGURE 4.11: Loss in dB from individual simulations of single frequency sine waves from 0.1 to 10 GHz at 100 MHz intervals from just DC losses and also losses fixed at 1.5 GHz. Line parameters: Width 22 mil, thickness 1.5 μm, dielectric thickness 10 mil, dielectric constant 3.5, loss tangent 0.004

with the VNA measured results in Figure 4.9, we can see that below 1.5 GHz, there is an overestimation of loss compared to the VNA measure and the signal dependent results. At 1.5 GHz there is a very close match in losses which is very encouraging as this is the frequency where the losses from the signal dependent model and the 1.5 GHz fixed loss model should be almost identical. Past 1.5GHz, as the losses become more apparent in the measured and signal dependent models, the losses that are fixed at 1.5 GHz have more and more error apparent in them, leading to an increasingly large underestimation of loss. This shows that the signal dependent approach, when considered across a larger frequency range, is more accurate than allocating a fixed value to losses in that same range.

One further simulation run was conducted whereby at each frequency tested, the values for frequency dependent losses were calculated and the model changed to include them before each simulation. The losses for this approach are found in Figure 4.12 where it is clear that when the losses for each frequency are calculated, the signal dependent model follows them very closely indeed, further confirming that the signal dependent algorithm works and works well. The coupled model as described in Figure 4.2 was then used to simulate differential microstrip lines. Using field solver parameters for Cm and Lm meant that the accuracy could be maintained to a large degree.

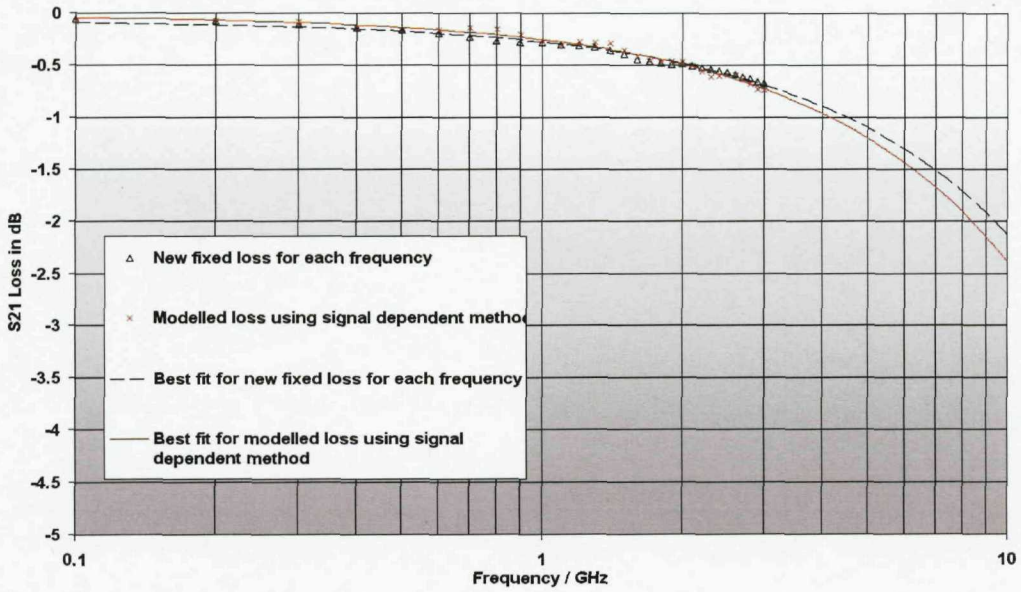

FIGURE 4.12: Loss in dB from individual simulations of single frequency sine waves from 0.1 to 10 GHz at 100 MHz intervals from using the signal dependent method and also allocating fixed frequency dependent losses for each frequency. Line parameters: Width 22 mil, thickness 1.5 μm, dielectric thickness 10 mil, dielectric constant 3.5, loss tangent 0.004

In order to drive the coupled line, two sinusoidal sources in anti-phase were used. Figure 4.13 shows the input and output signals of the pair, with the y axis in each graph from -1 to +1 V and the x axis from from 0 to 8 ns. The frequency of 2 GHz was chosen because both skin effect losses and losses through the dielectric medium are observable here.

A plot for the signal dependent dielectric conductance from the same simulation that created Figure 4.5 is found in Figure 4.14, where the line's last section is shown. It should be noticed in both the skin depth and conductance plots that the model that calculated these effects does not begin evaluating itself until the signal begins to change, or until the signal reaches that section. This is efficient and also the effects take a certain time to react to the signal, an instant value of skin depth or conductance is not given straight away, but is tended towards according to the linearisation of the time it takes for an EM field to affect the material properties.

Skew can be seen in a transmission line model of three corners with each corner having a 1 cm bend radius and 90° angle except the last which had a 180° angle. Each straight section of line was 2 cm long except the last which was 1 cm. The outer and inner line lengths were 0.134268 m and 0.133313 m in total respectively. This gave a difference

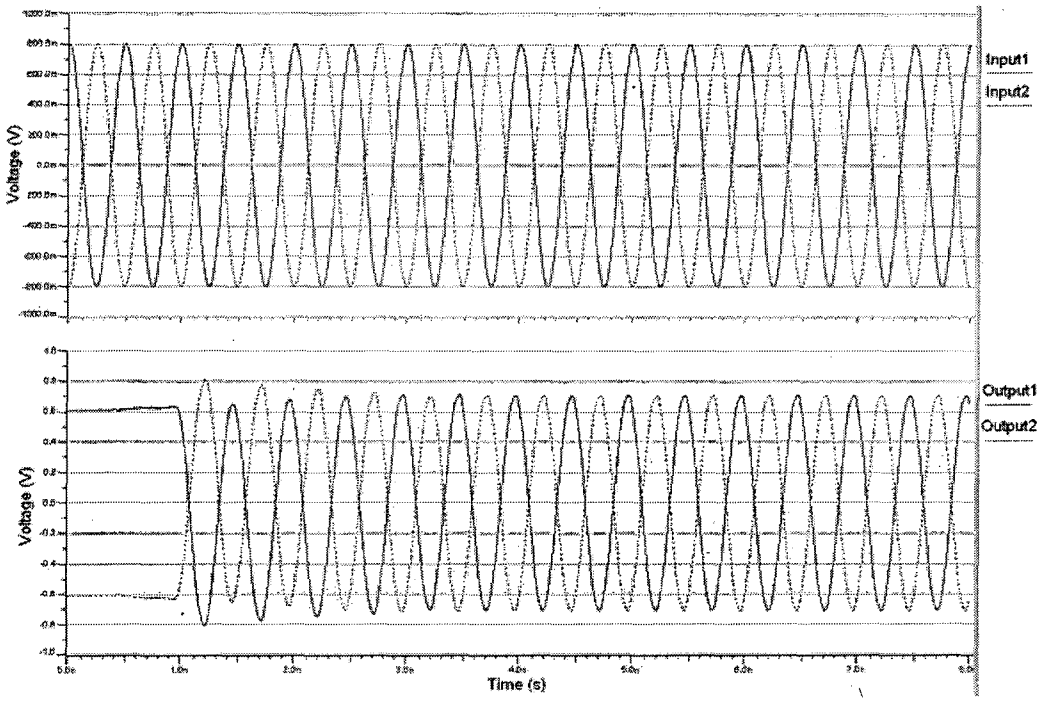

FIGURE 4.13: Sinusoidal input and output of the coupled pair of transmission lines

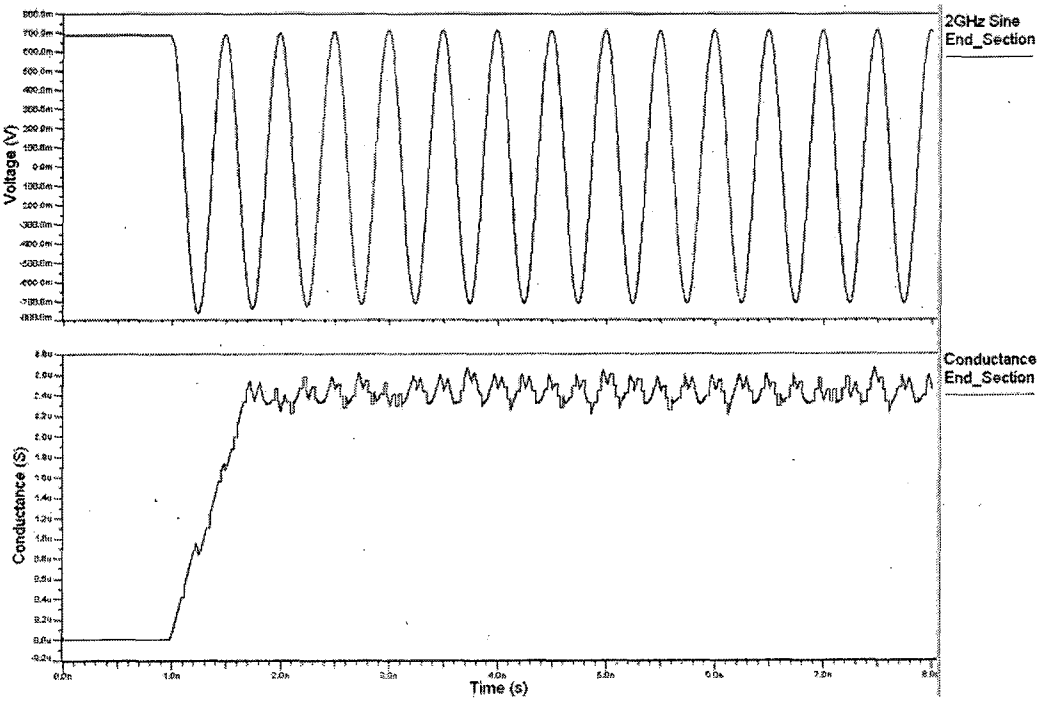

FIGURE 4.14: Dielectric conductance at both ends of a coupled line, stimulated by sinusoidal sources in antiphase

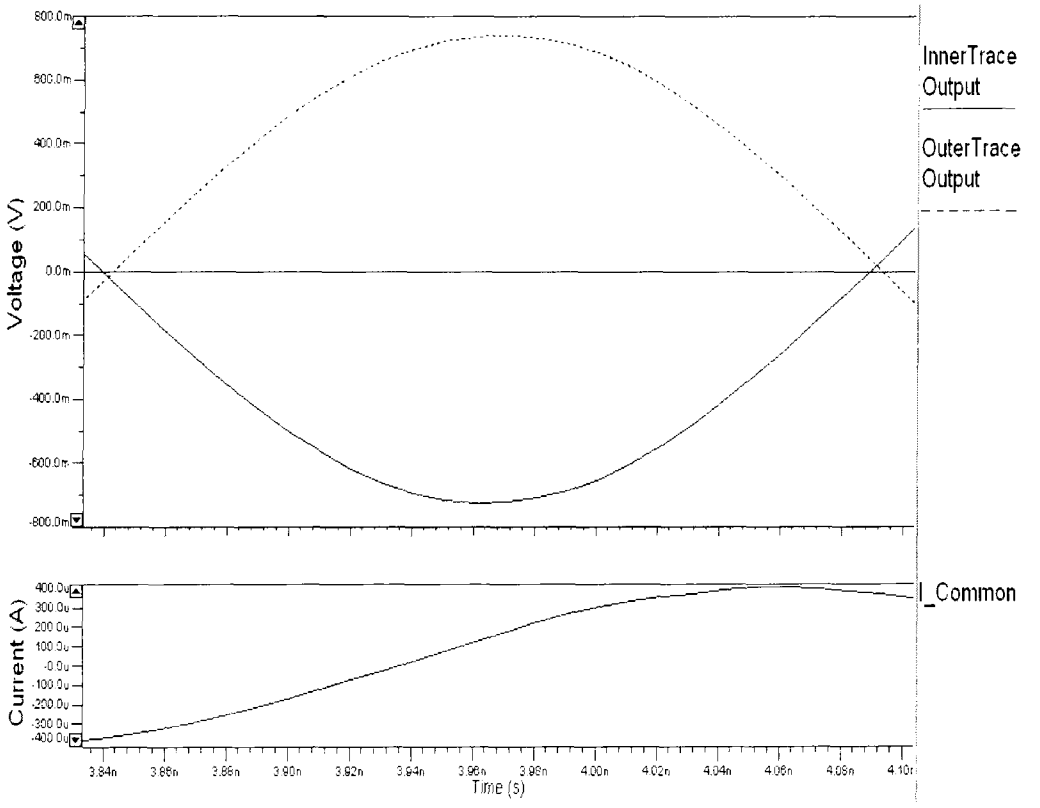

FIGURE 4.15: Part of the differential signal showing output 2 (outer bend) to be lagging output 1 (inner bend) at the zero crossing

of 0.000955 m between inner and outer traces of the pair which is a 4.3° mismatch between the traces at 2 GHz. The model reported 1.01 dB loss and 0.4 mA of common mode current by the end of the last section. The signal skew is too small to see with the whole waveform in view so Figure 4.15 shows a close up view of a single wavelength. It is seen that the signal on the inner, shorter trace, crosses the zero line before the outer, longer signal path.

4.6 Potential benefits of using a VHDL-AMS based time domain model of signal dependent effects in digital transmission media

Having now explored the novel methods for capturing signal dependent effects in the time domain using a known modelling language and tool, comments made in Section

3.3 can be re-iterated with some confidence.

The frequency is never known exactly unless there is a pure sinusoidal signal being transmitted, however, the bandwidth of the signal is nearly always available from transceiver specifications as provided by system architects. The bandwidth of the signal may be used to initialise the model and also to give appropriate timings within the model to avoid running it too many times and reducing efficiency.

Real data has no frequency and so losses will either be greater or less than assuming a fixed frequency of operation, in fact the more a signal changes, the more loss and distortion will be observed, less changes allow the signal dependent effects to abate somewhat.

It has been shown there is no need for components to have frequency dependent data attached to them with this method. We need only supply a bandwidth to the model for internal purposes.

The novel time domain method worked continuously without showing asymptotic behaviour through the use of simple modelling techniques known to help avoid such behaviour and careful coding work. These techniques involved adding 1.0 to parts of equations in the denominator that had the ability to fall to zero, thus avoiding the result going to infinity. This approach was valid as the other terms in the relevant part of the equation set were very large, and adding 1.0 would have no effect on the result of the equation. Also, the number 0.000001 was added to terms in equations where, when evaluated, could give zero causing the equation to evaluate to zero. In this case, any number greater than 0.000001 would have impacted the result as the terms that could go to zero were in themselves no greater than 1.0. Other modelling techniques used involved logging the greatest value a particular signal reached in a transmission line section in order to pass it to the next section so the next section would have a value to work with instead of calculating the maximum value itself, which would at that point be too late to do so.

Everyone from student to small electronics design house could benefit from this novel method of calculating signal dependent effects in the time domain as it appears easily portable to many circuit simulation tools, including ones available on student license. Although VHDL-AMS was used here, this method could also be used in a variety of programming languages also.

The code only ran as often as was required to maintain accuracy, thus providing an efficient algorithm.

4.7 Research truncation

At this point in the research into the implementation of a new methodology for modelling the skin effect and the losses to the dielectric medium, the sponsoring company made a business decision to close the division that the research was intended for. As with any project that has links to industry, it was always going to be a possibility that business conditions would change which could in turn affect the research the company is willing to fund or have use for. Since there was no longer a need for this successful modelling approach, all work had to be truncated at this juncture.

As a result of this truncation, there was of course work still to be done which will now be discussed.

A validation of the differential microstrip line model as opposed to just the single microstrip line case was intended. This would involve either using empirical data from an existing experiment or designing, building and measuring a new differential pair of transmission lines of similar dimensions to those already modelled.

The model was to be converted into a 'drop in' module for use any supporting mixed signal simulator that could be referenced either in code or via a graphical user interface (GUI). This would be essential for the system modelling engineer to have an easy to use model on hand that would be customisable in terms of geometry and fastest expected signal rise time.

Following integration into a mixed signal full scale system simulation, comparisons between the outputs of the simulation with zero losses and delays, a fixed loss and a delay, and our model in place of transmission lines could have been made, also with comparisons of simulation efficiency and memory resources. This could be achieved by creating a small test board with a differential pair and a single microstrip line on that turned corners and was around 6 to 10 inches between terminations to make any effects observable. A real data sequence could be been sent through the simulator and the board using the the various approaches just described. It would be hoped that our model would most closely match the real digital data that emerged from the test board.

It would have been a very important task to attempt to apply the new modelling approach to different HDLs and programming languages such as Verilog-AMS and SystemC-AMS. Also it would be interesting to attempt to create and apply the algorithm / model in some system modelling development tool's own proprietary environments and languages.

The following chapters describe the closely related area research the sponsor redirected our attention to where it was possible to use knowledge already gained in the area of transmission lines and modelling.

Chapter 5

Proposal and Analysis of New Methodologies for Skew and EMI Management in Planar Lossy High Speed Digital Transmission Media

Most modern multi-gigahertz critical electronic data paths are controlled impedance differential pairs. Differential signalling relies on two signals being largely differential, i.e. being of equal and opposite amplitude at the same time. Irregularities such as temporal skew, connectors, pads, vias and driver output anomalies in either of the lines make the differential pair unbalanced, change the impedance [18, 128] and give rise to mode conversion. Mode conversion converts the differential signal into a common signal where a portion of the signal is in phase on each trace in the pair. Common mode currents cause Electro-Magnetic Interference (EMI) problems as well as signal integrity (SI) issues. This problem has been examined experimentally and also by using Finite Difference Time Domain modelling methods as previously stated. Both approaches revealed that EM loss is related to common mode currents as generated by temporal skew (delay) between the signals in the pair. Previous research only examined the problem at 1 GHz. This research used Agilents GENESYS® simulation package with EMPOWER/ML®, their 2.5D field solver add-in, the tool is shown to be useful in EM loss analysis. New ground is broken by extending the discovered trends up to 15 GHz and it is shown that EM losses and mode conversion caused by temporal skew have the potential to be serious problems, particularly in backplanes or inter-chip busses. The common mode

component of the signal is unusable at the differential receiver and is another loss in the system. This work reveals problems where existing methods of length matching methodology, when used with higher frequencies, increase mode conversion and further degrade signal integrity. In fact it is shown that existing methodology can make the problem worse than having no length matching at all. Three different approaches using the new methodology of engineering the interconnect geometry to match the length of the pair at a specific or dominant frequency whilst keeping common mode, EM loss and signal reflections to a minimum are given. This is effectively optimising the de-skew.

5.1 Validation of the tool for analysing skew and EMI effects in high speed digital transmission media

Before the tool, Genesys® with EMPOWER/ML®, could be used to provide further evidence of skew to aid in the determination of effective skew compensation methodology, it required validating. Genesys® need not be validated here for transmission line modelling as it has been peer reviewed on several occasions [129,130,131]. EMPOWER/ML® is validated for the use of calculating EM loss by performing simulations with all physical losses removed from a real, previously physically measured and also modelled microstrip patch antenna (MPA) [23, 132].

5.1.1 Tool management of physical losses

In order to prove that when an option in the tool to 'Ignore Physical Losses' was checked, it did as it stated. It was necessary to do this in order for the next part of the validation process, explored in the next section, where the tool is validated for EM loss calculation. The theory here is that if there are no physical losses then the only loss would be due to EM losses. Six experiments were set up, Figure 5.1.1 lists them. A 50 Ω single ended microstrip line was used for test purposes. The loss tangent (or dissipation factor) of the substrate was chosen to be relatively and artificially high so the losses would be more apparent in the output of the simulation.

Figure 5.2 shows that experiments numbered 1 through 4 inclusive gave the same result. This result shows that when 'Ignore Physical Losses' is selected, in experiments 1

Number in Fig. 5.2	Physical Losses	Metal Loss	Substrate Loss Tangent
1	Ignored	Lossless	0.00
2	Ignored	Lossy	0.00
3	Ignored	Lossy	0.04
4	Included	Lossless	0.00
5	Included	Lossy	0.00
6	Included	Lossy	0.04

FIGURE 5.1: Table showing experiments conducted to explore 'Ignore Physical Losses'

through 3 inclusive, S_{21} shows no loss across the frequency range. The minor perturbations are due to reflections from line mismatch between the 50 Ω driver and how the tool calculated characteristic impedance. The experiments are self validating when experiment number 4 is considered. Here, physical losses were not ignored but the metal and substrate were made lossless by setting the resistance to zero and loss tangent to zero. Again, the result of zero losses was obtained showing that selecting 'Ignore Physical Losses' is the same as having a lossless metal and a lossless substrate, the only sources of physical loss in the system. Results 1 through 4 lie on top of each other at the top of the graph and results 5 and 6 are the next to plots in turn going down the graph.

5.1.2 Tool validation against a microstrip patch antenna

The copper MPA that was characterised experimentally is in Figure 5.3 and was taken from [23]. Manipulation of internal tool variables [133] led to Equation 5.1 which gives energy that did not leave the system through a port of a four port system and was hence, due to the elimination of physical losses, radiated:

$$1 - (S_{11}S_{11}^* + S_{21}S_{21}^* + S_{31}S_{31}^* + S_{41}S_{41}^*) \tag{5.1}$$

where stars denote conjugation. Using the first two terms of Equation 5.1 to create a plot of return loss (S_{11}), Figure 5.4 shows the physically measured MPA radiated losses from Garg [23] and also the EM losses that EMPOWER/ML® calculated. Excellent agreement between existing experimental measurements and simulation results is observed. Any discrepancies in the modelled MPA can be attributed to incomplete technical data on the modelled MPA, propagation medium losses and physical circuit losses not being fully taken into account. No alteration of or variation to the model was required in order to make the modelled graph and the experimental graph agree to a better degree. Large

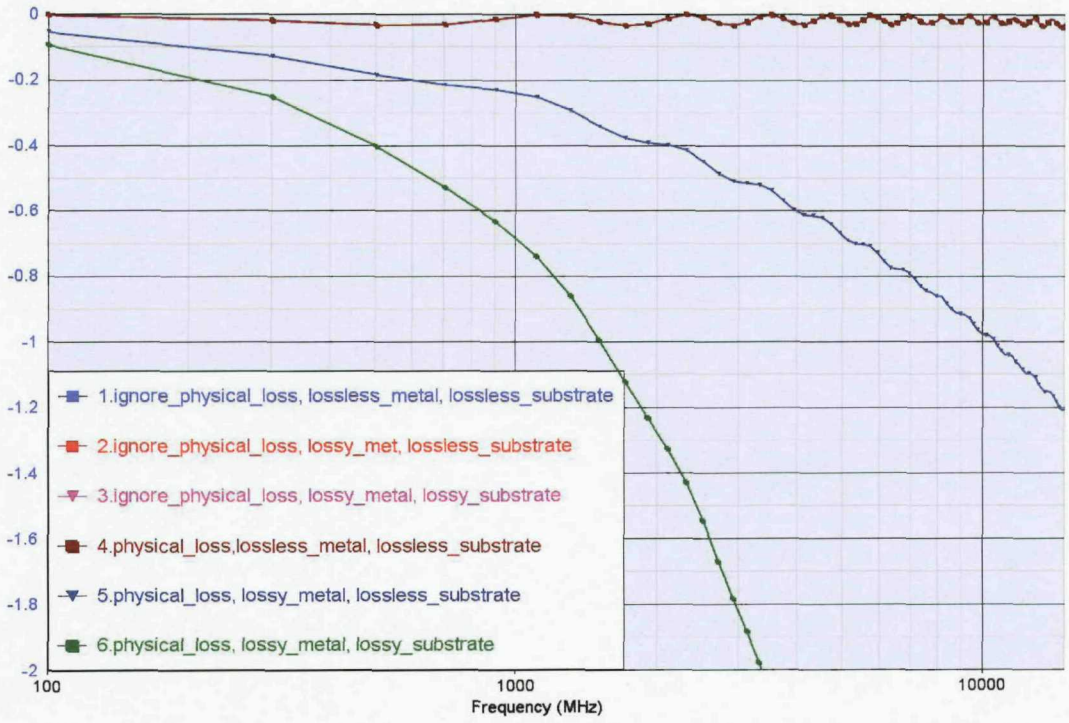

FIGURE 5.2: Amount of loss in dB whilst exploring the 'Ignore Physical Losses' function in EMPOWER/ML®. Experiments 1 to 4 inclusive are in the line at the top, experiment 5 is in the middle and experiment 6 is the line showing most loss at the bottom.

dips in S_{11} show that at the particular frequency, almost no energy was reflected back to the single launch port, and with all physical losses ignored and no other port by which to exit, the energy had to be radiated. The Genesys results in Figure 5.4 appear to have more volatility in them because the tool evaluated more frequencies between 0.1 and 15 GHz than were measured in the experiment, this providing a higher resolution of EM loss with frequency. The Genesys results are always slightly less than the experimental ones as the Genesys results do not show physical losses. These will not be very large due to the larger distance to ground through the dielectric this lowering dielectric losses and also a very wide area thus lowering skin effect losses. Figure 5.4 therefore shows that EMPOWER/ML® has been achieved an excellent match and we can place reliance on this tool for EM loss modelling.

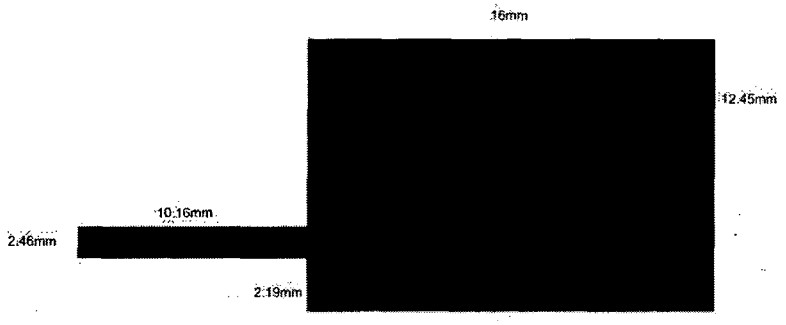

FIGURE 5.3: Microstrip patch antenna used for validation of the tool.

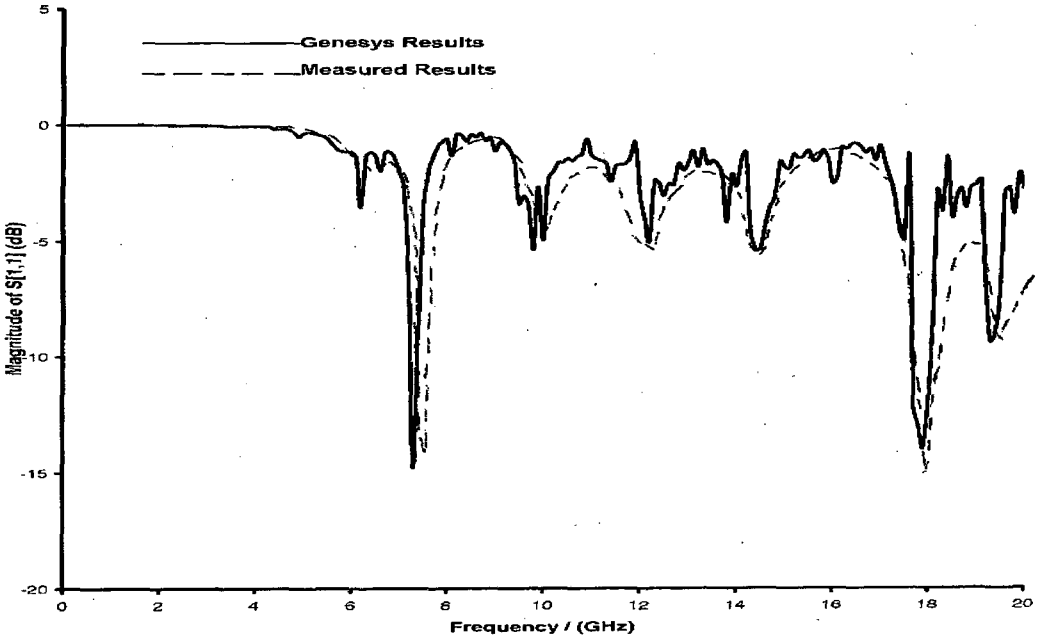

FIGURE 5.4: Tool validation showing return loss, dashed line is existing measured data and solid line is EMPOWER/ML® modelled return loss

5.1.3 Tool validation against previous skew and EMI experimental work

One of the objectives laid out in Chapter 2 was to ascertain whether trends from previous work by Knighten and Hoeft [10,21] still continue past 1 GHz. The same approach as in the previous section was applied to model skew and EM losses in a differential microstrip pair as skew was increased from 0 to 80 ps. EMPOWER/ML® was used to produce S-Parameters for a microstrip pair of the dimensions and characteristics as per Figure 5.1.3

Parameter	Value	Units
Length	3	inches
Width (t)	12	mil
Separation (s)	6	mil
Thickness (t)	0.71	mil
Dielectric height (h1)	8	mil
Dielectric constant (ε_r)	3.48	–
Odd mode impedance (Z_{0o})	49.8	Ohms
Even mode impedance (Z_{0e})	72.1	Ohms
Odd mode relative ε_r	2.411	–
Even mode relative ε_r	2.836	–

FIGURE 5.5: Parameters for the differential microstrip pair under test

It can be seen from Figure 5.1.3 that the odd and even modes experience different relative dielectric constants. The velocity a signal travels at in a given medium is governed by the relative dielectric constant according to Equation 5.2:

$$c_r = \frac{c_0}{\sqrt{\varepsilon_r}} \tag{5.2}$$

where c_r and c_0 are the speed of light in a medium and speed of light in free space respectively. Hence it is clear that even mode signals will travel more slowly than odd mode signals.

The S-Parameters were imported into a Genesys® generic four port component. A component in this case is a high level abstract construct used in Genesys® purely as a vessel in which to place data obtained elsewhere, such as experimental data or data from a previous simulation. Two ideal centre tapped transformers were used either side of the four port to generate a differential signal and to also allow termination of both even and odd modes if any were generated. The schematic for the described system is given in Figure 5.6. Genesys® was used to introduce skew into one side of the differential pair by using the delay element in Figure 5.6. Skew was increased from 0 to 80 ps and a linear frequency sweep was performed at each 10 ps interval to determine the amount of common mode signal generated. This was found by adding any signal that exited the system through the centre taps of the transformers, terminated in the common mode impedance to minimise reflections. The results are given in Figure 5.7, where the illustrative results from Figures 2.7, 2.8, 2.9 and previous works are corroborated. Increasing skew causes common mode signals to increase. From studying Figure 5.7 we can see that at 10 GHz, with around 52 ps of skew, the amount of common mode reaches a maximum and begins to decrease thereafter. This signifies the differential

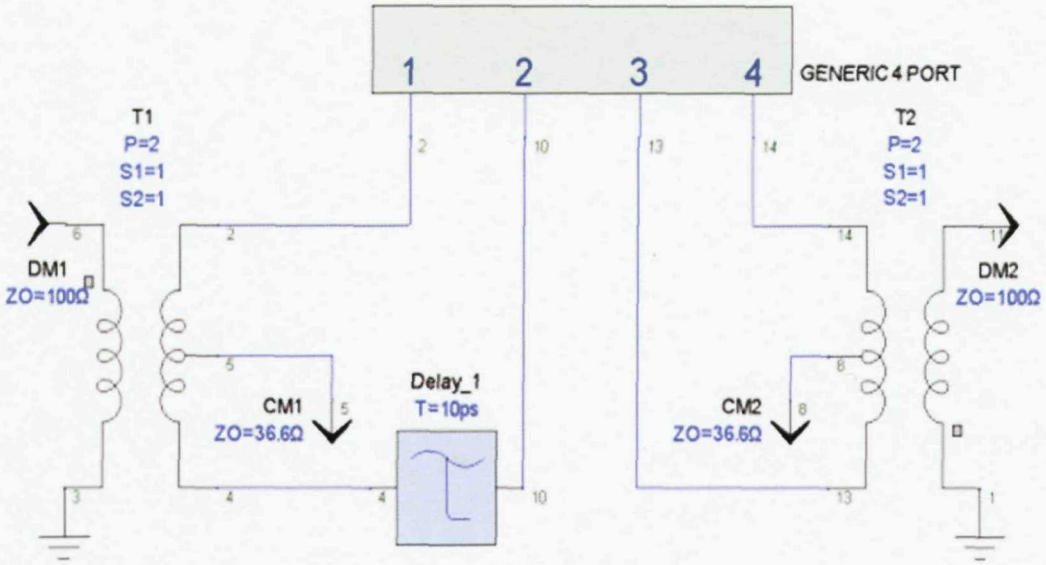

FIGURE 5.6: Genesys differential driver schematic set up showing generic four port where S-parameters are imported into.

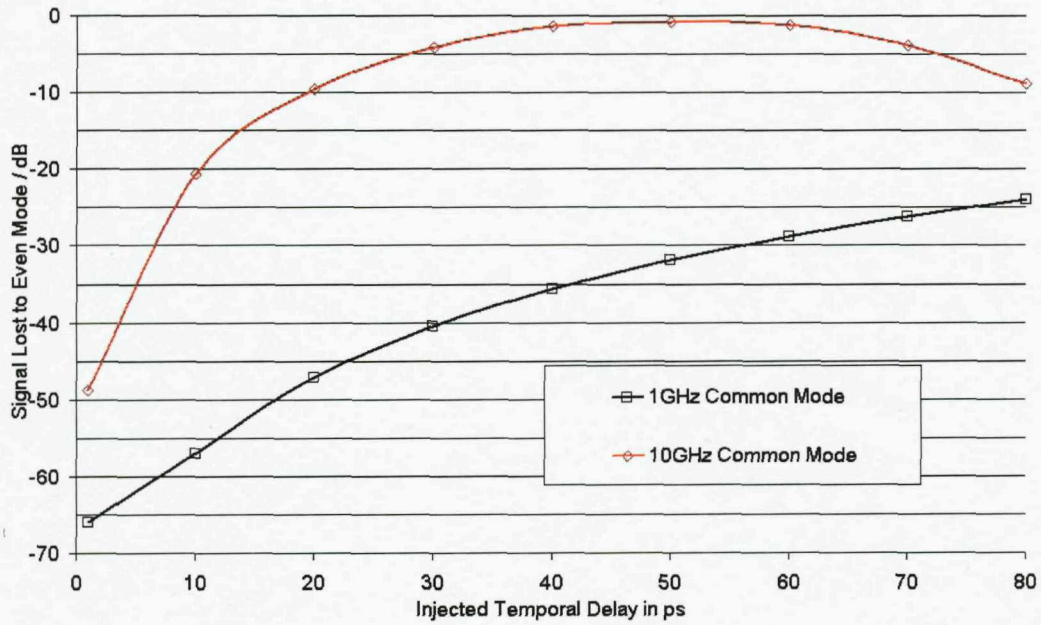

FIGURE 5.7: Skew in a differential microstrip line from 0 to 80 ps at 1 and 10 GHz to show the mode conversion increases with frequency and skew

signals have been skewed by 180° and the signal with this amount of skew is almost totally common mode. Mutual EM field cancellation will almost entirely cease and the return current will have to flow entirely through the return plane. According to the literature this should lead to increased EM losses. Previous results are confirmed

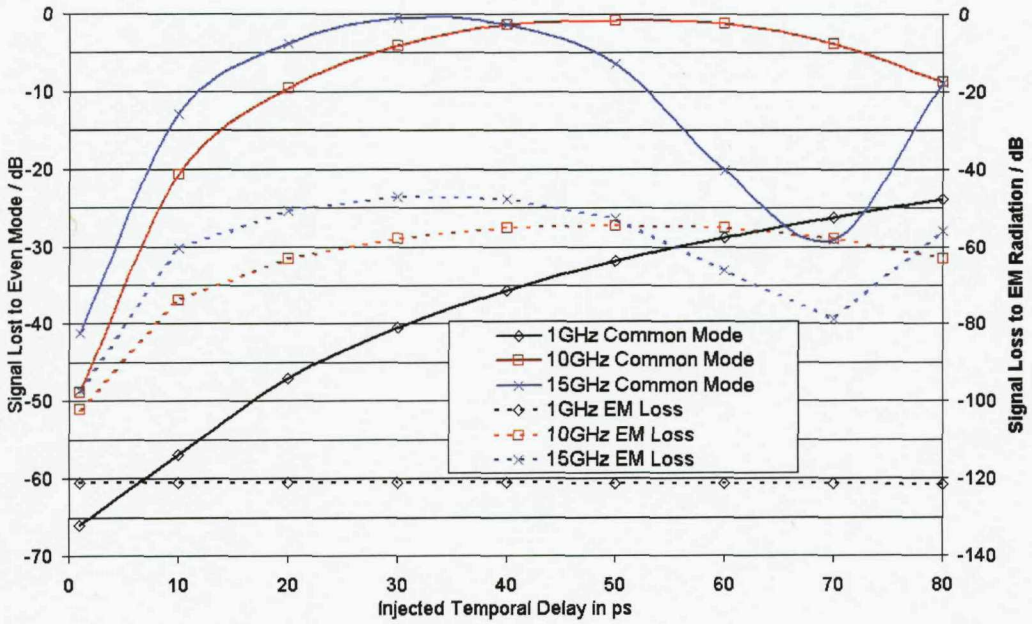

FIGURE 5.8: EM losses follow skew. There are more EM losses at higher frequencies

because as the common signal increases, causing subsequently less field cancellation, increased electro-magnetic losses are observed. Increases in frequency also increase EM losses. At 1 GHz a 2.8 times increase in the common mode portion of the signal is observed between 1 and 10 ps of skew, showing the common portion to increase at 8.94 dB/decade, agreeing with previously measured work by Knighten and Hoeft [10, 21] which measures 9 dB /decade. Knighten measured actual increases in the common current whereas here we are simulating increases in the portion of the signal that is common to both traces. These two quantities are equivalent however as we do not know the amount of current the previous work started with, we cannot say what portion of it is in the common mode and compare the results graphically. We can only compare the numbers. The previous work stated that these increases in skew were still considered to be very much less than the rise time of the signal. Figure 5.8 shows this trend does not continue with increases in frequency or skew, where the skew becomes comparable to the signal rise time. When skew nears half a wavelength, e.g. the 10 GHz case much like the IEEE specification [15], near 52 ps of skew most energy will be common to the traces and unusable at the receiver. If skew approaches a whole wavelength, such as at approximately 47 ps in the 15 GHz case where the common mode signal falls to a minimum again, the signal will be mostly differential again (in a frequency domain sense, that is) due to a 360° skew. However, the 360° delay would most likely render the digital signal unusable, depending on the application. Guidelines for tolerable amounts

of skew are generally not given, however, it was found by experimentation that, a simple 180° bend in the differential pair described produces in the region of 12 ps of skew at 10 GHz. Figure 5.8 shows this converts almost 10% of the signal to common mode at 10 GHz and 23% at 15 GHz. This will be a serious problem as losses to the common mode are generally not considered to be much of a problem currently and are not factored into loss budgets. EM losses were previously linked to common mode currents, showing one follows the other. Figure 5.8 shows this was correct at the snap-shot of frequency. However, as frequency increases further, EM loss for the equivalent temporal skews also increases proportional to somewhere between f^3 and f^4, depending on exact geometry. This agrees with existing mathematical analysis by Ramo [11]. EM losses approach half a percent of total energy in the pair under test. It is noted this is a straight differential pair with only an introduced delay and no other asymmetries to cause EM loss. Mode conversion in this case is always the greater loss.

5.2 Potential problems with existing skew compensation methodologies currently in use

From here on, a differential microstrip line identical to that described in Figure 5.1.3 of length 6000 mil (6 inches) will be used for all simulations unless otherwise stated.

Currently used methods of de-skewing a signal involve placing some form of geometry at the end of the pair of metal tracks to increase the length of one trace to match the length of the other following a length mis-matched as created by corners etc. The main problem however with this approach of de-skewing at the end near termination is not the generic 45° snaking wiglets used to match the length but the fact the even mode signal travels more slowly than the odd mode signal. This effect is fully observable in Figures 5.9 and 5.10, where experiments were carried out involving five 45° snaking wiglets being placed 100 mil, 2980 mil and 5405 mil from a skew 10 ps event on a 6000 mil differential pair. Another two experiments were also carried out where no skew and 10 ps of skew were introduced but no de-skew was provided as controls by which to analyse the de-skewed experiments. Frequencies ranged between 0.1 and 15 GHz with physical losses included. This corresponded to placing de-skew immediately after, some distance away and just before termination on the differential pair. The exact distances the wiglets were placed at were chosen at random and have no significance other than

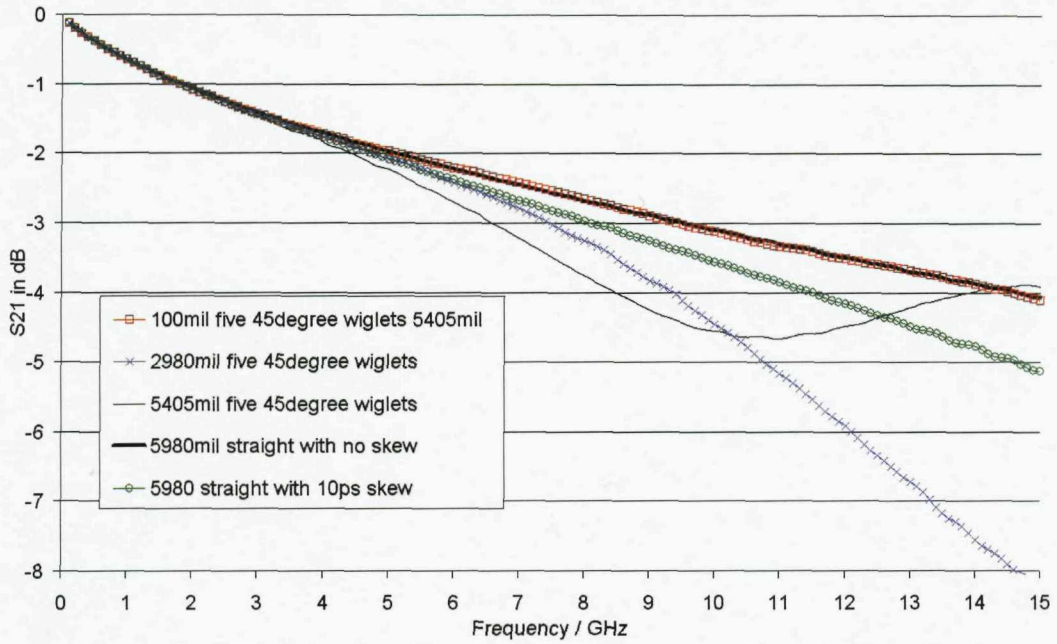

FIGURE 5.9: S_{21} loss with five 45° snaking wiglets placed 0.100", 2.980" and 5.405" from a 10 ps skew event on a 6.000" differential pair

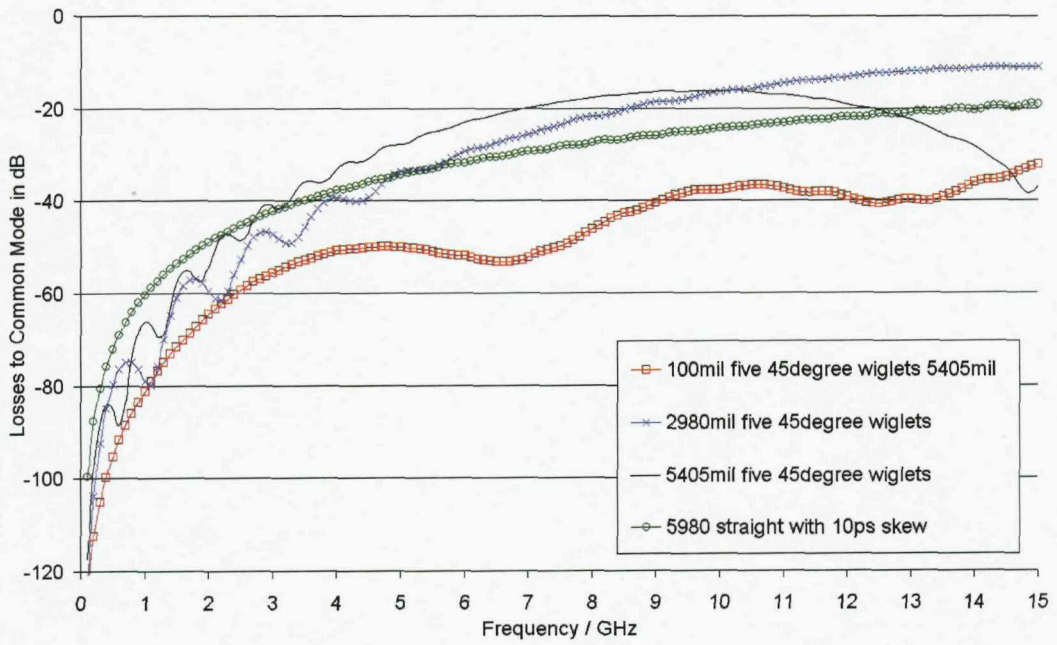

FIGURE 5.10: Losses to common mode with five 45° snaking wiglets placed 0.100", 2.980" and 5.405" from a 10 ps skew event on a 6.000" differential pair

to provide constant, repeatable results by placing wiglets in further simulations in the same place.

Figure 5.9 clearly shows that increasing the distance between the skew and de-skew geometry increases insertion loss in the pair. Below approximately 3 GHz, all approaches to de-skewing a differential pair are equally valid with similar losses. After approximately 3 GHz, the various skew compensation approaches begin to separate. The most important result of this experiment is the comparison between 10 ps of skew with no de-skew geometry and all other results. By examining these comparisons it is possible to show that at some point, using skew compensation geometry can result in more losses than not using it at all. From the data presented for the geometry in question, this point occurs when using five 45° snaking wiglets placed after 5405 mil at approximately 3 GHz. Placing the wiglets closer at 2980 mil from the skew moves this point to approximately 5.5 GHz. Placing de-skew immediately after the skew is the best approach with little difference in S_{21} loss between this approach and a straight differential pair of equal length with no skew at all present. Placing de-skew immediately after the skew is always better than not de-skewing at all according to Figure 5.9.

In considering Figure 5.10 and comparing it with Figure 5.9, the losses to the common mode rise as S_{21} falls. Common mode losses are the energies that exited the system through the centre taps of the transformers. Any signal will always be attenuated no matter what mode it is in, so any reflected common mode will be attenuated as it travels back towards the launching transformer. Rising common mode losses coinciding with rising S_{21} losses are clear indication that mode conversion is a significant loss mechanism. Mode conversion is occurring as a direct result of the difference in flight times of the two modes that are created. As de-skew geometry is moved further from the skew, the odd and even modes separate due to their differing velocities, adding considerably to losses. Immediately after the skew event, the modes begin to separate, if de-skew is placed immediately after the skew, the signals and modes in each trace are realigned, the even mode is converted back into the odd mode and nearly all of the differential signal is preserved. If however some distance is allowed to pass before de-skew geometry is effected, the even mode will trail behind the odd mode, observed as an increase in signal amplitude immediately following the main differential signal occurring at the same instant in time on both traces in the pair. This increase in the signal that is common to both traces will fall further and further behind the differential signal until ultimately it will detach from the differential signal altogether. It is somewhere approaching this point that any de-skew used will make signal integrity worse than with no de-skew at all. This is because the common mode signal will encounter the de-skew, and because it is common to both traces and approaching becoming completely distinct from the differential signal at this point, will be skewed and be split into two parts comprising

differential and common portions. These portions will be nothing to do with the original differential signal and will appear as inter-symbol interference on the pair, seriously degrading signal integrity. The original differential signal will of course also encounter the de-skew, although as the common portion of the signal is separated, the same thing will happen to what is left of the differential portion. It will be skewed by the de-skew geometry and will separate into common and differential portions. At this point there will be two common mode signals and two differential signals travelling along the differential pair. The differential receiver will reject the common portions but will still see two differential signals. Also not yet mentioned is the fact that the retardation of the common signal and the second differential signal could encroach into the next signal on the pair sent after the first. This would lead to inter-symbol interference (ISI) and close the eye diagram down, thus increasing data error rates as would the generation of any common signals or secondary differential signals. The energy from the initial signal is now being shared amongst four distinct signals. Figure 5.9 shows this effect where the plot of '5405mil five 45degree wiglets' which represents a skew of 10 ps, followed by 5.405 inches of a straight differential pair, then 10 ps of de-skew at the end, shows large losses until roughly 11 GHz where losses begin to decrease and at just over 14 GHz, the losses are less than with no skew at all. This is clear indication that the energy travelling in the even mode has fallen so far behind the odd mode that it is now overlapping considerably with the next '1' or '0' that had been sent next from the driver. This is how there is showing more energy that with no skew at all as there is energy from two 1's or 0's overlapping.

Further study of Figures 5.9 and 5.10 shows that in the worst case scenario of placing de-skew at the end of the pair at 5405 mil from the skew, losses appear to decrease, as does mode conversion to the common mode. This decrease in loss indicates the common mode has fallen more than 180° behind the differential mode, most likely making the signal unrecoverable. The tool used for analysis does not distinguish between usable energy in the modes, only how much is in each mode at one instant and frequency. If losses increase and then decrease it can only mean that one half of the signal has begun to integrate with the next signal (period) in the line, reducing mode conversion and increasing S_{21} again.

In summary from the data gathered thus far, the most important loss mechanism in a differential pair is physical loss and the second most important loss mechanism is skew compensation location. The third most important loss mechanism from the data gathered thus far would be the length or duration of the de-skew geometry. Five 45°

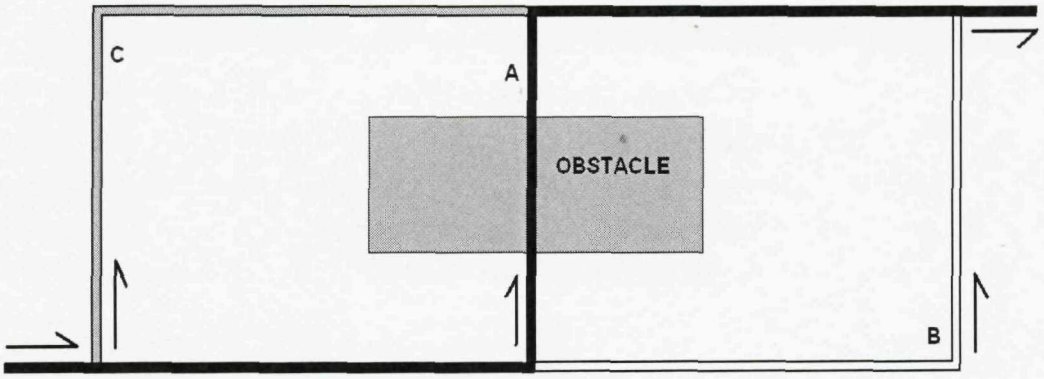

FIGURE 5.11: Various choices for routing around an obstacle such as a microstrip. All paths travel from (0,0) to (4,1), units in inches

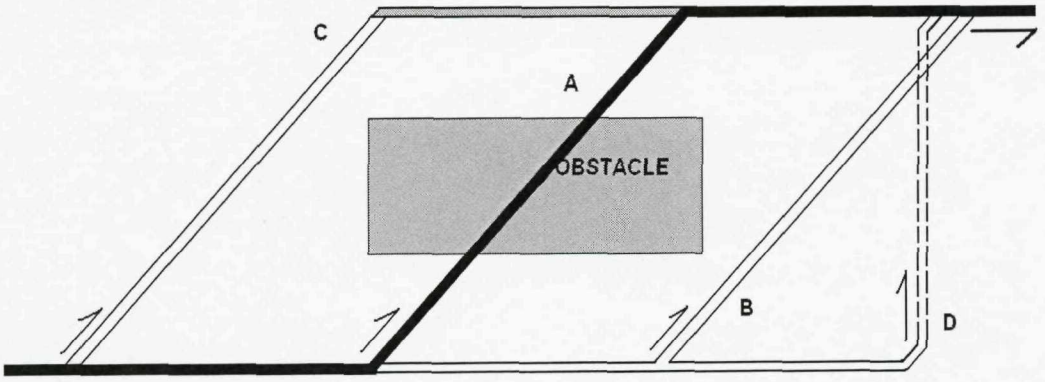

FIGURE 5.12: Various choices for routing around an obstacle such as a microstrip. All paths travel from (0,0) to (4,1), units in inches

wiglets only de-skew approximately 2 ps per wiglet, this means that skew exists for a longer distance on the pair with this distance dependent on pair geometry, giving the modes more chance to separate and less chance of fully recovering the signal.

And so it is seen that existing skew compensation methodology, if used incorrectly, can harm signal integrity more than it can help it. A new methodology requires investigating. A practical example follows illustrating these points.

5.2.1 Practical example: Routing around a PCB obstruction

Using this result in the real example of having to route a differential pair around an obstacle such as a microchip, it is possible to find the path of least loss that preserves

signal integrity the best. Figures 5.11 and 5.12 show the problem and possible routing paths. Placed into a cartesian context, the pair must travel from (0,0) to (4,1) where the units are inches in this case. The figures respectively show routing paths using 90° bends and 45° bends. Considering the 90° bend case, all paths are of equal length. It is only where the bends are placed that differs. Path A would travel through the obstacle, path B would travel as far as possible before having to turn and path C makes the turn as soon as possible. In Figure 5.12, the same paths exist however there is an extra route. This route involves making two 45° turns to take the route North instead of at a 45° angle. Two more 45° turns are made to take the route back East and make the connection. The paths A through C inclusive in Figure 5.11 correspond to A through C in Figure 5.13 which is the results for the 90° bend example. Paths A through D in Figure 5.12 correspond to A through D in Figure 5.14 which contains the 45° bend examples.

Studying the results in Figures 5.13 and 5.14, because physical losses are almost identical for all routes in each case due to the line lengths all being equal and physical loss being the primary loss mechanism, the plots lie almost on top of each other and are indistinguishable. It is clear that the shortest routes, using the 45° corners give least loss. For this reason, the same line styles have been used in the graphs. Physical losses are on the left axes of the graphs and common mode losses are on the right axes. The amount of energy converted to the common mode in each graph shows the effects of skew and mode separation are confirmed as second order effects that increase with frequency. By very close inspection of the data that was used to create the graph, the path providing least common mode loss is the path that makes the first turn as late as possible which agrees with results previously obtained, the effect is very small. This is primarily because the amount of skew introduced is small, only of the order of 2 ps and also, there is in paths B, C and D in both examples, only 1inch before the de-skew. Using 45° bends provides the shortest route around the obstacle. Considering the 'cut' corners in Figure 5.12, although these provide the shortest route, the additional corners provide additional sites for reflection to occur and also for mode conversion to take place, this is shown in the results by there being most loss and increased losses to the common mode also. It would be prudent from studying this example that, when an obstacle has to be routed around, the highest priority is to take the shortest route. After this, any bends in the pair should be left as late as possible to avoid unnecessary mode separation and subsequent loss of SI.

We can say from results obtained so far in this chapter that, the farthest point at which

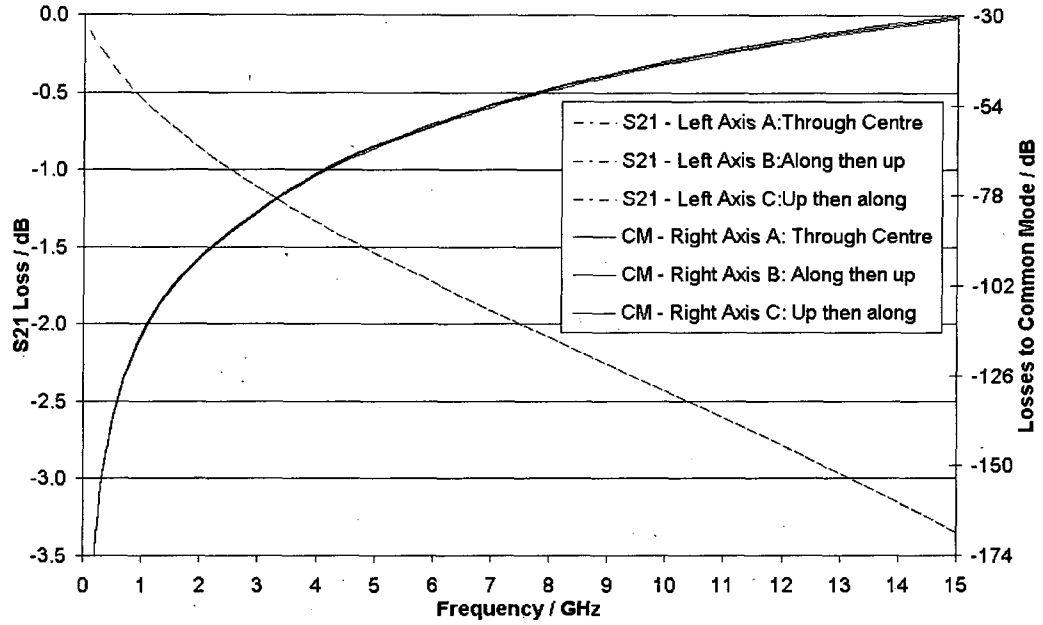

FIGURE 5.13: S_{21} losses and losses to the common mode in dB using 90° bends to route paths from (0,0) to (4,1)

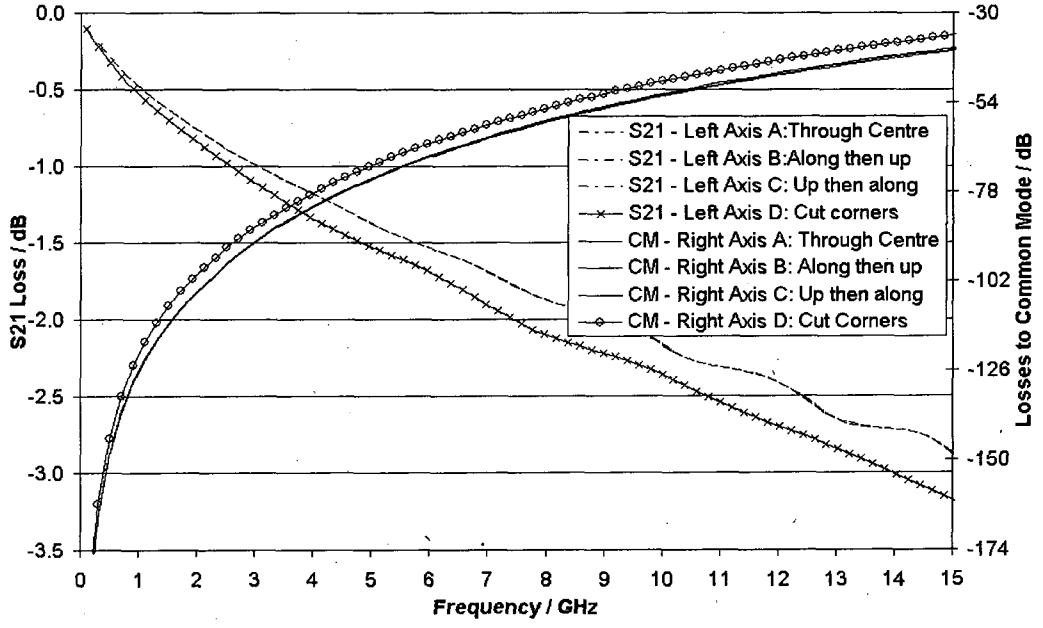

FIGURE 5.14: S_{21} losses and losses to the common mode in dB using 45° bends to route paths from (0,0) to (4,1)

a signal can be de-skewed depends on geometry, amount of skew and frequency. If de-skew is placed after this point, then the de-skew geometry will add to signal integrity issues.

5.3 Effective new methodologies for skew compensation in high speed planar digital transmission media

From the previous section, it is evident that placing de-skew as close as possible to skew events reduces loss through the preservation of signal integrity. As frequencies increase, this better practice will become a necessity, but exactly how that is achieved is still as yet unclear. As previously stated, matching length does not necessarily mean that two signals forming a differential or common signal will arrive concurrently or within a given tolerance. To this end, and also with the aim of preserving signal integrity and hence reducing losses further, different wiglet (skew compensation) geometries will be examined. It is hoped to ascertain which wiglet geometries provide the smallest reflections (lowest S_{11} measurement) and give the best amount of de-skew at the required frequency. The tolerance adopted will be ± 0.5 ps at 10 GHz from the desired amount of skew because 1 ps is 1% of the period at 10 GHz, so is an acceptably small error from the desired amount of de-skew. 10 GHz was chosen because many of the skew effects such as mode separation are most prevalent and observable at this frequency, also this frequency is now an industry standard [15]. The aim will be to match the propagation time in each trace in a pair by negating the skew caused almost exactly at the main frequency of interest instead of matching the length of the whole pair.

5.3.1 Engineering single skew compensation wiglets to improve signal integrity in coupled planar transmission media

Figure 5.15 shows the parameters of the wiglets which will be changed in order to minimise S_{11} and attempt to produce an exact amount of de-skew at a given frequency. The height gives the distance from the top edge of the trace to the top edge of the wiglet. The pitch gives the wiglet's internal width between its two inner sides, measured from edge to edge. The separation, used in subsequent sections is measured from the right side of one wiglet to the left side of the next. As well as the parameters in Figure 5.15, the type of corners in the wiglets were investigated. Wiglet types investigated are the 90° bends in Figure 5.15, the optimally mitered bend [134] and also curved corners where the curve radius was changed. Increasing curve radius softens and elongates the corner, taking longer to turn a corner. The latter two are found in Figure 5.16. The first aim was to examine all wiglet types and find single wiglets that presented a delay of 10 ps each at lowest S_{11}. The best candidates from many tested by varying the parameters

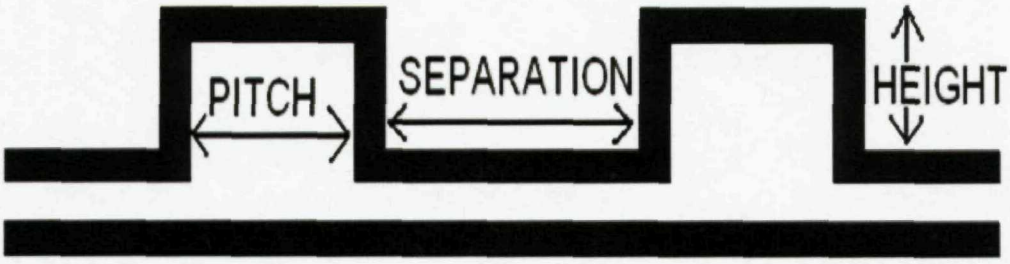

FIGURE 5.15: Wiglets showing dimensions to be varied

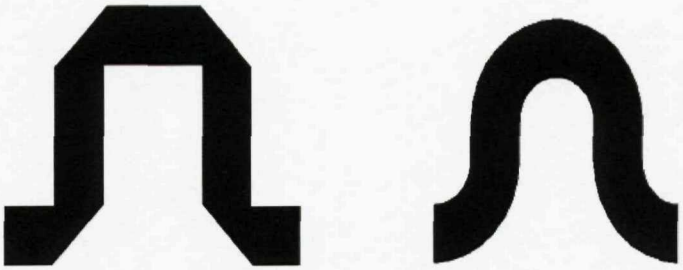

FIGURE 5.16: Optimally mitered wiglets and curved wiglets

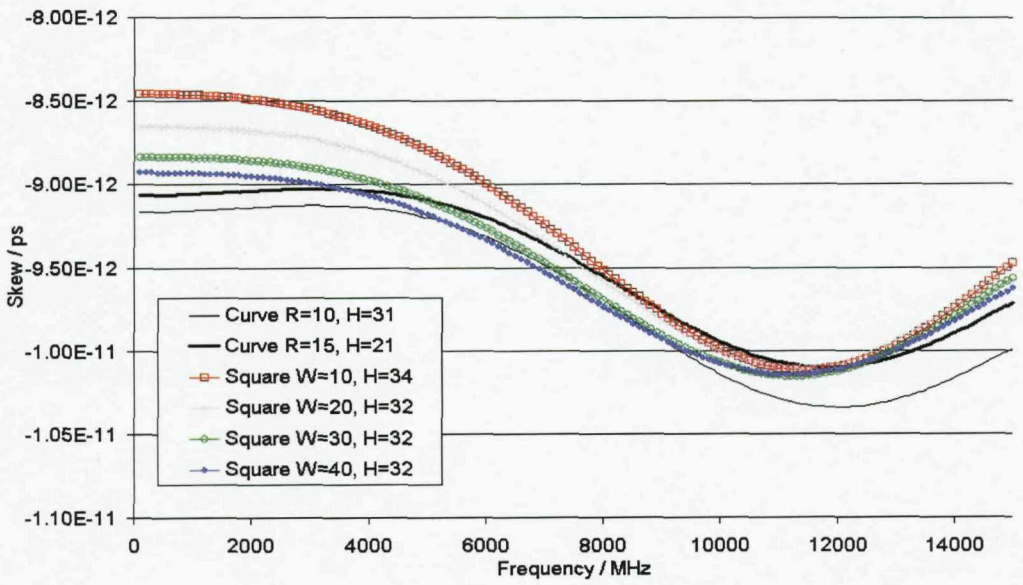

FIGURE 5.17: Single wiglets giving closest to 10 ps of skew at 10 GHz. R:Radius, W:Width, H:Height. Units in mils.

descried, are found in Figures 5.17 and 5.18. As designed, with EMPOWER/ML®, the skew is 10 ps at 10 GHz. Analysis of the best candidates for skew compensation wiglets to give 10 ps of skew at 10 GHz led to Figure 5.18. It should be noted the

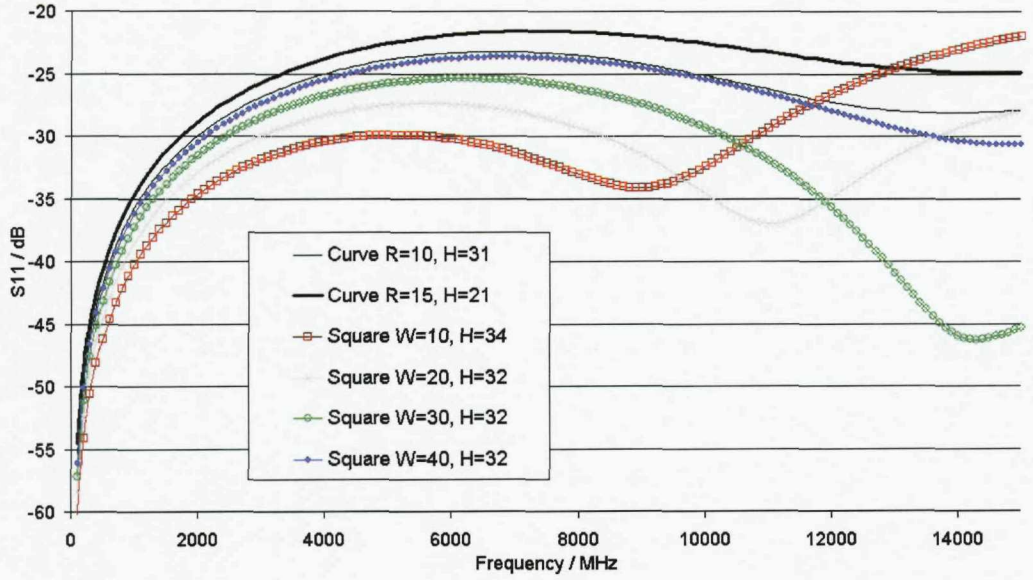

FIGURE 5.18: S_{11} for single wiglets giving closest to 10 ps of skew. R:Radius, W:Width, H:Height. Units in mils.

absence of more curved and optimally mitered wiglets from Figure 5.18. It was found that for wiglets giving a skew of 5 ps, these wiglet types were indeed comparable and in some cases gave better S_{11} performance than those in Figure 5.18. However, for skews above 5 ps, these wiglet types (curved and optimally mitered) gave significantly worse S_{11}. So much so that any benefit of using them would have been vastly outweighed by the amount of reflection they caused. The optimally mitered wiglet dimensions and their S_{11} profiles with frequency that gave 10 ps of skew at 10 GHz are found in Figure 5.19whilst the curved wiglet dimensions and their S_{11} profiles with frequency that gave 10 ps of skew at 10GHz are found in Figure 5.20.

It is now possible to select the wiglet that gives the best reflection performance. From studying previous Figures 5.7, 5.9, 5.13, 5.10 and 5.14 it became apparent that below 3 GHz and in pairs up to 6" in length, it did not particularly matter when or how de-skew was accomplished. The period of the signal was not small enough to be affected by, from results of experiments carried out, up to 10 ps of skew.

After 3 GHz, the signal period is small enough that skew begins to noticeably interfere with signal integrity and loss. The 0.1 to 15 GHz range was divided into three sections according to trends that appeared in the results. These three sections were 0.1 to 6.9 GHz, 7 to 9.9 GHz and 10 to 15 GHz. The centre frequency of each range was chosen as the frequency at which to engineer a single de-skew wiglet to provide the desired

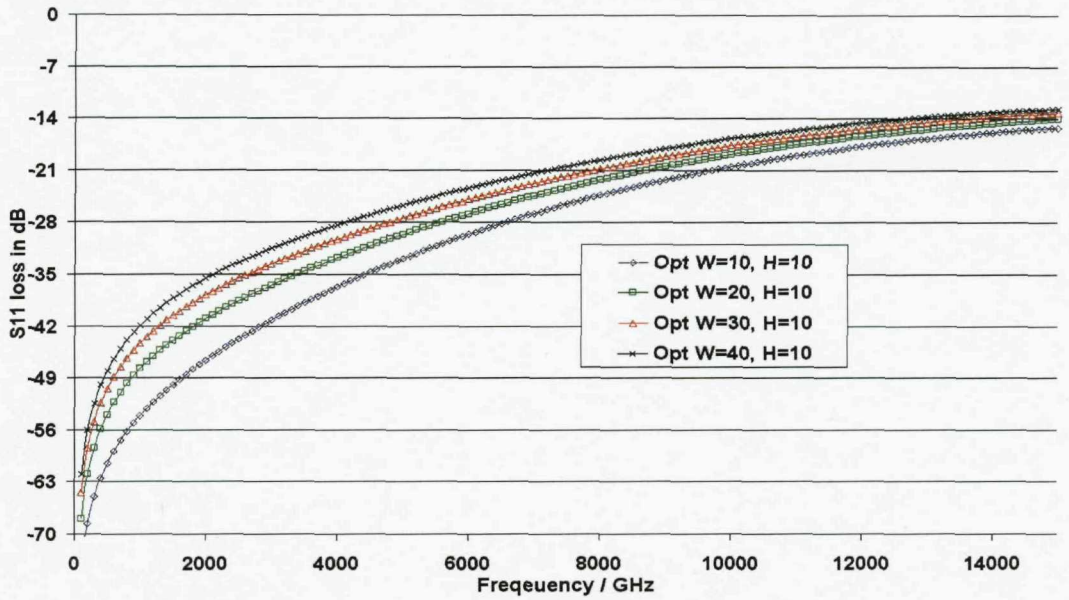

FIGURE 5.19: S_{11} for single optimally mitered wiglets giving closest to 10 ps of skew. W:Width, H:Height. Units in mils.

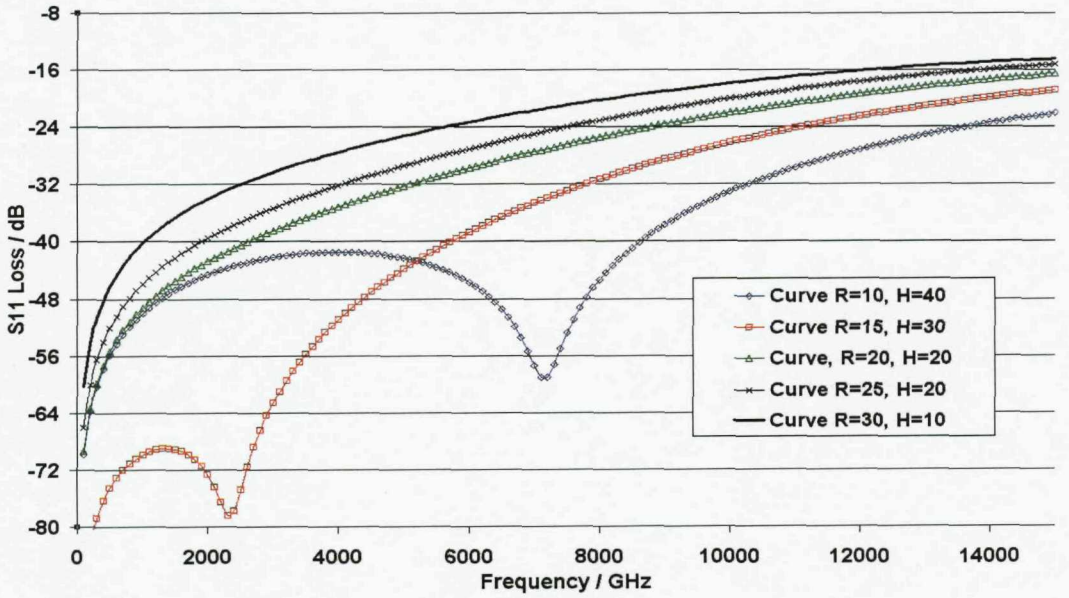

FIGURE 5.20: S_{11} for single curved wiglets giving closest to 10 ps of skew. R: Radius of curve, H:Height. Units in mils.

de-skew. In the 0.1 to 9.9 GHz frequency range, a square wiglet of width 10 mil and height 34 mil gives lowest S_{11}. The lowest amount of reflection is -60.0 dB and the highest is -31.0 dB in that range. In the 10 to 15 GHz range a square wiglet of width 30 mil and height 32 mil is best. The amount of reflection ranges between -46.3 and -29.3

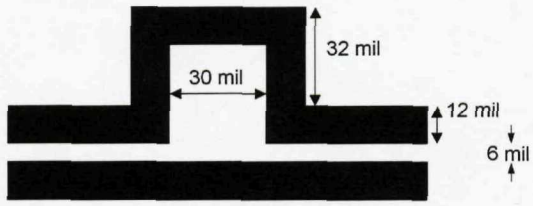

FIGURE 5.21: Scale drawing with same aspect ratio of the ideal wiglet that gives minimum S_{11} and closest to 10 ps of de-skew in the 10 to 15 GHz bracket

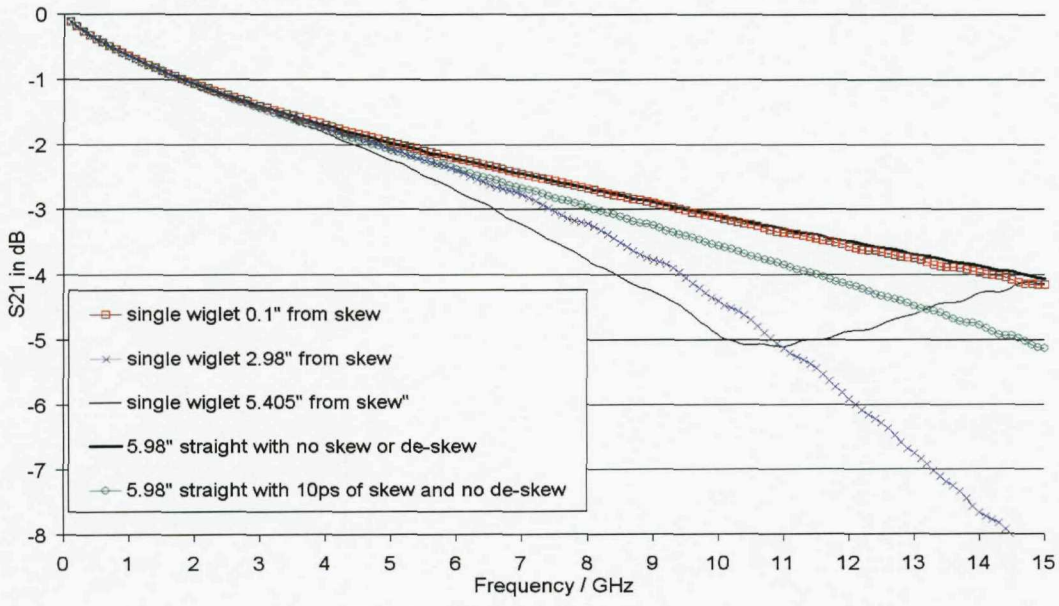

FIGURE 5.22: S_{21} loss with a single wiglet placed 0.100", 2.980" and 5.405" from a 10 ps skew event

dB. A scale drawing of the ideal wiglet for this frequency range is found in Figure 5.21, the aspect ratio has been maintained. All other wiglets although providing the correct skew compensation provided much higher reflections (impedance discontinuities).

These 'best 10ps wiglets' were placed 0.100", 2.980" and 5.405" after 10 ps of skew on 6.000" of differential microstrip line. The same experiment set up was used as in Figure 5.6. The amount of common signal was measured by summing the energy that left the system by the common mode impedance terminated centre taps of the transformers. Results are in Figure 5.22.

Close examination of Figures 5.9, 5.10, 5.22 and 5.23 shows great similarity in shape of curve as well as S_{21} and losses to the common mode. This is because as previously stated, the primary loss mechanism is physical loss, hence placing the de-skew at exactly the same places and using the same length of line in each experiment means the physical

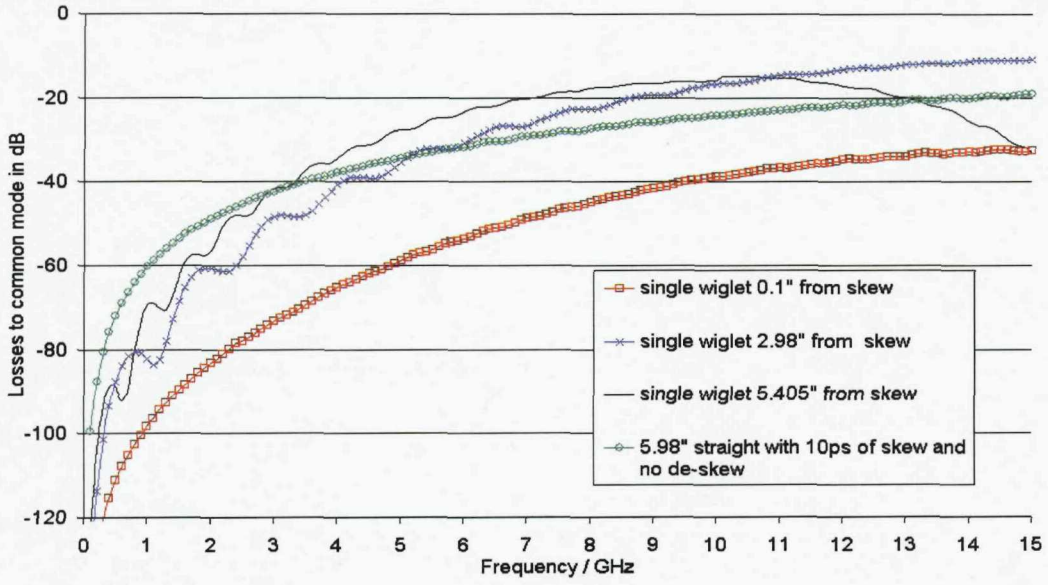

FIGURE 5.23: Losses to common mode with a single wiglet placed 0.100", 2.980" and 5.405" from a 10 ps skew event

losses will be the same and dominate all other loss mechanisms. This further adds weight to the argument for placing de-skew as close as possible to the skew.

It is still possible however to make some statements comparing single 'engineered' wiglets specific to a frequency grouping with the generic 45° wiglets as shown in Figure 2.6 as applied for all frequencies.

Using a single engineered wiglet in the 10 to 15 GHz range at any position after the skew, results in slightly more loss than multiple 45° wiglets. However, in the single wiglet case, because it has been engineered to have exactly the correct amount of de-skew, it only begins to become worse than not de-skewing at all at approximately 6 GHz. The five 45° wiglets become worse than not de-skewing at all around 5.5 GHz. Also evident is the fact that no matter what sort of de-skew is used, as long as it is placed immediately after the skew, very little deviation from the plot of a straight pair with no skew at all is seen.

Considering the mode conversion losses, i.e. the energy that was converted from the differential mode to the common mode, the single wiglet generally shows a slight decrease in the amount of common mode losses across the frequency range. This is because there is only one wiglet and a very short distance for the signal to experience a discontinuity and approaching half an inch less over which the modes can separate. Using five

wiglets presents five opportunities for the signal to 'see' an impedance discontinuity and experience mode conversion or reflection.

As the de-skew is moved further away, and the modes separate, the de-skew becomes less and less effective which is why the common mode losses for both cases are very similar for de-skew placed at a distance from the skew. The impact de-skew has on the skewed signal will be far less observable.

From the above analysis it can be said again that the closer to the skew the de-skew is placed the more effective it is. Engineering a single wiglet to have a specific de-skew time at a specific frequency in place of several generic wiglets has its advantages but these are only slightly better than the generic equivalent. Below 3 GHz, de-skew can be placed up to 5.405" from the skew using the 45° or a single engineered wiglet without making signal integrity worse than not using de-skew at all. After certain distances, depending on frequency, placing de-skew geometry makes SI worse than not placing it at all.

5.3.2 Engineering multiple skew compensation wiglets to improve signal integrity in high speed coupled planar transmission media

Having investigated using a single engineered wiglet to minimise S_{11}, S_{21} and common mode losses, the use of multiple engineered wiglets was to be investigated. Using a single tall wiglet to provide 10 ps of de-skew gives the signal the opportunity to 'see' itself on the other side of the wiglet. In a tall wiglet which provides all the de-skew in one small space, the distance around the wiglet approaches and indeed may exceed half a wavelength. This presents a voltage gradient across the wiglet and the far side of the wiglet experiences the rising and falling voltages of the near side through the electric field much like a capacitor. This results in cross talk as the signal couples across the wiglet. This will degrade SI by increasing mode conversion. The problem becomes worse at higher frequencies. A way round this is to either increase the pitch of the wiglet, meaning the field between the wiglet sides will be weaker and hence less cross talk will result. Also, if the height of the wiglet is reduced, the path around the wiglet becomes shorter and at the frequencies under investigation, half a wavelength will not fit inside a wiglet. This means that one side of the wiglet will experience nearly the same signal as the other side and less cross talk will result. Again, disadvantages of this

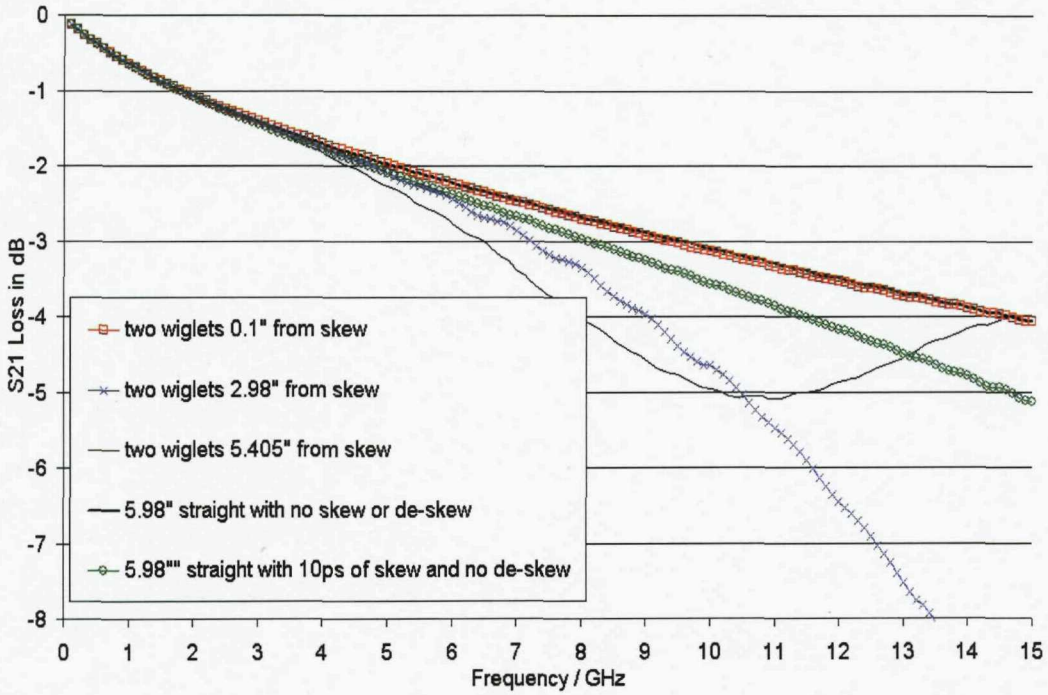

FIGURE 5.24: S_{21} losses for two wiglets placed 0.100", 2.980" and 5.405" from a 10 ps skew event. Also shown are differential pairs of equal length with no skew as well as a pair with skew but no de-skew

approach would be the fact it takes longer to de-skew so mode separation will occur for longer. Using multiple wiglets also means there are more sites for discontinuities to affect the signal. The best single wiglets were again taken and reduced in height to provide 10 ps of skew across two and three wiglets in a chain. The wiglets were separated each by 26 mil as a trade off between de-skewing in a short a space as possible and avoiding cross talk between wiglets. Figures 5.24 and 5.25 show S_{21} and common mode losses for two wiglets whereas Figures 5.26 and 5.27 show losses for three wiglets.

Figures 5.22, 5.24 and 5.26 show S_{21} losses for one, two and three engineered wiglets placed 0.100", 2.980" and 5.405" from a 10ps skew event. Close examination reveals the longer the de-skew geometry is left and the greater the number of wiglets used to create the de-skew geometry, the more loss is observed. This agrees with previous statements and confirms that the more sites or opportunities for mode conversion there are, the higher the losses associated with mode conversion will be. However, if multiple de-skew wiglets are used immediately, 0.100" from the skew in this case, less losses are observed. This means that to reap the benefits of multiple wiglets, they must be used in very close proximity to the skew. At higher frequencies, in the 10 to 15 GHz bracket,

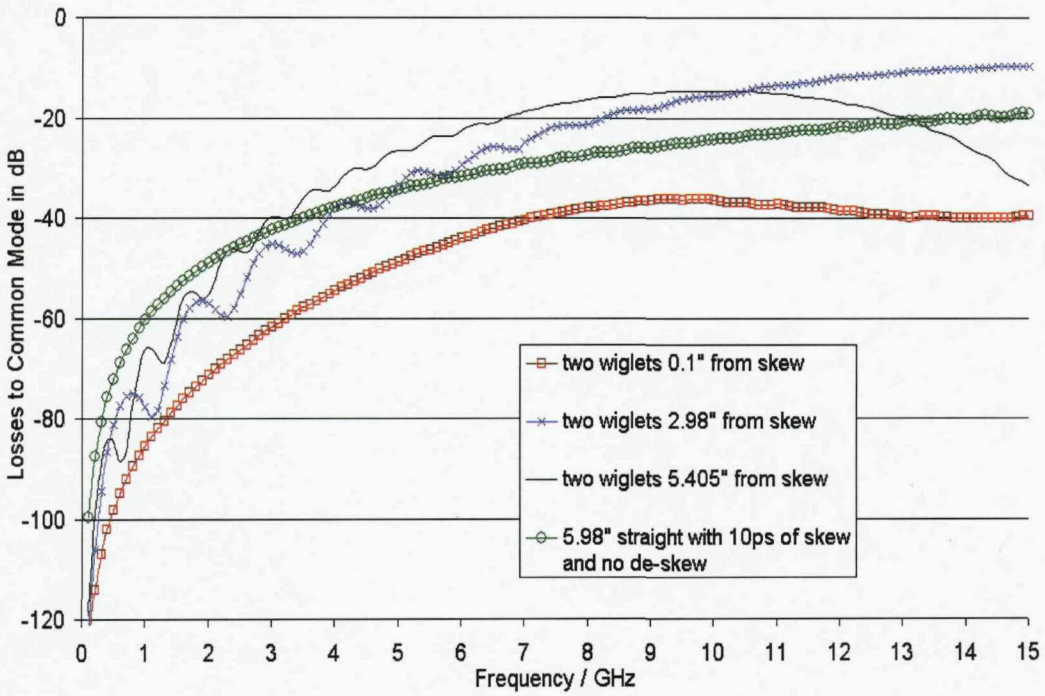

FIGURE 5.25: Losses to common mode for two wiglets placed 0.100", 2.980" and 5.405" from a 10 ps skew event. Also shown are differential pairs of equal length with no skew as well as a pair with skew but no de-skew

losses were seen to improve with multiple wiglets. This is due to the wider pitches that keep mode conversion within the wiglet to a minimum. The graph for three de-skew wiglets is almost identical to that for five 45° wiglets.

Considering Figures 5.23, 5.25 and 5.27 showing common mode losses for one, two and three de-skew wiglets, higher losses are observed for multiple wiglets placed some distance from the skew, confirming analysis of the associated S_{21} graphs.

The S_{11} performance of one, two and three wiglets at each frequency was also considered. Ordinarily, if skew effects at high frequency are removed from the problem, the location of de-skew geometry has almost negligible effect on S_{11}. This is because the impedance discontinuity that is the wiglet(s), will cause the same amount of reflection, regardless of the location on the pair. With skew present at higher frequencies however, and with the impedance being an instantaneous measure of the ratio of voltage to current, different amounts of skew and the location of the wiglets will, in fact affect S_{11}. Figure 5.28 shows S_{11} for frequencies between 0.1 and 15 GHz, using one, two and three wiglets chosen for their best performance within each frequency bracket. The frequency brackets again are 0.1 to 6.9 GHz, 7 to 9.9 GHz and 10 to 15 GHz. Again, these

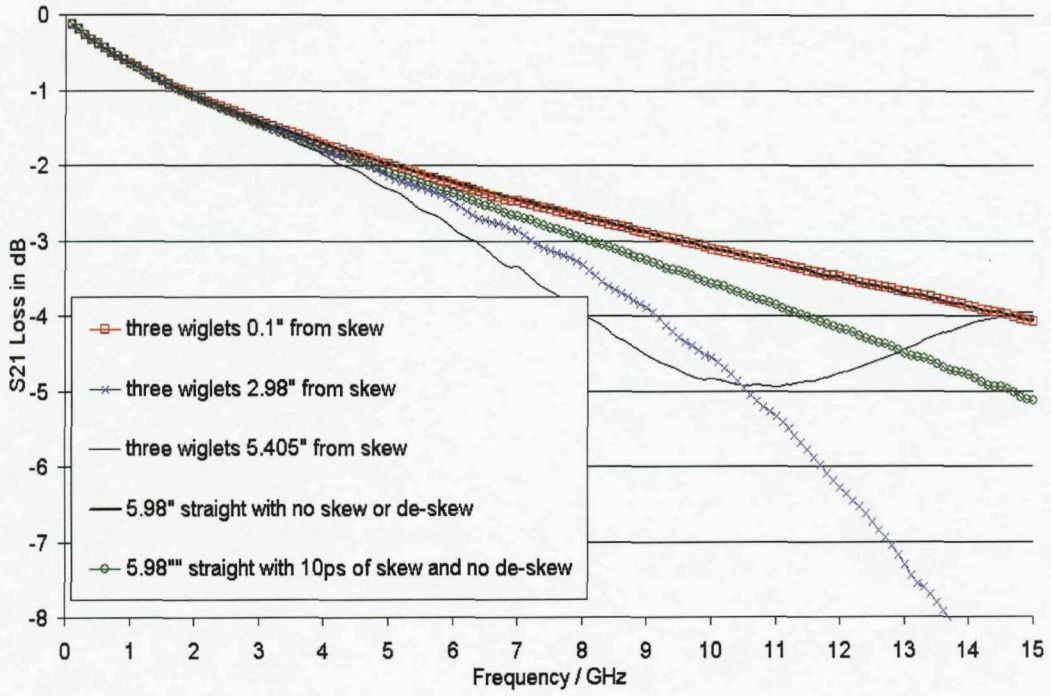

FIGURE 5.26: S_{21} losses for three wiglets placed 0.100", 2.980" and 5.405" from a 10 ps skew event. Also shown are differential pairs of equal length with no skew as well as a pair with skew but no de-skew

brackets were chosen partly for convenience after it was discovered that the amount of de-skew, mode conversion and delay a wiglet presented were frequency dependent. Additionally, following further inspection of initial results, the trends observed aided in the final definition of these frequency brackets where trends were observed that led to the exact location of the ranges to be defined. Study of Figure 5.28 shows some very interesting results. The entire frequency range was considered, and using the mean of each line in the graph as the average amount of loss due to reflection, the lowest amount of loss was at an average of -30.86 dB and was given by three wiglets. The highest amount of loss due to reflection was an average of -25.32 dB given by five 45° wiglets. This gives an average of 2.6% less loss due to reflections alone if three engineered wiglets are used across the frequency range, instead of a generic one size fits all solution. These results are an average across the frequency range comparing the methods giving the best and worst S_{11} performances across the entire range, but do not consider that different methods may give more or less loss within each frequency bracket. Examining each frequency bracket in closer detail reveals that there are even greater savings in loss due to S_{11} to be made. The biggest savings in each bracket now follow. In the 0.1 to 6.9 GHz bracket, at best case, 7% less losses are observed by using either one, two or three

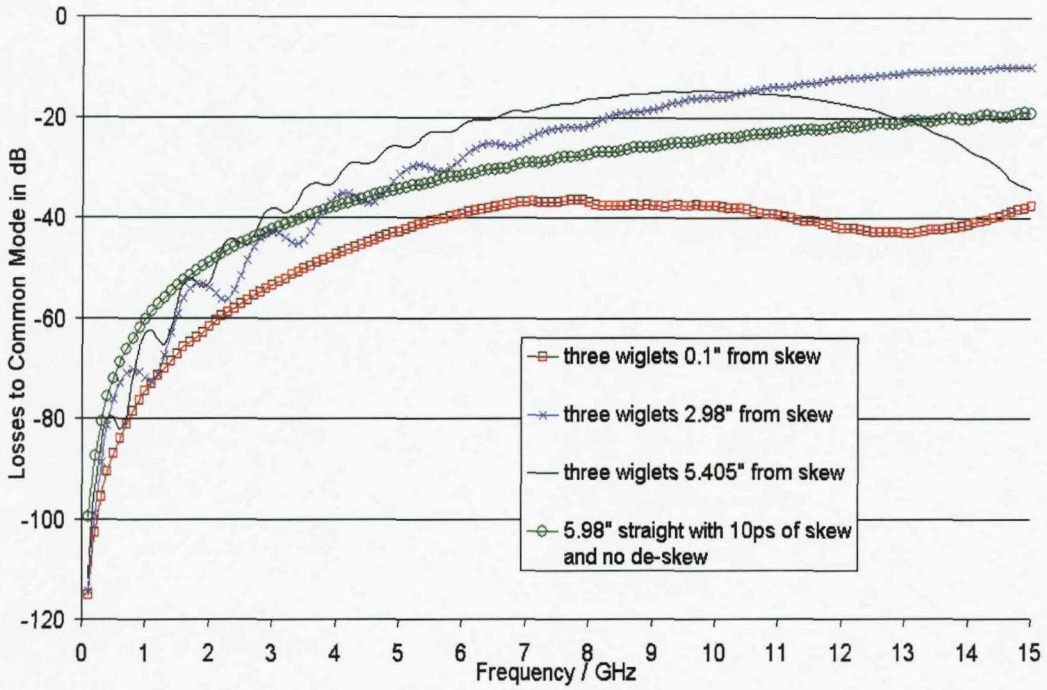

FIGURE 5.27: Losses to common mode for three wiglets placed 0.100", 2.980" and 5.405" from a 10 ps skew event. Also shown are differential pairs of equal length with no skew as well as a pair with skew but no de-skew

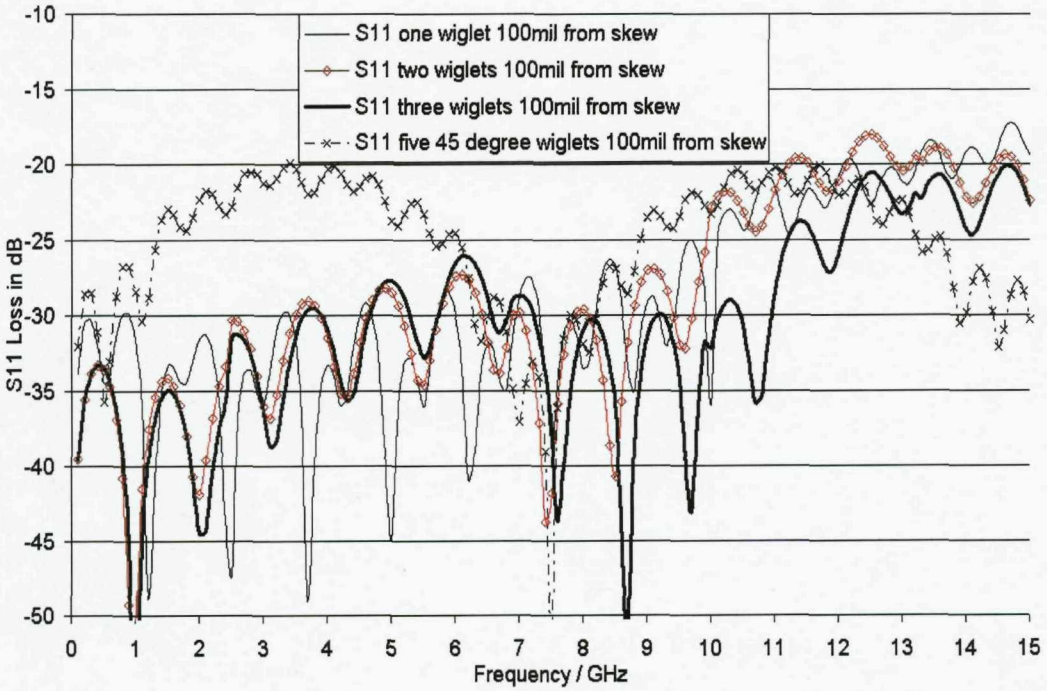

FIGURE 5.28: S_{11} losses for one, two, three and five 45° wiglets placed 0.100" from a 10 ps skew event

engineered wiglets instead of the generic solution. In the 7 to 9.9 GHz range, 6% less loss is achieved by using three engineered wiglets, using one and two wiglets in this same bracket still presents a saving, however, not by as much, meaning the impedance match is not quite as good. In the 10 to 15 GHz frequency range the best possible saving is of 10%. Interestingly enough this saving is made by using five 45° wiglets which appear to give the lowest S_{11} in this range.

To summarise, neither the single engineered wiglet nor the use of two engineered wiglets as temporal skew compensation offered the best S_{11} performance out right. At lower frequencies, if de-skew is performed immediately, either one, two or three engineered wiglets present lowest S_{11} losses. Higher frequencies show definite trends that place multiple wiglets as better performers than single wiglets. This is because at high frequency, cross talk can become prohibitively high as the amount of signal coupled between two traces is directly proportional to the rate of change of the signal on the trace affecting the victim. Using wiglets that have a low profile (that have a smaller height) as well as being engineered to provide the exact amount of de-skew, becomes increasingly important as frequency increases as this minimises cross talk and reduces mode conversion losses. Mode conversion occurs through cross talk all along the differential pair whenever there is a potential gradient between the traces. However, there are increased opportunities for it to happen in a taller wiglet as at higher frequencies near half a signal period may be inside the wiglet at the same time. This considerably increases cross talk within the wiglet due to the potential gradient between each side.

In order to show more conclusive evidence and gain more insight into the benefits derived, if any, of using the engineered single and multiple wiglets compared with using the generic five 45° wiglets, the de-skew geometry itself was tested at choice frequencies. The frequencies chosen were 3.5, 8.5 and 12.5 GHz, these were chosen to correspond to the centre points of the three frequency brackets already chosen. An amount of skew was introduced to the pair that contained the skew compensation wiglets designed to de-skew 10 ps of skew at each of the frequencies. The injected skew was varied from 4 to 16 ps. It was expected to see maximum S_{21} (highest amount of signal transmission between transmitting and receiving ends) and minimum common mode losses at 10 ps of injected skew where the de-skew should exactly match it. All wiglet types were placed 0.100" from the skew in turn to mostly eliminate mode separation from the outcome and to maintain consistency. By comparing losses due to reflections (S_{11}), total losses (S_{21}) and common mode losses, it should be possible to say which is the

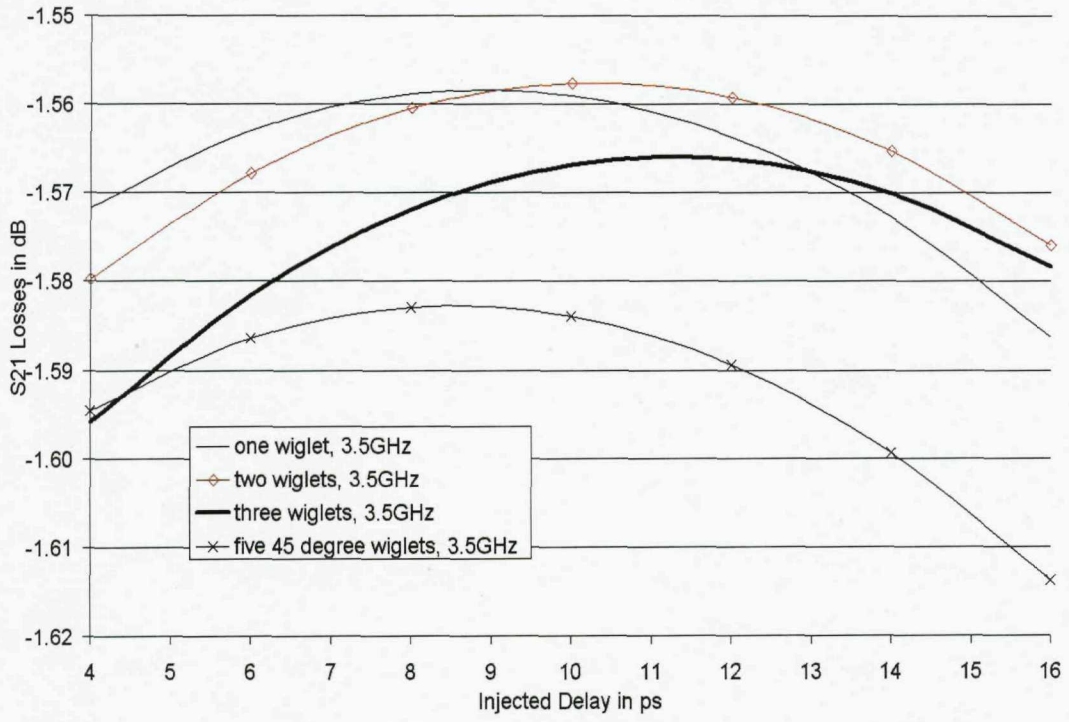

FIGURE 5.29: S_{21} losses for one, two, three and five 45° wiglets placed 0.100" from a 10 ps skew event. Injected delay is varied from 4 to 14 ps for frequencies between 0.1 and 6.9GHz

greater loss mechanism at each frequency range and for each type of skew compensation geometry. From this it will aid in the understanding of the best skew compensation strategies and methodologies. Considering Figures 5.29 and 5.30 in the 0.1 to 6.9 GHz range, the engineered wiglets show least total S_{21} loss at 10 ps. The five 45° wiglets show least loss at 8ps however overall in this range, they also show most loss. One, two and three engineered wiglets all out performed the generic wiglets in terms of total loss. Considering the common mode losses for the same experiment in Figure 5.30, all losses to the common mode are less than the S_{11} losses. This indicates that it is perhaps more important to match the impedance of the wiglet than to consider the exact amount of de-skew required and the number of wiglets used to achieve this. This brings an amendment to the importance of the individual loss factors in the system. The biggest loss mechanism remains physical loss, the second biggest mechanism appears to be impedance mismatch with the third and fourth biggest loss mechanisms being skew compensation position and exactly how that is achieved respectively. Figure 5.31 shows only 0.5% difference in loss between using five 45° wiglets and using two wiglets which are the best and worst loss performances in the 7 to 9.9 GHz frequency range respectively. The associated common mode losses graph in Figure 5.32 shows

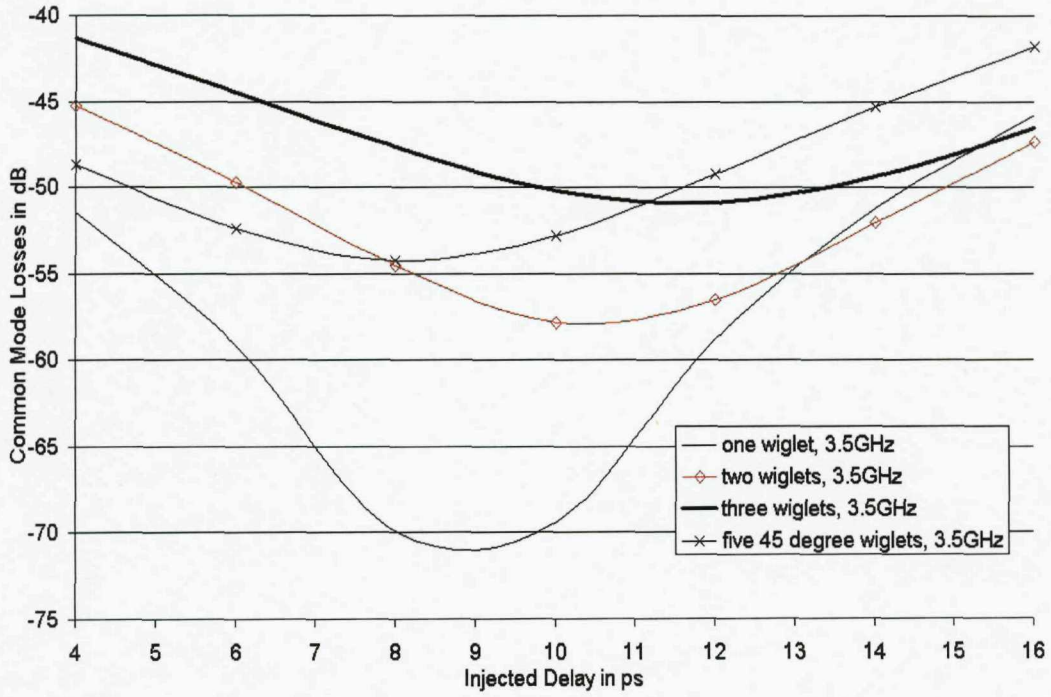

FIGURE 5.30: Common mode losses for one, two, three and five 45° wiglets placed 0.100" from a 10 ps skew event. Injected delay is varied from 4 to 14 ps for frequencies between 0.1 and 6.9 GHz

the same order of best and worst loss performers as the S_{21} chart. There is again also a 0.5% difference in loss between the best and worst cases. This, combined with the fact that losses to the common mode are of the same order of magnitude as S_{11} losses in this case, implies that there is a good impedance match with little reflection and lesser effect of the number of wiglets is observable. The generic wiglets give less mode conversion losses. In the 10 to 15 GHz range in Figure 5.33, over 1% extra loss is observed from using a single wiglet versus using three or five wiglets. Incremental improvements can be seen as the number of wiglets is increased. The same trend applies to the common mode losses in Figure 5.34, which are an order of magnitude less loss than the losses caused by impedance mismatch as observed in the S_{11} graph in Figure 5.28. In this graph, the losses follow the same order as in Figures 5.33 and 5.34. Once again the impedance mismatch is shown to be the second largest loss mechanism after physical losses if de-skew is performed immediately.

From the data gathered in this section, in order to ensure good signal integrity, the shortest path must be taken to minimise physical losses. Next, any skew must be compensated for as soon as possible using de-skew wiglets that are matched as closely as

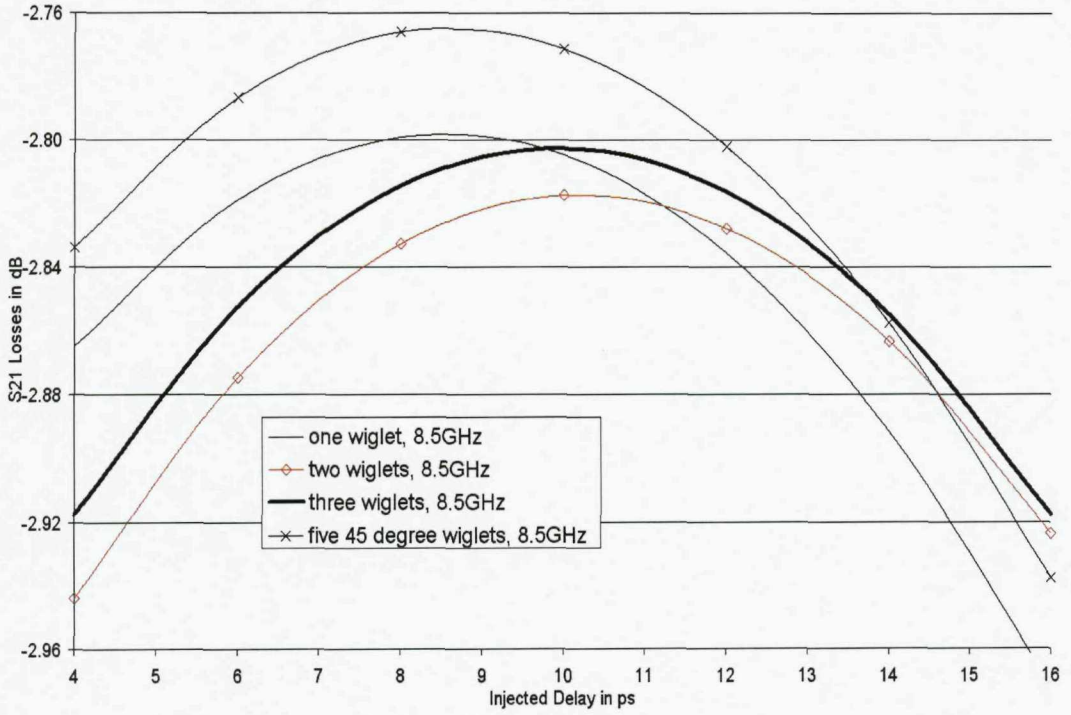

FIGURE 5.31: S_{21} losses for one, two, three and five 45° wiglets places 0.100" from a 10 ps skew event. Injected delay is varied from 4 to 14 ps for frequencies between 7 and 9.9 GHz

possible to the impedance of the differential pair to appear transparent to the signal. Finally, as frequency is increased past 10 GHz multiple low profile wiglets should be used.

Further work on this topic would consist of investigating methods of impedance matching skew compensation geometry. This could be done by making the wiglet go single ended or engineering the wiglet by using time domain reflectometry (TDR) type techniques to 'tune out' the inductive and capacitive responses to match those of the differential pair. Both of these approaches are yet to be investigated and are recommended as a continuation to this work.

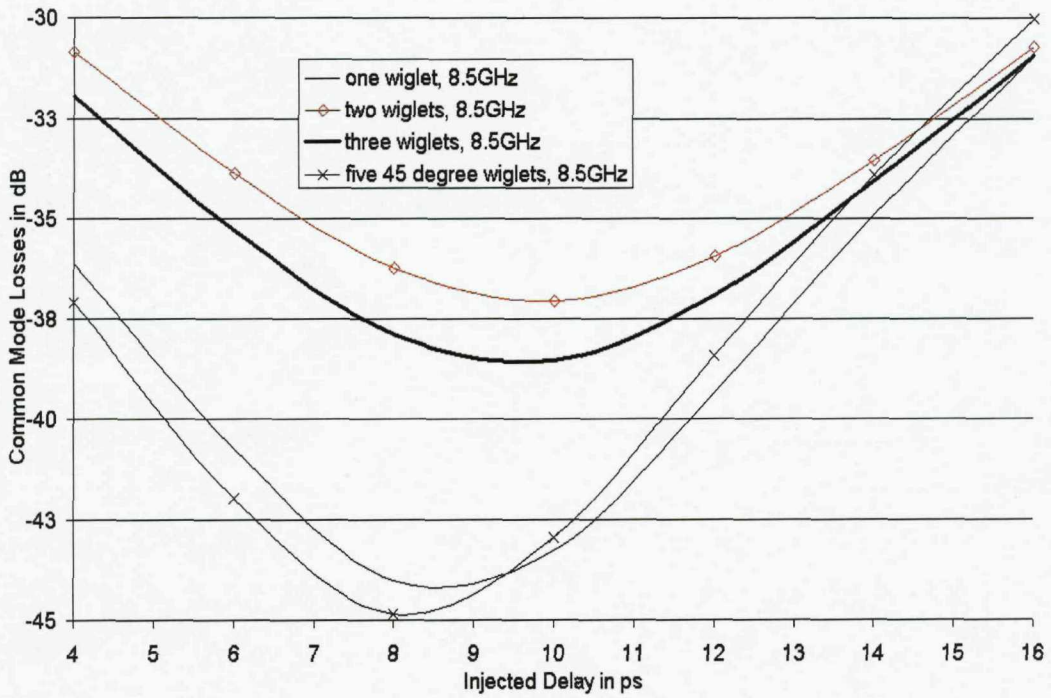

FIGURE 5.32: Common mode losses for one, two, three and five 45° degree wiglets placed 0.100" from a 10 ps skew event. Injected delay is varied from 4 to 14 ps for frequencies between 7 and 9.9 GHz

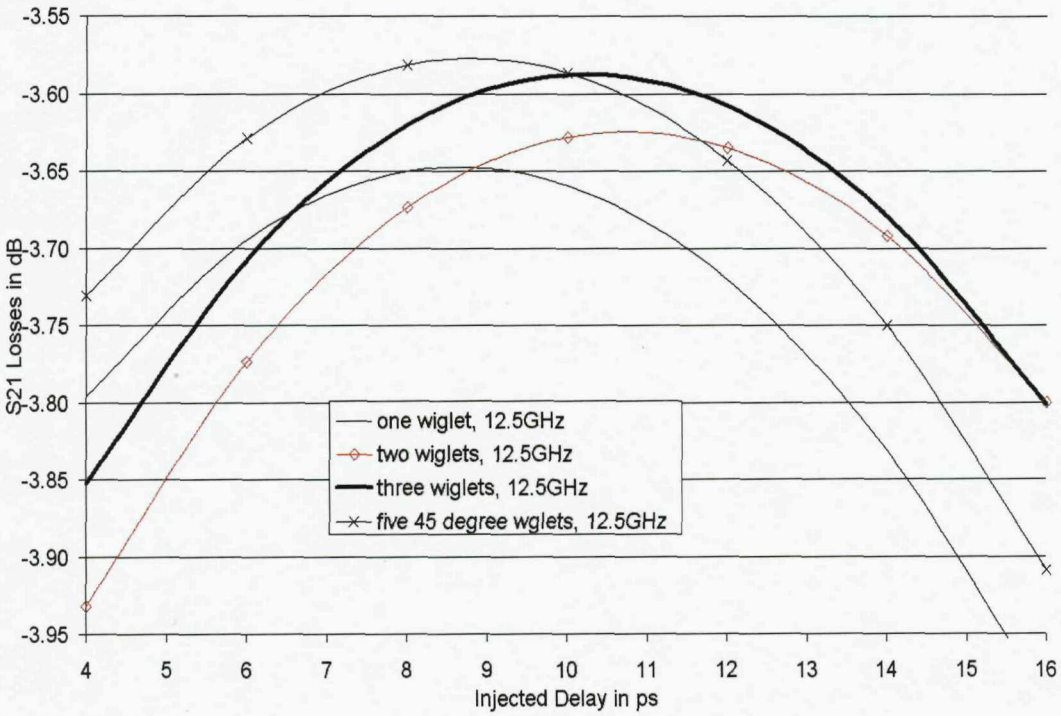

FIGURE 5.33: S_{21} losses for one, two, three and five $45_{\circ}$ wiglets places 0.100" from a 10 ps skew event. Injected delay is varied from 4 to 14 ps for frequencies between 10 and 15 GHz

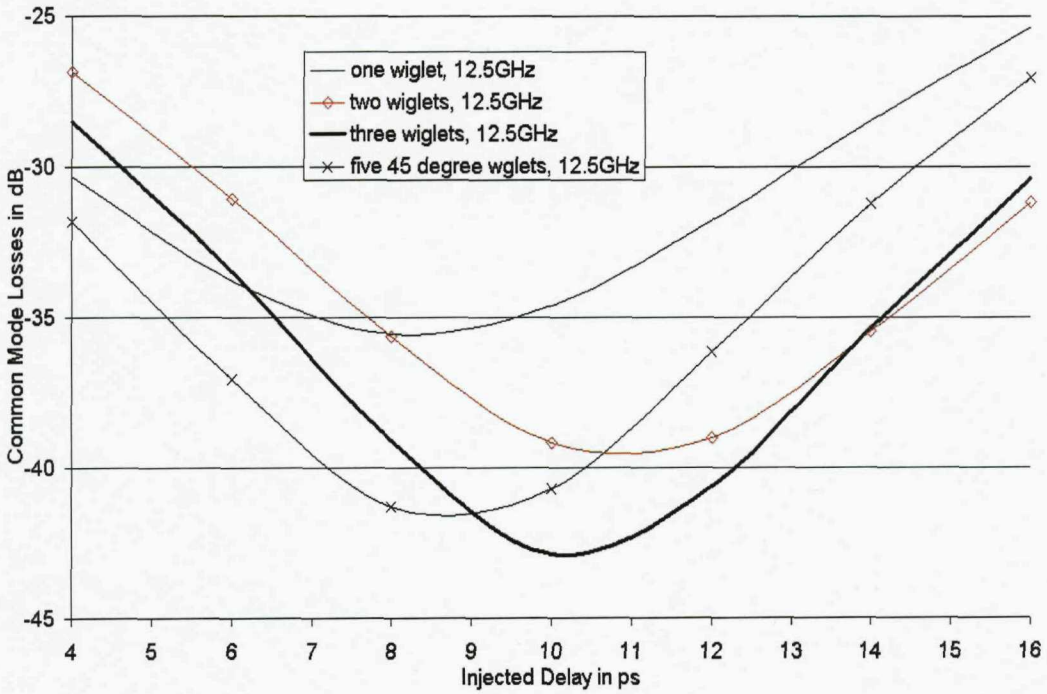

FIGURE 5.34: Common mode losses for one, two, three and five 45_{o} wiglets places 0.100" from a 10 ps skew event. Injected delay is varied from 4 to 14 ps for frequencies between 10 and 15 GHz

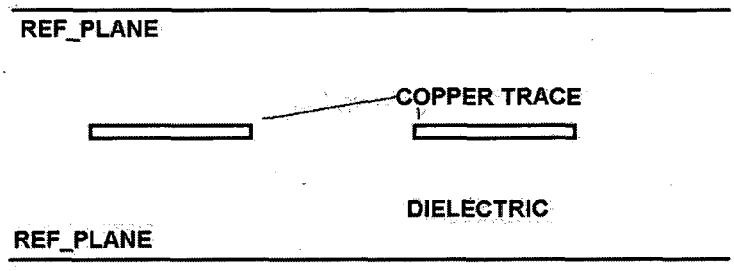

FIGURE 5.35: Stripline geometry between two reference planes

5.3.3 Homogenising the dielectric medium in which the transmission media is situated to improve signal integrity

As previously stated the difference in the odd and even mode relative dielectric constants causes the modes to travel at different velocities. This is the reason skew compensation geometry becomes less effective as it is effected further from the skew event. If however, the relative dielectric constants were the same number, such as in stripline geometries shown in Figure 5.35, then the modes would not separate and de-skew could potentially be placed wherever it most suited the designer. Moving to a stripline based geometry requires five PCB layers as it is shielded top and bottom by reference planes. The next best thing could be to use buried microstrip line. This would require four layers as no top plane would be needed. This means that most of the field from the signal will be contained within the dielectric on top and below the microstrip pair, meaning both odd and even modes will experience a much similar relative dielectric constant. Figure 5.3.3 gives the parameters for such a buried microstrip line. The geometry under test occupies less area on its plane than the unburied microstrip line by 3mils. If multiple buried pairs were used this could allow a higher density of routing to be achieved.

The odd and even mode dielectric constants are 1.770 and 1.795 respectively, a difference of only 0.025 or 1.4%. Comparing this with the microstrip equivalents of 2.411 and 2.836 for odd and even modes respectively, the difference in the unburied case was 15.0%.

For example, over 3" of microstrip line at 10 GHz, if a signal common to each trace travelling in the even mode were generated through length mismatch, the modes after after 3" would be skewed by 120° resulting from 33.4 ps difference in flight time caused by dissimilar modal velocities, seriously compromising SI. For the same distance and frequency, 8.6° of skew between the modes results from only 2.4 ps difference in flight

Parameter	Value	Units
Length	3	inches
Width (t)	8	mil
Separation (s)	1	mil
Thickness (t)	0.71	mil
Dielectric height (h1)	6	mil
Dielectric height (h2)	4	mil
Dielectric constant (ε_r)	3.48	–
Odd mode impedance (Z_{0o})	32.2	Ohms
Even mode impedance (Z_{0e})	102.5	Ohms
Odd mode relative ε_r	1.770	–
Even mode relative ε_r	1.795	–

FIGURE 5.36: Parameters for the buried differential microstrip pair under test

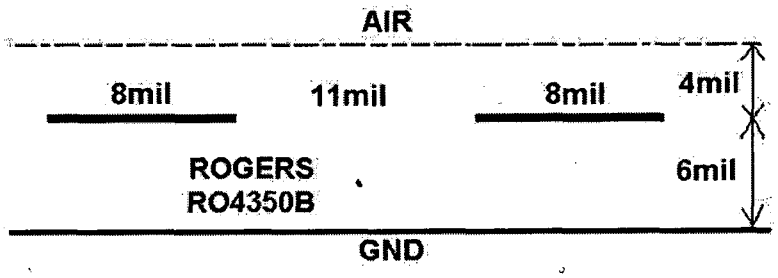

FIGURE 5.37: Diagram showing buried microstrip line as described in Figure 5.3.3

times resultant from having very similar relative dielectric constants. This is a good example showing how buried microstrip line could help to preserve SI. The disadvantages of using buried microstrip line instead of microstrip line are that it requires another board layer and also it has higher inherent physical losses. These higher losses are due to skin effect and dielectric conductance. Skin effect is worse because each half of the pair in this case is only 8 mil wide compared to 12 mil used for the microstrip examples in this work. This gives less surface area for surface currents to flow in and so increases the resistance. Dielectric conductance is also higher because the pair is 2 mil closer to the ground plane causing capacitance to increase, which according to Equation 2.6 also increases conductance.

The same experiments were conducted as in Sections 5.3.1 and 5.3.2 in order to find the best wiglets providing 10 ps of skew compensation across the three frequency ranges whilst also providing minimum S_{11}. Once found these wiglets were again used in experiments where skew compensation geometry was moved further away from the skew to 0.100", 2.980" and 5.405" away. The amount of signal lost overall (S_{21}) and the

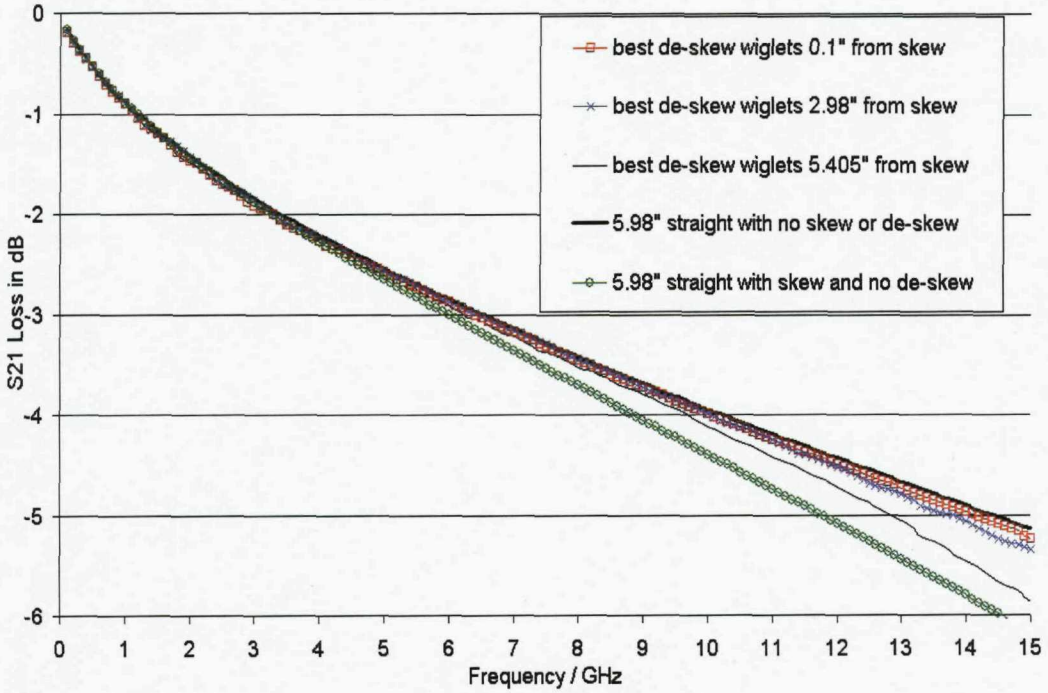

FIGURE 5.38: 10 ps of skew compensation placed 0.100", 2.980" and 5.405" after skew on 6.000" of buried microstrip line. Also shown are two plots of straight buried microstrip with no compensation both with (circles) and without (thick solid line) skew.

amount of signal lost to the common mode are plotted in Figures 5.38 and 5.39 respectively. For comparison, also plotted were the same results but this time using five 45° wiglets at the same locations. These results for buried microstrip are found in Figures 5.40 and 5.41. S_{11} for all listed results where de-skew is placed 0.100" from the skew is given in Figure 5.42. Analysis of the results for buried microstrip line and comparison with results for normal microstrip line supports all previous findings and predictions. Figure 5.38 shows a similar pattern of loss with frequency, with increased losses for experiments where de-skew is moved further from skew. Immediately noticeable is that in using buried microstrip, there are far greater inherent physical losses than in normal microstrip line. For example, at 3 GHz using normal microstrip all losses for all de-skew geometries are approximately -1.4 dB, whereas using buried microstrip line these losses rise to -1.9 dB. This gives an extra 0.5 dB or 5.6% further losses. Examining the cases for no skew with no de-skew, or more simply put, a straight differential pair, again the buried case shows more loss. The normal microstrip differential pair at 10 GHz shows -3.2 dB loss and the buried case shows -4 dB loss giving an extra 8.8% more loss for the same frequency. At 15 GHz the respective losses have increased to -4.1 dB and -5.2dB which is 11.9% more loss. As frequency is increased, physical loss

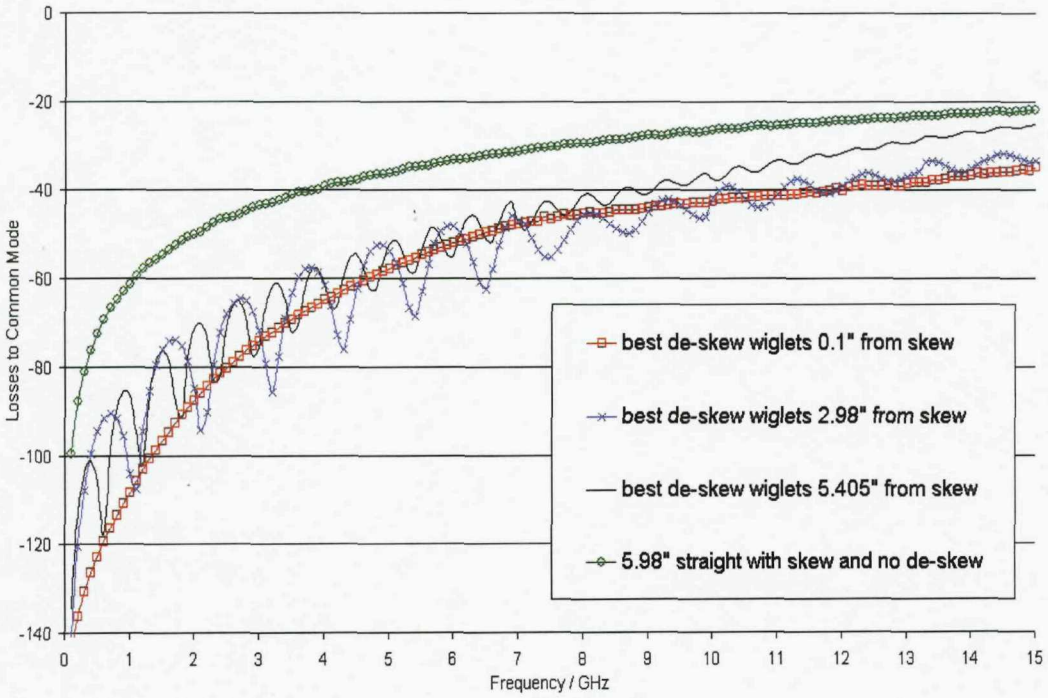

FIGURE 5.39: 10 ps of skew compensation placed 0.100", 3.100" and 5.405" after skew on 6.000" of buried microstrip line. Also shown is a plot of straight buried microstrip with skew but no de-skew.

increases faster in the buried case. Again, this is explained by greater skin effect and dielectric conductance losses in the buried case, both of which are frequency dependent. No common mode losses are given for these cases because common signal is too low to be graphed properly.

The cases where there is 10 ps of skew but no skew compensation geometry show the reference point at which compensating for skew is either having no effect or making signal integrity worse. Considering the cases for skew with no de-skew in both normal and buried microstrip, the overall (S_{21}) loss for normal microstrip at 10 GHz is -3.6 dB. In the buried case this figure is -4.4 dB. The difference is the same as for the straight differential pairs with skew compensation. There are near identical losses to the common mode in both cases also, confirming that the extra loss is due to physical loss and not mode conversion. This also reinforces statements made previously pertaining to length (physical loss) as being the dominant loss mechanism in transmission lines.

Considering differences in signal integrity between normal and buried microstrip pairs, the buried case appears to offer far superior signal integrity over the normal case. In the normal (microstrip) case, as the de-skew geometry is moved further away from the

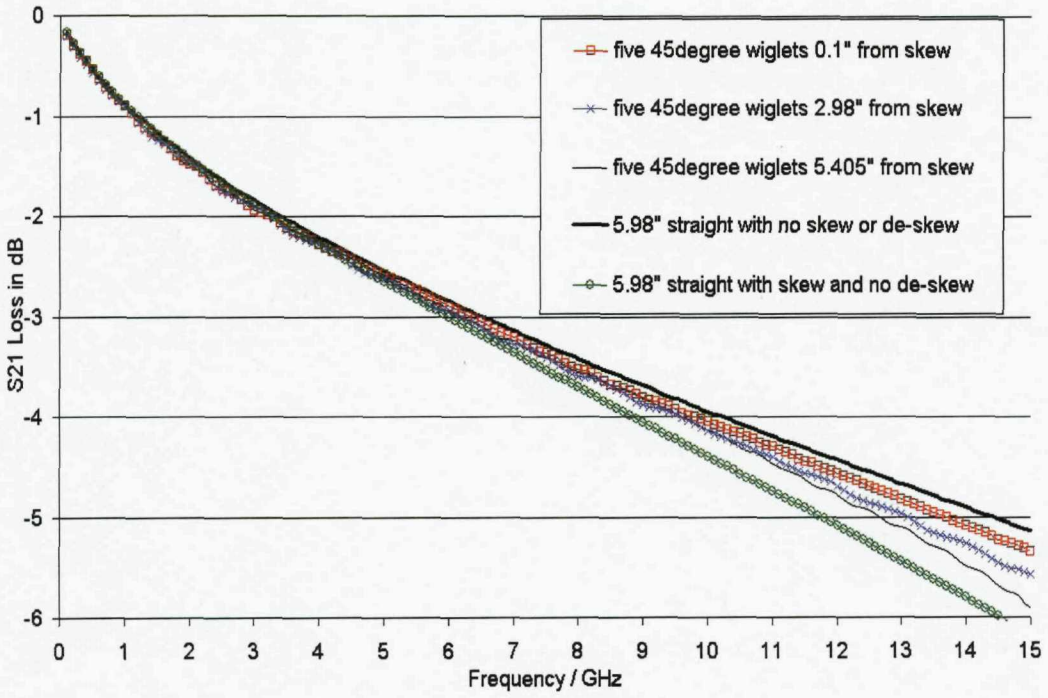

FIGURE 5.40: 10 ps of skew compensation placed 0.100", 3.100" and 5.405" after skew on 6.000" of buried microstrip line using generic five 45° wiglets. Also shown are two plots of straight buried microstrip with no compensation both with (circles) and without (thick solid line) skew.

skew, overall losses deviate much more quickly from the ideal straight line case with immediate de-skew than the buried case. For example, in the normal case at approximately 3 GHz, with de-skew placed 5.405" from skew, the amount of physical loss begins to deviate in a non-uniform manner. In the buried case, this non-uniform deviation does not begin to occur until approximately 10 GHz. Considering skew compensation geometry placed at 2.980" from the skew, the normal case begins deviation from the normal physical loss curve around 5GHz, whereas the buried case does not deviate at all over the entire 6" pair up to 15 GHz. The deviation from the expected loss curve in the normal case is due to mode separation, the buried case restricts mode separation through the homogenised medium by making relative dielectric constants near equal. This in turn means that almost all of the signal split between the odd and even mode will be able to be recombined back into the odd mode only, thus preserving signal integrity.

Examining common mode losses where the skew compensation has been moved further from the skew, apart from the immediate de-skew case, using buried microstrip line reduces the common mode component remaining following the use of skew compensation geometry. All skew compensated cases never present more than -28 dB (4.0%)

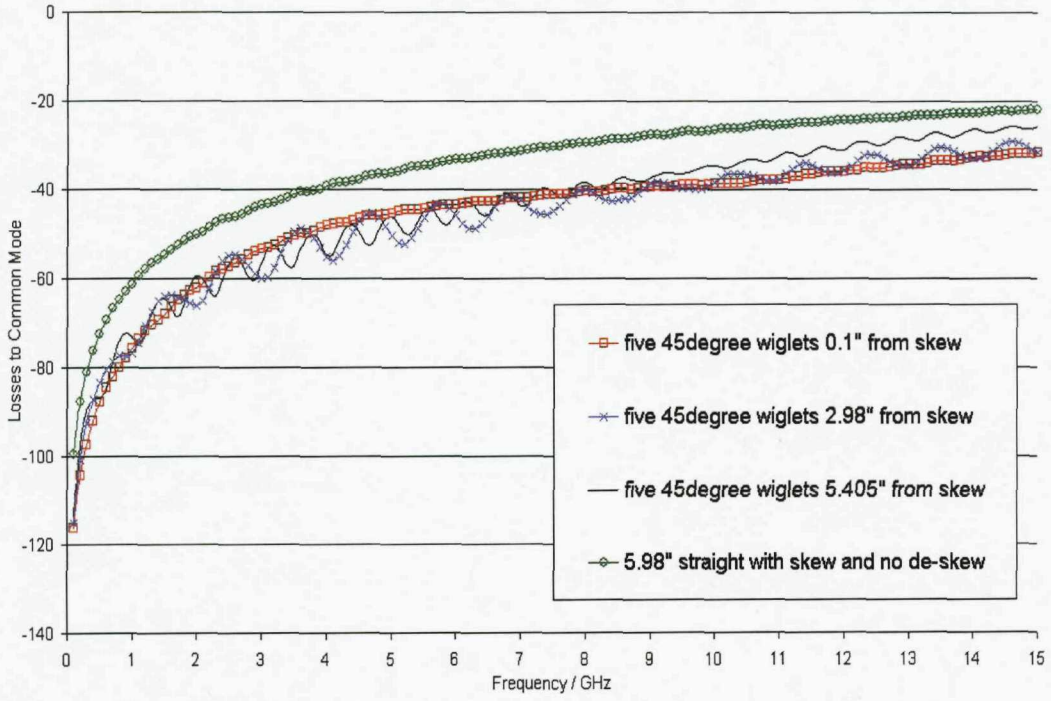

FIGURE 5.41: 10 ps of skew compensation placed 0.100", 3.100" and 5.405" after skew on 6.000" of buried microstrip line using generic five 45° wiglets. Also shown is a plot of straight buried microstrip with skew but no de-skew.

loss to common mode signal in the buried case whereas in the normal case the common mode signal peaks at -15 dB (17.8%)loss. Also in the normal case, with the skew compensation placed at 5.405" from the skew, the losses begin to decrease past 10 GHz, indicating complete mode separation by more than 180° and showing almost a purely common signal. The buried case does not show such a trend as the modes are never allowed to separate this much. As de-skew geometry is moved further from skew in the normal case compared to the buried case, the common signal increases more as compensation is placed further from the skew than in the buried case. The common signal also increases at a greater rate at lower frequencies in the normal case compared to the buried case. This is because modes separate at the same rate regardless of frequency, the difference being in the buried case, the modes travel at near the same velocity so separation takes a longer distance.

Comparing buried microstrip engineered wiglets providing the exact amount of skew compensation required whilst also giving minimum S_{11} against the generic 45° wiglet case again, common mode signals are reduced using engineered wiglets. Using de-skew up to 2.980" from skew, the engineered wiglets keep common signals under -40

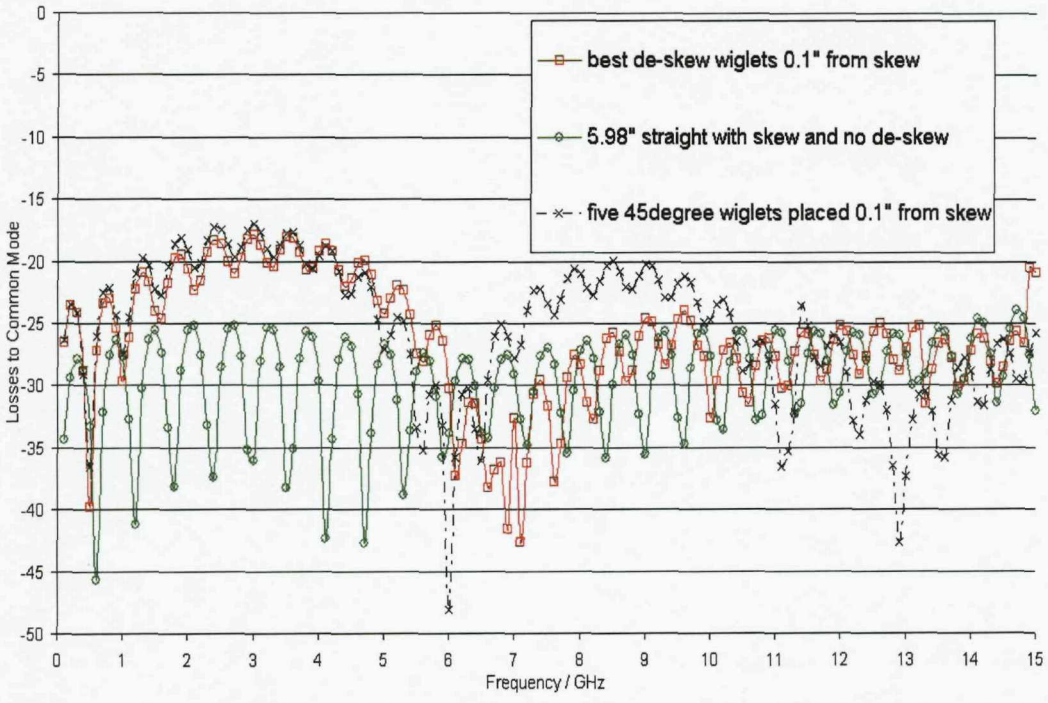

FIGURE 5.42: Comparison between a generic solution of five 45° wiglets and a frequency engineered solution of exactly 10 ps of skew compensation placed 0.100" after skew on 6.000" of buried microstrip line. Also shown is a plot of straight buried microstrip with skew but no de-skew (circles).

dB (under 1%) up to 11 GHz. The 45° wiglets in the same scenarios keep common signals under -40 dB up to only 8 GHz. Also obvious is that the engineered buried wiglets present less overall physical loss than the generic 45° wiglets for all cases.

To complete the analysis of buried microstrip line, the S_{11} profiles shall be examined and compared. Examining only cases of immediate skew compensation, under 7 GHz, using either generic or engineered wiglets presents the same levels of signal reflection. From 7 to 10 GHz, the generic solution present a further -5 dB (4.4%) loss. We can say from the above that using a buried microstrip line gives larger inherent physical loss however signal integrity can be preserved over longer distances and higher frequencies allowing skew compensation to be placed much further away from the skew. This would give the designer more flexibility in how they dealt with skew compensation. Buried microstrip could potentially offer greater common mode protection for sensitive transceivers used with circuits that could potentially produce large amounts of skew and hence common signal. It appears very much worthwhile engineering wiglets for minimum S_{11} as this can further preserve signal integrity.

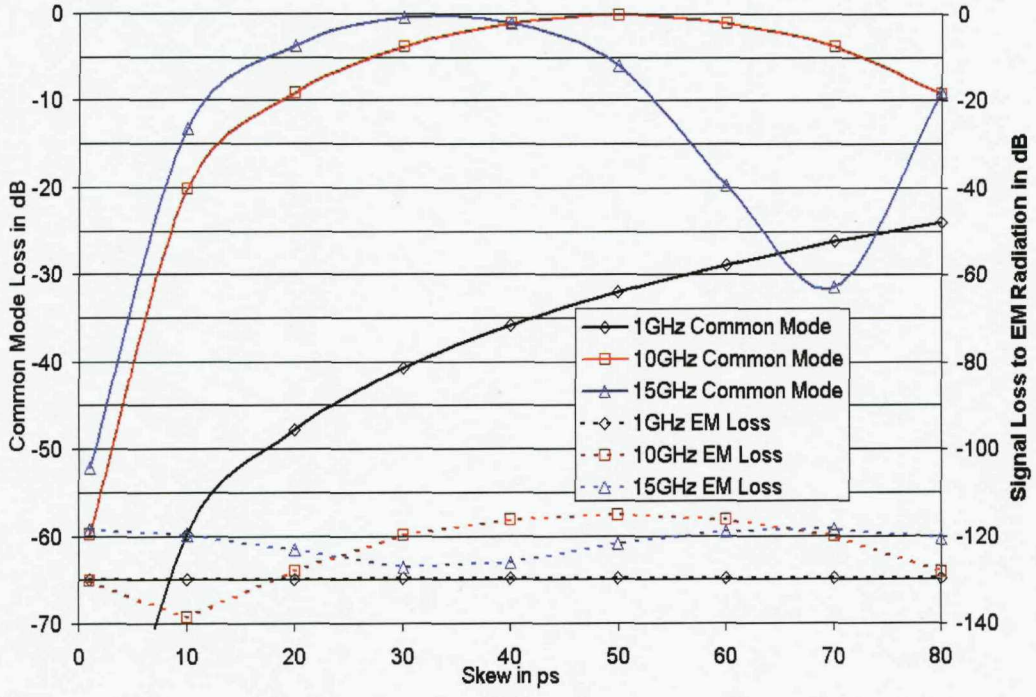

FIGURE 5.43: Losses to common mode increase with skew, EM losses near zero due to proximity to ground plane of the buried copper differential pair.

These figures are for single instances of skew, followed by subsequent skew compensation that in themselves may not pose much of a problem. However, if this pattern were to repeat over the length of a longer differential pair, the multiple reflections, multiple mode separations and re-alignments could ultimately severely affect signal integrity. As an example, for a signal in the 7 to 10 GHz band, using the generic solution for skew compensation would present a further 4.4% loss each time it is used, coupled with the not quite exact skew compensation each time it is used would, over the course of an A to B link, present significant extra losses. Finally, examining the signal loss to electromagnetic radiation for the buried case in Figure 5.43 and comparing to Figure 5.8, there are near identical amounts of common signal produced as skew is increased from 1 to 80 ps. In the buried case, EM loss peaks at only $0.2\text{x}10^{-4}\%$ whereas in the normal case the figure is much higher at almost 0.5%. This reduction is primarily due to the closer proximity to the ground plane of the buried microstrip line. In the non-buried case, the EM loss clearly follows the amount of skew however there is no discernable pattern in the buried case. Placing copper traces as close to the ground plane as possible eliminates EM loss from the system however as previously stated, physical losses are increased. This approach appears be beneficial in helping equipment pass EMI standards and also

in enabling signal integrity to be preserved over longer distances at the cost of signal amplitude.

Chapter 6

Discussion and Further Work

This section will summarise the research objectives and make comment on respective successes before giving a set of guidelines for consideration when laying out high speed data paths on printed circuit boards. There will also be an outline of ways in which this research could be extended.

6.1 Summary of research objectives and accomplishments

The research was divided into two main parts, the first was a novel signal-dependent time domain model of single and edge coupled lossy transmission line. A new methodology was developed for hardware description language (HDL) based modelling of high speed planar lossy microstrip structures in the time domain offering better than 0.1 dB error when compared to experimental measurements from near DC up to 7 GHz. The salient feature of the model was the use of signal variation rate instead of frequency to determine the non-linear effects of skin depths and dielectric conductance as well as the linear signal skew effects for loss calculation. A highly efficient, customisable and scalable model was implemented in VHDL-AMS for use in system level high speed time-domain mixed-signal simulations, especially for applications involving very high speed digital switch fabrics. As a result there now exists a highly configurable transmission line model for use in large system level analogue and digital mixed signal simulations. The model offers better accuracy than a simple loss and delay approach by

considering the signal shape when determining losses. A purely time domain based approach did not easily provide all relevant information of a differential pair required for a complete analysis to fully research skew and EM loss so a frequency based approach was employed in the second major part of this research.

The second major part of the research explored the use of current methods of length matching in differential microstrip and buried microstrip transmission lines when used with data-rates up to 15 GHz. It was shown that using current methods of length matching to compensate for temporal skew could make worse mode conversion and EM loss than with no length matching at all. A new methodology was suggested whereby interconnect geometry can be engineered to match the length of a pair at a specific or dominant frequency, whilst also minimising reflections. This was achieved through appropriate engineering of de-skew wiglets (skew compensation geometry), through variation of their position, geometry and number. From this research, it is obvious that signal skew and associated mode conversion are facts of life that cannot be totally avoided, and as frequency increases, these become more problematic. Therefore 'skew and EMI management' should be employed as opposed to the common approach taken of 'length matching' currently widely in use. The following set of guidelines for the management of skew in high speed circuit routing were formed.

6.1.1 Guidelines for skew compensation and EM loss management

The following points are in order of priority where the first has the largest impact on signal integrity and each subsequent point has less and less impact. When routing a trace from A to B, for good skew management, the points should be followed however, some may not be compatible with others in the specific situation so the point above should always take precedence.

•Take the shortest route

The shortest route between A and B should be taken because physical loss is always the dominant loss mechanism. Physical loss increases with length and decreasing trace width and decreasing return plane to trace spacing. Tradeoffs will occur as it is beneficial to have thin, closely spaced traces that are close to the return plane for reasons of routing density, immunity to external noise sources and lowering of EM loss and interference.

•Use buried differential microstrip pairs or differential stripline pairs

Changing to a buried or shielded geometry can increase trace density due to thinner traces and offer the benefits of stripline, primarily the homogenisation of the dielectric medium surrounding the differential pair, and near total immunity to external EM sources. This has the major benefit of presenting near identical relative dielectric constants meaning the odd and even mode travel at the same velocity. If the modes travel at the same velocity, a misaligned signal can always be realigned to give near 100% odd mode again because the modes never separate. Buried differential pairs offer nearly the same dielectric constants for each mode and so mode separation, although observable, is severely reduced. This allows skew compensation to be placed wherever the designer so chooses, which according to this research is up to 6" away up to 15 GHz without affecting signal integrity. It should be possible to place de-skew even further than 6" away at higher frequencies however this cannot be said for certain as this research is limited to 15 GHz and 6" lines for consistency. Careful selection of buried trace geometry would be required as the closer proximity of the geometry under test in this research to the ground plane and the thinner traces increased physical losses. The tradeoff is on one hand, an increased physical loss with greater assurance given on signal quality over longer traces at higher frequencies, or on the other hand, less physical loss but the potential for worse signal integrity with normal differential microstrip unless careful skew management is employed.

•Match all parts of the line to the terminations

Signal reflection has a directly proportional relationship between the impedance of all parts of the trace and the terminations. If only one part of a 100 Ω terminated trace falls in impedance to 90 Ω, this presents a 5% loss in signal that can never be recovered that will also reflect and interfere with other parts of the signal (data). In the context of this research this applies to skew compensation structures, referred to as 'de-skew', 'wiglets' or 'length matching'. It would be highly prudent to engineer these wiglets to reflect the signal as little as possible or, put another way, to allow the signal to pass with minimal impact on signal integrity.

•Compensate for skew as soon as possible

Signal skew causes mode conversion and EM loss. If an odd mode signal is skewed by turning a corner, an odd and even mode component are created with signal energy being divided between them according to the amount of skew that has occurred. If the signal is de-skewed immediately there is minimal impact on signal quality and loss. If

however normal differential microstrip line is used and skew compensation is left until further down the pair, due to the differing velocities of each mode, the modes will separate over the distance. This means the de-skew designed to compensate for the original amount of skew will be less effective at re-aligning the modes. If left too late, skew compensation can be detrimental to signal quality. The point along the pair at which skew compensation geometry becomes ineffective or worsens signal quality, is found closer to the skew as frequency increases.

•Turn corners as late as possible

If corners are turned as late as possible, there will be a greater portion of the signal path that is of uniform impedance and free from skew, giving less distance for any mode separation to occur due to the different velocities of the modes, this will inherently mean that the de-skew is placed nearer the skew event, or corner in this case. It should be noted that once a signal has been skewed, it will never be returned to 100% pure odd mode as some energy will be converted to even mode and become very slightly detached from the related odd mode. There is no way of returning this very small part of the signal back to useful data, and the longer it is left before de-skewing, the less energy will be available for realignment.

•Use engineered skew compensation

Engineering de-skew wiglets as opposed to using generic ubiquitous length matching techniques can further preserve signal integrity with minimal extra design time and effort. This is achieved by designing the skew compensation to have the exact amount of de-skew required to re-align the modes to within $\pm$ 0.5ps. Once the exact de-skew time is achieved the wiglet's height, width and corner type can be changed to minimise reflection, by matching the impedance to the line.

•Use multiple engineered de-skew wiglets

Higher frequencies (above 6 or 7 GHz) can benefit from using two or three engineered wiglets as opposed to a single one. This has the benefits of minimising the common mode signal and preserving signal integrity, provided they are placed as close to the skew as possible.

6.1.2 Further work

The skew and EM loss management work coud be extended by considering the following points:

•The buried microstrip pair should be further investigated to find a geometry that presents minimum loss while retaining the benefits of a buried geometry.

•The engineered wiglets should be investigated further with the possibility of a software based time domain reflectometry approach. This would enable a fast, scientific and efficient approach to be taken to engineering a wiglet that gave minimal reflections and cross talk. Specifically, an investigation to see whether the wiglet becomes inductive or capacitive when certain dimensions and frequency were changed.

•Experimental validation and comparison with existing techniques of the best approaches to skew compensation should be conducted with a vector network analyser (VNA), time domain reflectometry (TDR), and bit error rate testing (BERT). This would validate the best approaches to skew and EM loss management in planar high speed data transmission structures. It would be expected to see less loss and less error.

•Incorporation of EM losses into a mixed signal time domain model could be a possibility although quite how this could be achieved and whether the effort would justify the result are questionable.

The work on the time domain modelling of effects that are dependent on the signal could be extended by considering the following points:

•The differential microstrip line model could be validated against experimental results by designing, building and measuring a differential pair of transmission lines and subsequently modelling the pair with the new method and comparing results.

•The model was to be converted into a 'drop in' module for use any supporting mixed signal simulator that could be referenced either in code or via a graphical user interface (GUI). This would be essential for the system modelling engineer to have an easy to use model on hand that would be customisable in terms of geometry and fastest expected signal rise time.

•The outputs from a mixed signal system level simulation could be compared against outputs of a real test board using real data where the simulation would use zero losses and delays, a fixed loss and a delay, and our model in place of transmission lines. This would also allow a comparison of the amount of memory and time taken to run the different simulation approaches. It would be hoped that our model would most closely match the real, time domain, digital data that emerged from the test board.

•The new modelling approach could be applied to different HDLs and programming languages such as Verilog-AMS and SystemC-AMS. Also it would be interesting to attempt to create and apply the algorithm / model in some system modelling development tool's own proprietary environments and languages.

References

[1] H. W. Johnson and M. Graham. *High Speed Digital Design, A Handbook of Black Magic.* Prentice-Hall, New Jersey, 1993. ISBN 0-13-395724-1.

[2] H. W. Johnson and G. Martin. *High Speed Signal Propagation, Advanced Black Magic.* Prentice Hall, New Jersey, 2003. ISBN 0-13-084408-X.

[3] N. K. Das and D. M. Pozar. Full-wave spectral-domain computation of material, radiation, and guided wave losses in infinite multilayered printed transmission lines. *Microwave Theory and Techniques, IEEE Transactions on*, Vol. 39(1):54–63, 1991. ISSN 0018-9480.

[4] B. E. Spielman. Dissipation loss effects in isolated and coupled transmission lines. *Microwave Theory and Techniques, IEEE Transactions on*, Vol. 25(8):648–656, 1977. ISSN 0018-9480.

[5] W. T. Beyene N. Cheng F. June S. Hao D. Oh and C. Yuan. Performance analysis of multi-gigahertz parallel bus with transmit pre-emphasis equalization. In *Microwave Symposium Digest, 2005 IEEE MTT-S International*, page 4, 2005. ISBN 01490-645X.

[6] IEEE standard VHDL analog and mixed-signal extensions. *IEEE Std 1076.1-2007 (Revision of IEEE Std 1076.1-1999)*, pages c1–328, 2007.

[7] E. Christen and K. Bakalar. VHDL-AMS-a hardware description language for analog and mixed-signal applications. *Circuits and Systems II: Analog and Digital Signal Processing, IEEE Transactions on [see also Circuits and Systems II: Express Briefs, IEEE Transactions on]*, Vol. 46(10):1263–1272, 1999. ISSN 1057-7130.

[8] J. D. Jackson. *Classical Electrodynamics.* John Wiley and Sons, Inc., Ontario, 3rd edition, 1999. ISBN 0-471-30932.

[9] L. N. Dworsky. *Modern transmission line theory and applications.* Krieger Publishing Company, Melbourne, FL, 1st edition, 1979. ISBN 0894642766.

[10] J. L. Knighten N. W. Smith J. T. DiBene and L. O. Hoeft. EMI common-mode current dependence on delay skew imbalance in high speed differential transmission lines operating at 1 gigabit/second data rates. In *Quality Electronic Design, 2000. ISQED 2000. Proceedings. IEEE 2000 First International Symposium on*, pages 309–313, 2000. ISBN 0-7695-0525.

[11] S. Ramo J. R. Whinnery and T. Van Duzer. *Fields and Waves in Communication Electronics.* John Wiley and Sons, 1994. ISBN 0471585513.

[12] A. Hirose. EP225.3 - waves, fields, and optics, Sept - Dec 2000. Class Notes from University of Saskatchewan, Department of Physics and Engineering Physics. http://physics.usak.ca/ hirose/ep225/ep225fp.htm.

[13] K. M. Coperich J. Morsey A. C. Cangellaris and A. E. Ruehli. Physically consistent transmission line models for high-speed interconnects in lossy dielectrics. *Advanced Packaging, IEEE Transactions on [see also Components, Packaging and Manufacturing Technology, Part B: Advanced Packaging, IEEE Transactions on]*, Vol. 25(2):129–135, 2002. ISSN 1521-3323.

[14] PCIe base spec. 1.1, 2005. PCI-SIG, http://www.pcisig.com.

[15] Approved draft revision of: IEEE standard for information technology telecommunications and information exchange between systems local and metropolitan area networks specific requirements part 3: Carrier sense multiple access with collision detection (csma/cd) access method and physical layer specifications amendment: Ethernet operation over electrical backplanes (amendment to IEEE std 802.3-2002), 2007.

[16] G. Blando. Losses induced by asymmetry in differential transmission lines. In *DesignCon 2006*, Santa Clara, CA, 2006.

[17] T. Hubing N. Hubing and C. Guo. Effect of delay sew and transition time differences on the common-mode component of differential signals. Technical report, UMR EMC Laboratory Technical Report: TR01-8-002, October 1 2001.

[18] S. B. Smith S. S. Agili and V. Balasubramanian. Theory and measurement of unbalanced differential-mode transmission lines. In *DesignCon 2006*, Santa Clara, CA.95054, 2006.

[19] M. Bucker and J. Gerling. Cancellation of common mode currents due to differential or counter-directed signals. In *Electromagnetic Compatibility, 2002. EMC 2002, IEEE International Symposium on*, volume Vol. 2, pages 627–632, MN, USA, 2002. ISBN 0-7803-7264-6.

[20] T. E. Braxton. The effect of bus driver devices on transmission line emission. In *Electromagnetic Compatibility, 1988. Symposium Record. IEEE 1988 International Symposium on*, pages 317–321, Seattle, WA, USA, 1988.

[21] L. O. Hoeft J. L. Knighten J. T. DiBene and M. W. Fogg. Spectral analysis of common mode currents on fibre channel cable shields due to skew imbalance of differential signals operating at 1.0625 gb/s. In *Electromagnetic Compatibility, 1998. 1998 IEEE International Symposium on*, volume Vol. 2, pages 823–827, Denver, CO, USA, 1998. ISBN 0-7803-5015-4.

[22] B. Kirk. Advanced design techniques to support next generation backplane links beyond 10gbps. In *DesignCon 2006*, Santa Clara, CA, 2006.

[23] R. Garg P. Bhartia I. Bahl and A. Ittipiboon. *Microstrip Antenna Design Handbook*. Artech House, Norwood, MA 02062, 2000. ISBN 0-89006-513-6.

[24] J. R. James. *Handbook of Microstrip Antennas*, volume 1 of *IEE Electromagnetic Waves Series 28*. Peter Peregrinus Ltd, London, UK, 1989. ISBN 0 863411509.

[25] R. Achar and M. S. Nakhla. Simulation of high-speed interconnects. *Proceedings of the IEEE*, Vol. 89(5):693, 2001. ISSN 0018-9219.

[26] S. B. Cohn. Characteristic impedance of the shielded-strip transmission line. *Microwave Theory and Techniques, IEEE Transactions on*, Vol. 2(2):52–57, 1954. ISSN 0018-9480.

[27] S. B. Cohn. Thickness corrections for capacitive obstacles and strip conductors. *Microwave Theory and Techniques, IEEE Transactions on*, Vol. 8(6):638–644, 1960. ISSN 0018-9480.

[28] B. W. Kernighan and D. M. Ritchie. *The C Programming Language*. Prentice Hall, Englewood Cloffs, NJ, USA, 2nd edition edition, 1988. ISBN 0131103628.

[29] S. Wieder. *Introduction to MathCAD for Scientists and Engineers*. McGraw-Hill, New York, 1992. ISBN 0079113060.

[30] HSPICE simulation and analysis user guide, 2003. Synopsis, Inc. Release U-2003.03-PA.

[31] W. Hayt and J. Kemmerly. *Engineering Circuit Analysis, 5th Ed.* McGraw-Hill Education, 1993. ISBN 978-0070274105.

[32] R. M. Barrett. Microwave printed circuits - a historical survey. *Microwave Theory and Techniques, IEEE Transactions on*, Vol. 3(2):1, 1955. ISSN 0018-9480.

[33] S. B. Cohn. Shielded coupled-strip transmission line. *Microwave Theory and Techniques, IEEE Transactions on*, Vol. 3(5):29, 1955. ISSN 0018-9480.

[34] J. D. Horgan. Coupled strip transmission lines with rectangular inner conductors. *Microwave Theory and Techniques, IEEE Transactions on*, Vol. 5(2):92–99, 1957. ISSN 0018-9480.

[35] S. B. Cohn. Characteristic impedances of broadside-coupled strip transmission lines. *Microwave Theory and Techniques, IEEE Transactions on*, Vol. 8(6):633–637, 1960. ISSN 0018-9480.

[36] W. J. Getsinger. Coupled rectangular bars between parallel plates. *Microwave Theory and Techniques, IEEE Transactions on*, Vol. 10(1):65–72, 1962. ISSN 0018-9480.

[37] R. R. Gupta. Fringing capacitance curves for coplanar rectangular coupled bars (correspondence). *Microwave Theory and Techniques, IEEE Transactions on*, Vol. 17(8):637–638, 1969. ISSN 0018-9480.

[38] B. Bianco L. Panini M. Parodi and S. Ridella. Some considerations about the frequency dependence of the characteristic impedance of uniform microstrips. *Microwave Theory and Techniques, IEEE Transactions on*, Vol. 26(3):182, 1978. ISSN 0018-9480.

[39] E. Bogatin and M. Resso. Differential impedance design and verification with time domain reflectometry. In *DesignCon 2000*, Santa Clara, US, 2000.

[40] J. R. Birchak and H. K. Haill. Characteristic impedance and coupling coefficients for multilayer pc boards. In *Test Conference, 1988. Proceedings. 'New Frontiers in Testing'., International*, pages 28–38, Washington, DC, USA, 1988. ISBN 0-8186-0870-6.

[41] E. Bogatin. Design rules for microstrip capacitance. *Components, Hybrids, and Manufacturing Technology, IEEE Transactions on [see also IEEE Trans. on Components, Packaging, and Manufacturing Technology, Part A, B, C]*, Vol. 11(3):253–259, 1988. ISSN 0148-6411.

[42] M. V. Schneider. Dielectric loss in hybrid integrated circuits. *Proceedings of the IEEE*, Vol. 57(6):1206–1207, 1969. ISSN 0018-9219.

[43] H. A. Wheeler. Transmission-line properties of a strip on a dielectric sheet on a plane. *Microwave Theory and Techniques, IEEE Transactions on*, Vol. 25(8):631, 1977. ISSN 0018-9480.

[44] S. Young-Soo L. Jeong-Cheol P. Hong-June and C. Soo-In. Empirical equations on electrical parameters of coupled microstrip lines for crosstalk estimation in printed circuit board. *Advanced Packaging, IEEE Transactions on [see also Components, Packaging and Manufacturing Technology, Part B: Advanced Packaging, IEEE Transactions on]*, Vol. 24(4):521–527, 2001. ISSN 1521-3323.

[45] Pacific Numerix Parasitic Parameters, 1996. Pacific Numerix Corporation, Scottsdale, AZ.

[46] R. S. Elliott. Pulse waveform degradation due to dispersion in waveguide. *Microwave Theory and Techniques, IEEE Transactions on*, 5(4):254–257, 1957. 0018-9480.

[47] N. Nahman. A discussion on the transient analysis of coaxial cables considering high-frequency losses. *Circuit Theory, IRE Transactions on*, Vol. 9(2):144, 1962. ISSN 0098-4094.

[48] R. L. Wigington and N. S. Nahman. Transient analysis of coaxial cables considering skin effect. In *IRE*, volume Vol. 45, pages 166–174, 1957. ISSN 0096-8390.

[49] A. Von Hippel. *Dielectrics and Waves*. John Wiley and Sons, New York, USA, 1954.

[50] J. I. Smith. The even- and odd-mode capacitance parameters for coupled lines in suspended substrate. *Microwave Theory and Techniques, IEEE Transactions on*, Vol. 19(5):424–431, 1971. ISSN 0018-9480.

[51] P. B. Johns and R. L. Beurle. Numerical solution of 2-dimensional scattering problems using a transmission line matrix. In *Proc. Inst. Elec. Eng.*, volume 118, pages 1203–1208, 1971.

[52] J. R. Whinnery and S. Ramo. A new approach to the solution of high frequency field problems. *IRE*, Vol. 32(May):284–288, 1944.

[53] G. Kron. Equivalent circuit of the field equations of maxwell. *IRE*, Vol. 32(May):289–299, 1944.

[54] J. R. Whinnery and W. Concordia. Network analyser studies of electromagnetic cavity resonators. *IRE*, Vol. 32(June):360–367, 1944.

[55] P. B. Johns. The solution of inhomogeneous waveguide problems using a transmission-line matrix. *Microwave Theory and Techniques, IEEE Transactions on*, Vol. 22(3):209, 1974. ISSN 0018-9480.

[56] W. J. R. Hoefer. The transmission-line matrix method–theory and applications. *Microwave Theory and Techniques, IEEE Transactions on*, Vol. 33(10):882, 1985. ISSN 0018-9480.

[57] E. F. Bernard. A transmission-line model for transient cacd programs. *Solid-State Circuits, IEEE Journal of*, Vol. 7(3):270–273, 1972. ISSN 0018-9200.

[58] Xerox Data Systems. Circ-tr users manual and reference guide. *Xerox Data Syst. Technical Notes*.

[59] D. Messerschmitt. A transmission line modeling program written in c. *Selected Areas in Communications, IEEE Journal on*, Vol. 2(1):148–153, 1984. ISSN 0733-8716.

[60] W. Lundry. Negative impedance circuits–some basic relations and limitations. *Circuit Theory, IRE Transactions on*, Vol. 4(3):132–140, 1957. ISSN 0098-4094.

[61] R. L. Veghte and C. A. Balanis. Dispersion of transient signals in microstrip transmission lines. *Microwave Theory and Techniques, IEEE Transactions on*, Vol. 34(12):1427–1436, 1986. ISSN 0018-9480.

[62] J. R. Brews. Transmission line models for lossy waveguide interconnections in vlsi. *Electron Devices, IEEE Transactions on*, Vol. 33(9):1356, 1986. ISSN 0018-9383.

[63] J. R. Brews. Characteristic impedance of microstrip lines. *Microwave Theory and Techniques, IEEE Transactions on*, Vol. 35(1):30, 1987. ISSN 0018-9480.

[64] X. Zhang J. Fang K. K. Mei and Y. Liu. Calculations of the dispersive characteristics of microstrips by the time-domain finite difference method. *Microwave Theory and Techniques, IEEE Transactions on*, Vol. 36(2):263–267, 1988. ISSN 0018-9480.

[65] A. R. Djordjevic T. K. Sarkar and R. F. Harrington. Time-domain response of multiconductor transmission lines. *Proceedings of the IEEE*, Vol. 75(6):743, 1987. ISSN 0018-9219.

[66] M. N. O. Sadiku and L. C. Agba. A simple introduction to the transmission-line modeling. *Circuits and Systems, IEEE Transactions on*, Vol. 37(8):991–999, 1990. ISSN 0098-4094.

[67] M. Wozny W. Carpenter and G. Stein. Identification of green's function for distributed parameter systems. *Automatic Control, IEEE Transactions on*, Vol. 15(1):155, 1970. ISSN 0018-9286.

[68] T. Leung and C. A. Balanis. Attenuation distortion of transient signals in microstrip. *Microwave Theory and Techniques, IEEE Transactions on*, Vol. 36(4):765–767, 1988. ISSN 0018-9480.

[69] P. Pramanick and R. R. Mansour. Dispersion characteristics of square pulse with finite rise time in single, tapered, and coupled microstrip lines. *Microwave Theory and Techniques, IEEE Transactions on*, Vol. 39(12):2117–2122, 1991. ISSN 0018-9480.

[70] G. L. Matthaei K. Kiziloglu N. Dagli and S. I. Long. The nature of the charges, currents, and fields in and about conductors having cross-sectional dimensions of the order of a skin depth. *Microwave Theory and Techniques, IEEE Transactions on*, Vol. 38(8):1031, 1990. ISSN 0018-9480.

[71] N. Fache and D. De Zutter. New high-frequency circuit model for coupled lossless and lossy waveguide structures. *Microwave Theory and Techniques, IEEE Transactions on*, Vol. 38(3):252, 1990. ISSN 0018-9480.

[72] T. Dhaene and D. de Zutter. Selection of lumped element models for coupled lossy transmission lines. *Computer-Aided Design of Integrated Circuits and Systems, IEEE Transactions on*, Vol. 11(7):805–815, 1992. ISSN 0278-0070.

[73] T. F. Hayes and J. J. Barrett. Modeling of multiconductor systems for packaging and interconnecting high-speed digital ic's. *Computer-Aided Design of*

Integrated Circuits and Systems, IEEE Transactions on, Vol. 11(4):424, 1992. ISSN 0278-0070.

[74] T. F. Hayes. *Packaging and interconnection of high speed digital circuits.* PhD thesis, University College, Cork, 1989.

[75] F. L. Mesa G. Cano F. Medina R. Marques and M. Horno. On the quasi-tem and full-wave approaches applied to coplanar multistrip on lossy dielectric layered media. *Microwave Theory and Techniques, IEEE Transactions on*, Vol. 40(3):524, 1992. ISSN 0018-9480.

[76] J. He N. S. Nahman and S. M. Riad. A causal skin-effect model of microstrip lines. In *Proc. of IEEE*, volume 2, pages 865–868, Atlanta, GA, USA, 1993. ISBN 0-7803-1209-0.

[77] C. Gordon. Time-domain simulation of multiconductor transmission lines with frequency-dependent losses. *Computer Design: VLSI in Computers and Processors, 1992. ICCD '92. Proceedings., IEEE 1992 International Conference on*, Vol. 11(11):222–228, 1992. ISSN 0278-0070.

[78] N. E. Hill W. E. Vaughan A. H. Price and M. Davies. *Dielectric Properties and Molecular Behaviour.* Van Nostrand Reinhold Co., London, 1969. ISBN 0442034113.

[79] Q. Yu and O. Wing. Computational models of transmission lines with skin effects and dielectric loss. *Circuits and Systems I: Fundamental Theory and Applications, IEEE Transactions on*, 41(2):107–119, 1994. TY - JOUR.

[80] L. W. Nagel. SPICE2: A computer program to simulate semiconductor circuits, May 9th 1975. Electronic Resource Number ERL-M520.

[81] D. M. Stubbs S. H. Pulko and B. Wilson. Extension of the transmission line matrix (tlm) method in its application to lumped networks. *Electronics Letters*, Vol. 31(21):1849–1851, 1995. ISSN 0013-5194.

[82] R. Gupta and L. T. Pileggi. Modeling lossy transmission lines using the method of characteristics. *Circuits and Systems I: Fundamental Theory and Applications, IEEE Transactions on [see also Circuits and Systems I: Regular Papers, IEEE Transactions on]*, Vol. 43(7):580–582, 1996. ISSN 1057-7122.

[83] M. S. Ghausi and J. J. Kelly. *Introduction to Distributed Parameter Networks with Application to Integrated Circuits*. Krieger, R. E., New York, 1968. ISBN 0-8827-5237-5.

[84] R. Gupta S.-Y. Kim and L. T. Pileggi. Domain characterization of transmission line models and analyses. *Computer-Aided Design of Integrated Circuits and Systems, IEEE Transactions on*, Vol. 15(2):184–193, 1996. ISSN 0278-0070.

[85] M. Hwangkhunnatham and E. Leelarasmee. A two level transient analysis of a circuit containing transmission lines modeled by segments of lumped elements. In *Circuits and Systems, 1998. IEEE APCCAS 1998. The 1998 IEEE Asia-Pacific Conference on*, pages 347–350, Chiangmai, 1998. ISBN 0-7803-5146-0.

[86] R. Berry. An optimal ordering of electronic circuit equations for a sparse matrix solution. *Circuits and Systems, IEEE Transactions on [legacy, pre - 1988]*, Vol. 18(1):40–50, 1971. ISSN 0098-4094.

[87] L. O. Chua and P. M. Lin. *Computer Aided Analysis of Electronic Circuits: Algorithms and Tehniques*. Prentice-Hall, 1975. ISBN 0-1316-5415-0.

[88] E. Chiprout. Interconnect and substrate modeling and analysis: an overview. *Solid-State Circuits, IEEE Journal of*, Vol. 33(9):1445–1452, 1998. ISSN 0018-9200.

[89] D. S. Gao A. T. Yang and S. M. Kang. Modeling and simulation of interconnection delays and crosstalks in high-speed integrated circuits. *Circuits and Systems, IEEE Transactions on*, Vol. 37(1):1–9, 1990. ISSN 0098-4094.

[90] J.-M. Jong B. Janko and V. Tripathi. Equivalent circuit modeling of interconnects from time-domain measurements. *Components, Hybrids, and Manufacturing Technology, IEEE Transactions on [see also IEEE Trans. on Components, Packaging, and Manufacturing Technology, Part A, B, C]*, Vol. 16(1):119–126, 1993. ISSN 0148-6411.

[91] I. Maio F. G. Canavero and B. Dilecce. Analysis of crosstalk and field coupling to lossy mtls in a spice environment. *Electromagnetic Compatibility, IEEE Transactions on*, Vol. 38(3):221–229, 1996. ISSN 0018-9375.

[92] M. Celik and A. C. Cangellaris. A general dispersive multiconductor transmission line model for interconnect simulation in spice. In *Computer-Aided Design, 1996. ICCAD-96. Digest of Technical Papers., 1996 IEEE/ACM International*

Conference on, pages 563–568, San Jose, CA, USA, 1996. ISBN 0-8186-7597-7.

[93] M. Celik A. C. Cangellaris and A. Yaghnour. An all-purpose transmission-line model for interconnect simulation in SPICE. *Microwave Theory and Techniques, IEEE Transactions on*, Vol. 45(10):1857–1867, 1997. ISSN 0018-9480.

[94] V. Jithesh and D. C. Pande. A review on computational emi modelling techniques. In *Electromagnetic Interference and Compatibility, 2003. INCEMIC 2003. 8th International Conference on*, page 159, 2003.

[95] K. M. Coperich J. Morse V. I. Matovski A. C. Cangellaris and A. E. Ruehli. Systematic development of transmission-line models for interconnects with frequency-dependent losses. *Microwave Theory and Techniques, IEEE Transactions on*, Vol. 49(10):1677–1685, 2001. ISSN 0018-9480.

[96] T. R. Arabi A. T. Murphy T. K. Sarkar R. F. Harrington and A. R. Djordjevic. On the modeling of conductor and substrate losses in multiconductor, multidielectric transmission line systems. *Microwave Theory and Techniques, IEEE Transactions on*, Vol. 39(7):1090, 1991. ISSN 0018-9480.

[97] S. Mei and Y. I. Ismail. Modeling skin and proximity effects with reduced realizable RL circuits. *Very Large Scale Integration (VLSI) Systems, IEEE Transactions on*, Vol. 12(4):437–447, 2004. ISSN 1063-8210.

[98] P. Silvester. Modal network theory of skin effect in flat conductors. *Proceedings of the IEEE*, Vol. 54(9):1147–1151, 1966. ISSN 0018-9219.

[99] S. Kim and D. P. Neikirk. Compact equivalent circuit model for the skin effect. In *Microwave Symposium Digest, 1996., IEEE MTT-S International*, volume 3, pages 1815–1818, San Francisco, CA, USA, 1996. ISBN 0-7803-3246-6.

[100] B. Seungyong A. Seungyoung P. Jongbae K. Joungho K. Jonghoon and C. Jeonghyeon. Accurate high frequency lossy model of differential signal line including mode-conversion and common-mode propagation effect. In *Electromagnetic Compatibility, 2004. EMC 2004. 2004 InternationalSymposium on*, volume 2, pages 562–566 vol.2, 2004. ISBN 0-7803-8443-1.

[101] M. Shizhong and Y. I. Ismail. Modeling skin and proximity effects with reduced realizable RL circuits. *Very Large Scale Integration (VLSI) Systems, IEEE Transactions on*, Vol. 12(4):437, 2004. ISSN 1063-8210.

[102] Mentor Graphics Corporation. Systemvision for mechatronic system modelling, www.mentor.com/systemvision, 2006.

[103] Agilent Technologies Inc. Genesys 2006.10 user guide, 1994-2006.

[104] U. Ko S. Schenck B. Van Eerden W. Locke M. Rumsey and J. Sackett. Mixed-signal ASIC simulation via an analog modeling package. In *ASIC Seminar and Exhibit, 1990. Proceedings., Third Annual IEEE*, pages P8/2.1–P8/2.4, Rochester, NY, USA, 1990. INSPEC Accession Number 4111873.

[105] M. Vlach. Modeling and simulation with saber. In *ASIC Seminar and Exhibit, 1990. Proceedings., Third Annual IEEE*, pages T/11.1–T/1111, Rochester, NY, 1990. INSPEC Accession Number 4111817.

[106] H. A. Mantooth and M. Vlach. Beyond SPICE with saber and MAST. In *Circuits and Systems, 1992. ISCAS '92. Proceedings., 1992 IEEE International Symposium on*, volume 1, pages 77–80 vol.1, San Diego, CA, 1992. ISBN 0-7803-0593-0.

[107] J. A. Barby S. E. Rehan and M. I. Elmasry. AHDL modelling to support top-down design of mixed-signal ASICs. In *ASIC Conference and Exhibit, 1994. Proceedings., Seventh Annual IEEE International*, pages 166–169, Rochester, NY, USA, 1994. ISBN 0-7803-2020-4.

[108] J. T. Smith and H. K. Brown. Mixed-signal circuit simulation system with behavioral modeling capability. In *Southcon/94. Conference Record*, pages 580–583, Orlando, FL, USA, 1994. ISBN 0-7803-9988-9.

[109] D. Dumlugol and D. Webber. Analog modeling using event-driven hdl's. In *VLSI Design, 1994., Proceedings of the Seventh International Conference on*, pages 53–56, Calcutta, India, 1994. 0-8186-4990-9.

[110] The MathWorks Inc. Matlab, 2007. http://www.mathworks.com.

[111] K. W. Current. Considerations for an analog and mixed-signal computer-aided design tool. In *Mixed-Signal Design, 2003. Southwest Symposium on*, pages 15–20, 2003. ISBN 0-7803-7778-8.

[112] S. Mu and M. Laisne. Mixed-signal modeling using simulink based-c. In *Behavioral Modeling and Simulation Workshop, 2005. BMAS 2005. Proceedings of the 2005 IEEE International*, pages 128–133, 2005. ISBN 0-7803-9352-x.

[113] L. B. Goldgeisser and G. Popescu. Modeling and simulation of mixed signal systems using a multi-lingual simulator. In *Circuits and Systems, 2005. ISCAS 2005. IEEE International Symposium on*, volume 5, pages 5178–5181, 2005. ISBN 0-7803-8834-8.

[114] P. R. Panda. Systemc - a modeling platform supporting multiple design abstractions. In *System Synthesis, 2001. Proceedings. The 14th International Symposium on*, pages 75–80, 2001. ISBN 1-58113-418-5.

[115] W. Mueller J. Ruf D. Hoffmann J. Gerlach T. Kropf and W. Rosenstiehl. The simulation semantics of systemc. In *Design, Automation and Test in Europe, 2001. Conference and Exhibition 2001. Proceedings*, pages 64–70, Munich, Germany, 2001. ISBN 0-7695-0993-2.

[116] H. Al-Junaid and T. Kazmierski. Analogue and mixed-signal extension to SystemC. *Circuits, Devices and Systems, IEE Proceedings -*, pages 682–690, 2005. ISSN 1350-2409.

[117] A. Vachoux C. Grimm and K. Einwich. Analog and mixed signal modelling with systemC-AMS. In *Circuits and Systems, 2003. ISCAS '03. Proceedings of the 2003 International Symposium on*, volume 3, pages III–914–III–917 vol.3, 2003. ISBN 0-7803-7761-3.

[118] A. Vachoux C. Grimm and K. Einwich. SystemC-AMS requirements, design objectives and rationale. In *Design, Automation and Test in Europe Conference and Exhibition, 2003*, pages 388–393, 2003. ISSN 1530-1591, ISBN 0-7695-1870-2.

[119] H. Al-junaid and T. J. Kazmierski. SEAMS - a SystemC environment with analog and mixed-signal extensions. In *Circuits and Systems, 2004. ISCAS '04. Proceedings of the 2004 International Symposium on*, volume 5, pages V–281–V–284, 2004. ISBN 0-7803-8251-x.

[120] OVI. Verilog HDL Language Reference Manual v1.0, 1991.

[121] 1076-2002 iEEE standard VHDL language reference manual, 2002. ISBN 0-7381-3247-0.

[122] Accelera. Verilog-AMS Language Reference Manual. Analogue and mixed signal extensions to Verilog HDL. version 2.2, 2004.

[123] H. Ming-ta and G. E. Sobelman. Modeling and verification of high-speed wired links with verilog-ams. In *Circuits and Systems, 2006. ISCAS 2006. Proceedings. 2006 IEEE International Symposium on*, page 4, 2006. ISBN 0-7803-9389-9.

[124] F. Pecheux C. Lallement and A. Vachoux. Vhdl-ams and verilog-ams as alternative hardware description languages for efficient modeling of multidiscipline systems. *Computer-Aided Design of Integrated Circuits and Systems, IEEE Transactions on*, Vol. 24(2):204–225, 2005. ISSN 0278-0070.

[125] A. R. Djordjevic M. B. Bazdar T. K. Sarkar and R. F. Harrington. *LINPAR for Windows: Matrix Parameters for Multiconductir Transmission Lines, Software and User's Manual, Version 2.0 Book and Disk edition.* Artech House Publishers, 1999.

[126] M. R. Burford and T. J. Kazmierski. A VHDL-AMS based time domain skin depth model for edge coupled lossy transmission stripline. In *Forum on Specification and Design Languages (ECSI-FDL05),*, pages 197–208, Lausanne, Switzerland, 2005. ISSN 1636-9874.

[127] S. A. Bokhari. Radiation from differential printed traces. In *Electromagnetic Compatibility, 2001. EMC. 2001 IEEE International Symposium on*, volume 1, pages 552–554, Montreal, 2001. ISBN 0-7803-6569-0.

[128] P. Acimovic. Novel band stop common mode filter for high speed digital data transmission. In *DesignCon 2007*, Santa Clara, CA, 2007.

[129] Eagleware-Elanix. Product note: Electrical to physical with advanced tline, 2002. PN13.

[130] Hittite Microwave Corporation. Designing with the HMC414MS8G PA using a low cost laminated printed circuit board, 2003. v.00.01.03.

[131] G. Wevers. A low-cost, two-stage low noise amplifier for 5 GHz to 6 GHz applications using the silicon-germanium BFP640 transistor,. *RF Design*, Vol. November 2003:12–28, 2003.

[132] D. M. Sheen S. M. Ali M. D. Abouzahra and J. A. Kong. Application of the three-dimensional finite-difference time-domain method to the analysis of planar microstrip circuits. *Microwave Theory and Techniques, IEEE Transactions on*, Vol. 38(7):849–857, 1990. ISSN 0018-9480.

[133] D. E. Bockelman and W. R. Eisenstadt. Combined differential and common-mode scattering parameters: theory and simulation. *Microwave Theory and Techniques, IEEE Transactions on*, 43(7):1530–1539, 1995. 0018-9480.

[134] R. J. P. Douville and D. S. James. Experimental study of symmetric microstrip bends and their compensation. *Microwave Theory and Techniques, IEEE Transactions on*, Vol. 26(3):175–182, 1978. ISSN 0018-9480.

Appendix A

Publications

M. Burford and T. Kazmierski, (2005) A VHDL-AMS Based Time Domain Skin Depth Model for Edge Coupled Lossy Transmission Stripline. In Proceedings of Forum on Specification and Design Languages (ECSI-FDL'05), ISSN 1636-9874, pp. 197-208, Lausanne, Switzerland, 27-30 September 2005.

M. Burford, P. Levin and T. Kazmierski, (2007) Skew and EMI Management in Differential Microstrip Lines up to 15GHz. In proceedings of Signal Propagation on Interconnects, ISBN 0-7803-7051-1, pp. 188-191, Genoa, Italy, 13-16 May 2007.

M. Burford, P. Levin and T. Kazmierski, (2008) Temporal Skew and Mode Conversion Management in Differential Pairs to 15GHz. Electronics Letters, ISSN 0013-5194, Vol. 44, Issue 1, pp. 35-37, January 3 2008.

Appendix B

VHDL-AMS Code for Signal Dependent Transmission Line Model

Testbenches for broad, edge and microstrip coupled lines

```
--AUTHOR:   Mark R Burford MEng (Hons) MIEE
--POSITION: Research Engineer
--PROJECT:  T-LINES
--latest update 02/09/2005
--MODULE:   broad
--
--Uses lumped laterally and distributed longitudinally RCLG t-line model
--
--User can define:  PHYSICAL DIMENSIONS OF LINE:  length, width, height and line
--seperation
--
-----------------------------------------------------------------
--HOW TO USE--
-----------------------------------------------------------------
--
-- 1>  Enter t-line dimensions with decimal points in metres;
-- 2>  Enter max. frequency of signal of the form 1GHz = 1.0e9;
-- 3>  Select a stimulus by un/commenting at end of code;
-- 4>  Simulate!  Long lengths and high frequencies may take hours!
--
-----------------------------------------------------------------

library IEEE_proposed;
use IEEE_proposed.electrical_systems.all;
library ieee;
use ieee.math_real.all;

entity broad_tb is
    generic(
        length      :   real    := 0.125; -- Length of trace
        freq        :   real    := 2.5e9; --Max frequency of operation
        UI_pc       :   real    := 0.125; --% of UI for tr & tf
        offset      :   real    := 0.0;
        amplitude   :   voltage := 0.8; --Amplitude of source
        height_ic   :   real    := 0.0000356; --1.4mil trace thickness
        width_ic    :   real    := 0.0001651; --6.5mil trace width
        h1          :   real    := 0.0007798; --30.7mil
        h2          :   real    := 0.0007798;
        line_sep    :   real    := 0.0003048; --12mil Seperation of lines
        roe         :   real    := 1.673e-8; -- Resistivity of trace
        Ur          :   real    := 1.0; --Relative permeability
        Er          :   real    := 4.0; --Relative permativity
```

```
        r_src       :   resistance := 1.0; -- First R in line
        r_load      :   resistance := 50.0; -- Load resistance of line
        g_line      :   real    := 1.0e11; -- conductance of FR4
        tan_delta   :   real    := 0.02; -- Loss tangent of dielectric
        surface_rms :   real := 1.0e-6      --Surface roughness rms in m
        );
end entity broad_tb;

architecture broad_tb_arch of broad_tb is

--TOP LEVEL TERMINALS
    terminal tin1, tin2, tout1, tout2   : electrical;

--QUANTITIES OF INTEREST (line parameters)
    quantity l_m_q  : inductance;
    quantity l_q    : inductance;
    quantity c_q    : capacitance;
    quantity cm_q   : capacitance;
    quantity Z0_odd_q : resistance;
    quantity rdc_q  : resistance;

--SECTIONS CALCULATION
    constant E0     : capacitance   := 8.85419e-12; --permittivity in vacuum F/m
    constant C      : real          := 3.0e8; --Speed of light in vacuum in m/s
    constant tr     : real          :=  ((1.0/freq)*UI_pc);  --tr == 1/8 UI
    constant sections : real  := Length*(SQRT(Er)) / (0.1 * tr * C);
                                                --sections as a 'real'

    constant U0     : real      := 1.2566e-6;       --permeability of free space
    constant PI     : real      := 3.141592653589; --Pi
    constant skin_onset : real  := amplitude/(UI_pc*(1.0/((1.0/(2.0*PI))*
    ((8.0*roe)/U0)*((width_ic+height_ic)/(width_ic*height_ic))**2)));

    constant skin_depth : real      := SQRT(roe/(PI*freq*U0*Ur));
    --constant Resist   : resistance:=
(1.678e-8)/(2.0*skin_depth*(width_ic+height_ic-(2.0*skin_depth)));

    constant resist         : real  := roe/(width_ic*height_ic);
    constant sr_onset       : real  := 1.0/(U0*PI*(1.0/roe)*(surface_rms**2));

    constant Z0_odd : resistance:=
                        (60.0/SQRT(Er))*log((1.9*b)/((0.8*width_ic)+height_ic));

--INDUCTANCE EQUATIONS
```

```
    constant delay_line   : real  := 1.0/(C/SQRT(Er));      --secs/m
    constant l_line       : inductance:= delay_line*Z0_odd; --Inductance of a line
--CAPACITANCE EQUATIONS
    constant c_line1      : capacitance:= 1.0/((z0_odd**2)/l_line);
    constant a            : real      := (1.0/(tanh(0.5*PI*(line_sep/b)))); -- a

    constant cap_m        : capacitance:=
                              -((2.0*E0*Er)/PI)*(1.0+2.66*(height_ic/b))*log(a);
--To find Lm....
    constant c_sum          : capacitance:= c_line1+cap_m;
    constant l_diff         : inductance := (Z0_odd**2)*c_sum;
    constant l_m            : inductance := (l_line - l_diff);

---Differential Impedance
    constant capac_fringing : capacitance:=

    Er*E0*(b/(line_sep*PI))*((log(b/(b-line_Sep))+((line_sep/(b-line_sep))
    *log(b/line_sep))));

    constant Zchar_cohn_diff: resistance :=
    (188.3*(b-line_sep)*line_sep)/(SQRT(Er)*((width_ic*b)+((capac_fringing/(E0*Er))
                           *line_sep*b)-((capac_fringing/(E0*Er))*line_sep**2.0)));

------Total capacitance of a line
    constant C_tot_line     : capacitance:= (3.30894e-9*SQRT(Er))/Zchar_cohn_diff;
------Coupling capac
    constant Cc             : capacitance:=
    ((E0*Er)/(2.0*PI))*(((1.0+(height_ic/line_sep))*
    log(1.0+(height_ic/line_sep)))-(height_ic/line_sep)*log(height_ic/line_sep));

------Total corrected capacitance of line
    constant C_tot_line1    : capacitance:= C_tot_line+(4.0*Cc);
-----New Differential Impedance
    constant Zchar_diff1    : resistance := (3.30894e-9*SQRT(Er))/C_tot_line1;

--DIELECTRIC ABSORPTION EQUATIONS
    constant gd_w       : real := 2.0*PI*tan_delta*c_line1; --in S/m.Hz
    signal init         : real := 2.0; --offset+amplitude;

begin

--PRINT QUANTITIES
l_m_q   == l_m;
l_q     == l_line;
```

```
c_q     == c_line1;
cm_q    == cap_m;
Z0_odd_q == Z0_odd;
rdc_q == resist;
--r_skin_q == Resist;
--gd_w_q    == gd_w*freq;
--skin_onset_q == skin_onset;

    n_sect : entity work.broad_gen
        generic map(
            res => (Resist*length)/(sections+2.0), --to see const freq resist.
            r_src => r_src,
            r_load => r_load,
            con => (g_line*length)/(sections+2.0),
            gd_w => (gd_w*length)/(sections+2.0),
            length => length,
            height => height_ic,
            width => width_ic,
            roe => roe,
            skin_onset => skin_onset,
            sr_onset => sr_onset,
            surface_rms => surface_rms,
            Ur => Ur,
            ind1 => (l_line*length)/(sections+2.0), --+2 for 1st and last sections
            ind2 => (l_line*length)/(sections+2.0),
            indmut => (l_m*length)/(sections+2.0),
            cap1 => (c_line1*length)/(sections+2.0),
            cap2 => (c_line1*length)/(sections+2.0),
            cap_m => (-cap_m*length)/(sections+2.0),
            amp => amplitude, --also passed to FDR
            sections => sections
            )
        port map(
            init => init,
            tin1 => tin1,
            tin2 => tin2,
            tout1 => tout1,
            tout2 => tout2,
            tref => ELECTRICAL_REF
            );

--STIMULI, SELECT IN PAIRS

--  vin1 : entity work.v_pwl_posnew_2_5ghz
```

```
--      generic map(off => 1.2, amp => amplitude)
--      port map(pos => tin1, neg => ELECTRICAL_REF);
--  vin2 : entity work.v_pwl_negnew_2_5ghz
---     generic map(off => 1.2, amp => amplitude)
--      port map(pos => tin2, neg => ELECTRICAL_REF);
--
--  vsin1 : entity work.v_sine
--      generic map(freq => freq, amplitude => amplitude,
--          phase => 90.0, offset => 1.2)
--      port map(pos => tin1, neg => ELECTRICAL_REF);
--  vsin2 : entity work.v_sine
--      generic map(freq => freq, amplitude => amplitude,
--          phase => 270.0, offset => 1.2)
--      port map(pos => tin2, neg => ELECTRICAL_REF);
----
--  vpulse : entity work.vpulse_2_5ghz
--      generic map(
--          amp => amplitude, off => 1.2
--          )
--      port map(
--          pos => tin1, neg => ELECTRICAL_REF
--          );
--  vpulse1 : entity work.vpulsepos_2_5ghz
--      generic map(
--      amp => amplitude, off => 1.2
--          )
--      port map(
--          pos => tin2, neg => ELECTRICAL_REF
--          );

    vstep : entity work.vstepneg_2_5ghz
        generic map(amp => amplitude, off=>offset)
        port map(pos => tin1, neg => ELECTRICAL_REF);
--- vstep1 : entity work.vstepos_2_5ghz
--      generic map(amp => amplitude, off=>offset)
--      port map(pos => tin2, neg => ELECTRICAL_REF);
---
end architecture broad_tb_arch;

--------------------------------
--EDGE COUPLED TESTBENCH-------
--------------------------------

--AUTHOR:   Mark R Burford MEng (Hons) MIEE
```

```
--POSITION: Research Engineer
--PROJECT:  T-LINES
--latest  on  02/09/2005
--MODULE:   edge
--
--        ------------------------------------
--    /\   width_ic  line_sep  /\
--    |     <------> <------>   |h2
--    |      _______        _\/____
--    |     |       |       |       |/\
--    |     |_______|       |_______|\/height_ic
--    plate_sep            /\
--    \/=h1+h2+height_ic   \/h1
--        ------------------------------------
--
--Uses lumped laterally and distributed longitudinally RCLG t-line model
-----------------------------------------------------------------
--HOW TO USE--
-----------------------------------------------------------------
-- 0>  Connect outside world to 'tin1' and 'tin2' with ground (ELECTRICAL_REF)
-- 1>  Enter t-line dimensions with decimal points.
-- 2>  Enter max. frequency of signal of the form 1GHz = 1.0e9;
-- 3>  Select a stimulus by un/commenting at end of code;
-- 4>  Simulate!  Long lengths and high frequencies may take hours!
--To view constants or signals just add a quantity and map it with
 'quantities of interest'
-----------------------------------------------------------------

library IEEE_proposed;
use IEEE_proposed.electrical_systems.all;
library ieee;
use ieee.math_real.all;

entity fdr_lw_gw_tb is
    generic(
        length      :   real := 0.125;      -- Length of trace / m
        freq        :   real := 2.5e9;      -- Max frequency of operation/Hz
        UI_pc       :   real := 0.125;      -- % of UI for tr & tf
        offset      :   real := 0.0;
        amplitude   :   voltage := 0.8;     -- Amplitude of source / V
        height_ic   :   real := 0.000018;   -- 0.7mil trace thickness / m
        width_ic    :   real := 0.0002032;  -- 8mil trace width / m
        h1          :   real := 0.000435;   -- 17.1mil gnd to line1 / m
        h2          :   real := 0.000435;   -- 17.1mil other gnd to line2 / m
```

```
        line_sep    :   real := 0.0003048;  -- 12mil Separation of lines / m
        roe         :   real := 1.673e-8;   -- Resistivity of trace Ohm m
        Ur          :   real := 1.0;        -- Relative permeability
        Er          :   real := 4.0;        -- Relative permittivity
        r_src       :   resistance := 1.0;  -- First R in line / Ohm
        r_load      :   resistance := 50.0; -- Load resistance of line /Ohm
        g_line      :   real := 1.0e11;     -- conductance of FR4 / S
        tan_delta   :   real := 0.02;       -- Loss tangent of dielectric
        surface_rms :   real := 1.0e-6      -- Surface roughness rms in m
        );
end entity fdr_lw_gw_tb;

architecture fdr_lw_gw_tb_arch of fdr_lw_gw_tb is

--TOP LEVEL TERMINALS
    terminal tin1, tin2, tout1, tout2   : electrical;

--QUANTITIES OF INTEREST (line parameters)
    quantity l_m_q  : inductance;
    quantity l_q    : inductance;
    quantity c_q    : capacitance;
    quantity cm_q   : capacitance;
    quantity Z0_q   : resistance;
    quantity rdc_q  : resistance;
--  quantity Z0_diff_q : resistance;
--  quantity r_skin_q  : resistance;
--  quantity gd_w_q : real;
--  quantity sr_ons : real;

--SECTIONS CALCULATION
    constant E0         : capacitance:= 8.85419e-12;
                                        --permittivity in vacuum F/m
    constant C          : real       := 3.0e8;
                                        --Speed of light in vacuum in m/s
    constant tr         : real       := ((1.0/freq)*UI_pc); --tr == 1/8 UI
    constant sections   : real       := Length*(SQRT(Er)) / (0.1 * tr * C);
                                                --sections as a 'real'

    constant U0             : real  := 1.2566e-6; --permeability of free space
    constant PI             : real  := 3.141592653589; --Pi
    constant skin_onset     : real  :=
                    amplitude/(UI_pc*(1.0/((1.0/(2.0*PI))*((8.0*roe)/U0)*
                    ((width_ic+height_ic)/(width_ic*height_ic))**2)));
--  constant skin_depth     : real  := SQRT(roe/(PI*freq*U0*Ur));
```

```
--  constant resist          : resistance:=
                               (1.76*(1.678e-8)/(2.0*skin_depth*(width_ic+
                               height_ic-(2.0*skin_depth))));

    constant resist          : resistance:= (roe)/(width_ic*height_ic);
    constant sr_onset        : real  := 1.0/(U0*PI*(1.0/roe)*(surface_rms**2));

--CHARACTERISTIC IMPEDANCE OF EDGE COUPLED TRIPLATE
    constant b               : real      := (h1+h2+height_ic);
    constant z0_odd          : resistance :=
                        (60.0/SQRT(Er))*log((1.9*b)/((0.8*width_ic)+height_ic));
                        --replace 0.347 with 0.748 for s <12
--  constant z0_diff         : resistance :=
                        2.0*Z0_odd*(1.0-0.748*exp(-2.9*(line_sep/h1)));

--INDUCTANCE EQUATIONS
    constant delay_line      : real       := 1.0/(C/SQRT(Er)); -- secs/m
    constant l_line          : inductance := delay_line*Z0_odd;
                                    -- Inductance of a line in nH/m

--CAPACITANCE EQUATIONS
    constant c_line1         : capacitance:= 1.0/((z0_odd**2)/l_line);
    constant a               : real       := (1.0/(tanh(0.5*PI*(line_sep/b))));

    constant cap_m  :capacitance:=
                             -((2.0*E0*Er)/PI)*(1.0+2.66*(height_ic/b))*log(a);

--To find Lm....
    constant c_sum           : capacitance:= c_line1+cap_m;
    constant l_diff          : inductance := (Z0_odd**2)*c_sum;
    constant l_m             : inductance := (l_line - l_diff);

--DIELECTRIC ABSORPTION EQUATIONS
    constant gd_w            : real := tan_delta*c_line1;
                                       -- in S/m.Hz so multiply by freq later

begin

--PRINT QUANTITIES
l_m_q == l_m;
l_q == l_line;
c_q == c_line1;
cm_q == cap_m;
Z0_q == Z0_odd;
```

```
--Z0_diff_q == Z0_diff;
rdc_q == resist;
--r_skin_q == (resist*length)/(sections+2.0);
--gd_w_q == gd_w*freq*2.0*PI; -- for sinusoidal simulation
--sr_ons == sr_onset;


    n_sect : entity work.fdr_lw_gw_gen
        generic map(
            res => (Resist*length)/(sections+2.0), --to see const freq resist.
            r_src => r_src,                        --1st 50ohm resistor
            r_load => r_load,                      --load resistor
            con => (g_line*length)/(sections+2.0), --DC conductance map
            gd_w => (gd_w*length)/(sections+2.0),  --AC conductance map
            length => length,
            height => height_ic,
            width => width_ic,
            roe => roe,
            skin_onset => skin_onset,              --skin onset freq
            sr_onset => sr_onset,
            surface_rms => surface_rms,
            Ur => Ur,
            ind1 => (l_line*length)/(sections+2.0), --+2 for 1st and last sections
            ind2 => (l_line*length)/(sections+2.0),
            indmut => (l_m*length)/(sections+2.0),
            cap1 => (c_line1*length)/(sections+2.0),
            cap2 => (c_line1*length)/(sections+2.0),
            cap_m => (-cap_m*length)/(sections+2.0),
            amp => amplitude,                      --also passed to SDR
            sections => sections
            )
        port map(
            init => init,
            tin1 => tin1,
            tin2 => tin2,
            tout1 => tout1,
            tout2 => tout2,
            tref => ELECTRICAL_REF
            );

--STIMULI, SELECT IN PAIRS

--  vin1 : entity work.v_pwl_posnew_2_5ghz
--      generic map(off => offset,  amp => amplitude)
```

```
--      port map(pos => tin1, neg => ELECTRICAL_REF);
--  vin2 : entity work.v_pwl_negnew_2_5ghz
--  generic map(off => offset,  amp => amplitude)
--      port map(pos => tin2, neg => ELECTRICAL_REF);
--
--  vsin1 : entity work.v_sine
--      generic map(freq => freq, amplitude => amplitude,
--          phase => 90.0, offset => offset)
--      port map(pos => tin1, neg => ELECTRICAL_REF);
--
--  vsin2 : entity work.v_sine
--      generic map(freq => freq, amplitude => amplitude,
--          phase => 270.0, offset => offset)
--      port map(pos => tin2, neg => ELECTRICAL_REF);

--  vpulse : entity work.vpulse_2_5ghz
--      generic map(amp => amplitude, off => offset)
--      port map(
--          pos => tin1, neg => ELECTRICAL_REF
--          );
--  vpulse1 : entity work.vpulsepos_2_5ghz
--      generic map(
--          amp => amplitude, off => offset
--          )
--      port map(
--          pos => tin2, neg => ELECTRICAL_REF
--          );
----
    step : entity work.vstepneg_2_5ghz
        generic map(
            amp => amplitude, off => offset)
        port map(
            pos => tin1, neg => ELECTRICAL_REF);
--  vstep1 : entity work.vstepos_2_5ghz
--      generic map(
--          amp => amplitude, off => offset)
--      port map(
--          pos => tin2, neg => ELECTRICAL_REF);


end architecture fdr_1w_gw_tb_arch;


-----------------------------------------
```

```
TESTBENCH FOR MICROSTRIP
-----------------------------------------

--AUTHOR:   Mark R Burford MEng (Hons) MIEE
--POSITION: Research Engineer
--PROJECT:  T-LINES
--latest  update 02/09/2005
--MODULE:   MICROSTRIP
--
--
--       width_ic  line_sep
--         <------> <------>
--          _______          _______
--         |       |        |       |/\
--         |_______|        |_______|\/height_ic
--    /\
--     |
--     |
--    \/h1
--    ----------------------------------
--
-------------------------------------------------------------------
--HOW TO USE--
-------------------------------------------------------------------
-- 0>  Connect outside world to 'tin1' and 'tin2' with ground
-- 1>  Enter t-line dimensions with decimal points.
-- 2>  Enter max. frequency of signal of the form 1GHz = 1.0e9;
-- 3>  Select a stimulus by un/commenting at end of code;
-- 4>  Simulate!  Long lengths and high frequencies may take hours!
--To view constants or signals just add a quantity and map it with
 'quantities of interest'
-------------------------------------------------------------------

library IEEE_proposed;
use IEEE_proposed.electrical_systems.all;
library ieee;
use ieee.math_real.all;

entity fdr_lw_gw_tb is
    generic(
        length      :   real := 0.125;      -- Length of trace / m
        freq        :   real := 2.5e9;      -- Max frequency of operation / Hz
        UI_pc       :   real := 0.125;      -- % of UI for tr & tf
        offset      :   real := 0.0;
```

```
        amplitude   :   voltage := 0.8;      -- Amplitude of source / V
        height_ic   :   real := 0.000035;    -- 1.4mil trace thickness / m
        width_ic    :   real := 0.0003;      -- 12mil trace width / m
        h1          :   real := 0.0005;      -- 20mil gnd to line1 / m
        h2          :   real := 0.000435;    -- 17.1mil other gnd to line2 / m
        line_sep    :   real := 0.000152;    -- 6mil Separation of lines / m
        roe         :   real := 1.673e-8;    -- Resistivity of trace Ohm m
        Ur          :   real := 1.0;         -- Relative permeability
        Er          :   real := 4.5;         -- Relative permittivity
        r_src       :   resistance := 1.0;   -- First R in line / Ohm
        r_load      :   resistance := 50.0; -- Load resistance of line /Ohm
        g_line      :   real := 1.0e11;      -- conductance of FR4 / S
        tan_delta   :   real := 0.02;        -- Loss tangent of dielectric
        surface_rms :   real := 1.0e-6       -- Surface roughness rms in m
        );
end entity fdr_lw_gw_tb;

architecture fdr_lw_gw_tb_arch of fdr_lw_gw_tb is

--TOP LEVEL TERMINALS
    terminal tin1, tin2, tout1, tout2   : electrical;

--QUANTITIES OF INTERTEST (line parameters)
    quantity l_m_q  : inductance;
    quantity l_q    : inductance;
    quantity c_q    : capacitance;
    quantity cm_q   : capacitance;
    quantity Z0_q   : resistance;
    quantity r_dc_q : resistance;
    quantity c_sum_q : capacitance;
    quantity Z0_diff_q : resistance;
--  quantity r_skin_q : resistance;
--  quantity gd_w_q : real;
--  quantity sr_ons : real;

--SECTIONS CALCULATION
    constant E0         : capacitance:= 8.85419e-12;
                                          --permittivity in vacuum F/m
    constant C          : real  := 3.0e8; --Speed of light in vacuum in m/s
    constant tr         : real  := ((1.0/freq)*UI_pc); --tr == 1/8 UI
    constant sections   : real  := Length*(SQRT(Er)) / (0.1 * tr * C);
                                            --sections as a 'real'

    constant U0             : real  := 1.2566e-6;   --permeability of free space
```

```
    constant PI             : real  := 3.141592653589; --Pi
    constant skin_onset     : real  := amplitude/(UI_pc*(1.0/((1.0/(2.0*PI))*
    ((8.0*roe)/U0)*((width_ic+height_ic)/(width_ic*height_ic))**2)));
--  constant skin_depth     : real  := SQRT(roe/(PI*freq*U0*Ur));
--  constant resist         : resistance:=
            (1.678e-8)/(2.0*skin_depth*(width_ic+height_ic-(2.0*skin_depth))));
--  constant resist         : resistance := roe/(width_ic*height_ic);
    constant sr_onset       : real  := 1.0/(U0*PI*(1.0/roe)*(surface_rms**2));

--CHARACTERISTIC IMPEDANCE OF EDGE COUPLED MICROSTRIP
    constant b              : real       := (h1);
    constant z0_odd         : resistance := (60.0/SQRT((0.457*Er)+0.67))*
                                    log((4.0*b)/(0.67*(0.8*width_ic)+height_ic));
                                        --replace 0.347 with 0.748 for s <12

    constant z0_diff : resistance :=
                            (2.0*Z0_odd)*(1.0-(0.48*exp(-0.96*(line_sep/b))));

--INDUCTANCE EQUATIONS
--  constant delay_line     : real := 1.0/(C/SQRT(Er));     --secs/m
    constant l_line         : inductance :=
          U0*Ur*(((3.71*((h1/width_ic)**0.041))+(0.018*((h1/width_ic)**(-0.73)))
          -(3.39*((h1/height_ic)**0.0006))) + (EXP(-1.89*(line_sep/h1)))*
          ((0.75*((h1/width_ic)**(-0.0052)))-(0.84*((h1/height_ic)**(-0.026)))));

--  constant l_m  : inductance :=
U0*Ur*((((-0.415*((h1/width_ic)**(-0.16)))-(2.38*((height_ic/width_ic)**1.18))  )
*((((line_sep/h1)+1.07)**(-2.6))) ) + (  (((line_sep/h1)+0.89)**(-2.03))*
  ((0.418*((h1/width_ic)**(0.13)))+ (1.37*((height_ic/width_ic)**1.09))  )   )   );

--CAPACITANCE EQUATIONS
constant a              : real      := (1.0/(tanh(0.5*PI*(line_sep/b))));
                                                -- a constant
constant cap_m  : capacitance:=
-((2.0*E0*Er)/PI)*(1.0+2.66*(height_ic/b))*log(a);
constant c_sum : capacitance := E0*Er*( ( (1.15*((width_ic/h1)**0.963))+
(1.07*((height_ic/h1)**0.049))) + (  (EXP(-3.52*(line_sep/h1)))*
((0.75*((width_ic/h1)**0.25))+(2.7*((height_ic/h1)**1.36)))  )   );
constant c_line1 : capacitance:= c_sum - cap_m;

--To find Lm....
    constant l_diff         : inductance := (z0_diff**2)*(-cap_m);
    --constant l_diff       : inductance := (Z0_odd**2)*c_sum;
    constant l_m            : inductance := (l_line - l_diff);
```

```
--DIELECTRIC ABSORPTION EQUATIONS
    constant gd_w     : real := 2.0*PI*freq*tan_delta*c_line1;
                                        --in S/m.Hz so multiply by freq later
    signal init       : real := offset+amplitude;
begin

--PRINT QUANTITIES
l_m_q == l_m;
l_q == l_line;
c_q == c_line1;
cm_q == cap_m;
Z0_q == Z0_odd;
Z0_diff_q == Z0_diff;
r_dc_q == resist;
c_sum_q == c_sum;
--r_skin_q == (resist*length)/(sections+2.0);
--gd_w_q == ((gd_w)*length)/(sections+2.0); -- for sinusoidal simulation
--sr_ons == sr_onset;


    n_sect : entity work.fdr_lw_gw_gen
        generic map(
        --  res => (resist*length)/(sections+2.0),  --to see const freq resist.
            r_src => r_src,                         --1st 50ohm resistor
            r_load => r_load,                       --load resistor
            con => (g_line*length)/(sections+2.0),  --DC conductance map
            gd_w => (gd_w*length)/(sections+2.0),   --AC conductance map
            length => length,
            height => height_ic,
            width => width_ic,
            roe => roe,
            skin_onset => skin_onset,               --skin onset freq
            sr_onset => sr_onset,
            surface_rms => surface_rms,
            Ur => Ur,
            ind1 => (l_line*length)/(sections+2.0), --+2 for 1st & last sections
            ind2 => (l_line*length)/(sections+2.0),
            indmut => (l_m*length)/(sections+2.0),
            cap1 => (c_line1*length)/(sections+2.0),
            cap2 => (c_line1*length)/(sections+2.0),
            cap_m => (-cap_m*length)/(sections+2.0),
            amp => amplitude,                       --also passed to SDR
            sections => sections
```

```
            )
        port map(
            init => init,
            tin1 => tin1,
            tin2 => tin2,
            tout1 => tout1,
            tout2 => tout2,
            tref => ELECTRICAL_REF
            );

--STIMULI, SELECT IN PAIRS

    vin1 : entity work.v_pwl_posnew_2_5ghz
        generic map(off => 1.2, amp => amplitude)
        port map(pos => tin1, neg => ELECTRICAL_REF);
    vin2 : entity work.v_pwl_negnew_2_5ghz
        generic map(off => 1.2, amp => amplitude)
        port map(pos => tin2, neg => ELECTRICAL_REF);

--  vsin1 : entity work.v_sine
--      generic map(freq => freq, amplitude => amplitude,
--          phase => 90.0, offset => 1.2)
--      port map(pos => tin1, neg => ELECTRICAL_REF);
--  vsin2 : entity work.v_sine
--      generic map(freq => freq, amplitude => amplitude,
--          phase => 270.0, offset => 1.2)
--      port map(pos => tin2, neg => ELECTRICAL_REF);
--  vpulse : entity work.vpulse_2_5ghz
--      generic map(amp => amplitude, off => 1.2)
--      port map(
---         pos => tin1, neg => ELECTRICAL_REF
--          );
--  vpulse1 : entity work.vpulsepos_2_5ghz
--      generic map(
--          amp => amplitude, off => 1.2
--          )
--      port map(
--          pos => tin2, neg => ELECTRICAL_REF
--          );
--
--  step : entity work.vstepneg_2_5ghz
--      generic map(
--          amp => amplitude)
--      port map(
```

```
--          pos => tin1, neg => ELECTRICAL_REF);
--  vstep1 : entity work.vstepos_2_5ghz
--      generic map(
--          amp => amplitude)
--      port map(
--          pos => tin2, neg => ELECTRICAL_REF);


end architecture fdr_lw_gw_tb_arch;
```

Appendix B.2

Generation Module

```
library IEEE_proposed;
use IEEE_proposed.electrical_systems.all;

library ieee;
use ieee.math_real.all;

entity fdr_lw_gw_gen is
    generic(
        res  : resistance;
        r_src    : resistance;   -- src resistance
        r_load   : resistance;   -- load resist
        con      : resistance;   -- conductance
        gd_w     : real;
        length   : real;
        height   : real;
        width    : real;
        roe      : real;
        skin_onset  : real;
        sr_onset: real;
        surface_rms : real;
        Ur       : real;
        cap1     : capacitance;  -- capacitance
        cap2     : capacitance;
        ind1     : inductance;   -- inductance
        ind2     : inductance;
        indmut   : inductance;
        cap_m    : capacitance;  -- mutual capacitance
        amp      : real;         -- signal amplitude
        sections: real           -- no' sections
        );
    port( --connect a vector up in the port here.
    init: in real;
        terminal tin1, tin2, tout1, tout2, tref : electrical
        );
end entity fdr_lw_gw_gen ;
```

```
architecture fdr_lw_gw_gen_arch of fdr_lw_gw_gen is

    constant int_sections : integer := integer(sections);

    terminal t1, t2 : electrical_vector(1 to (int_sections + 1));
    terminal t_r_src1, t_r_src2 : electrical;

    quantity vrs1 across irs1 through tin1 to t_r_src1;
    quantity vrs2 across irs2 through tin2 to t_r_src2;
    quantity vrl1 across irl1 through tout1 to tref;
    quantity vrl2 across irl2 through tout2 to tref;

    signal tfr : real_vector(0 to ((2*(int_sections+1))+2)):= (others=>0.0);


begin


vrs1 == irs1*r_src;
vrs2 == irs2*r_src;
vrl1 == irl1*r_load;
vrl2 == irl2*r_load;

--FIRST SECTION
    first_sect : entity work.fdr_lw_gw_nlist
    generic map(
        res => res,
        con => con,
        gd_w => gd_w,
        length => length,
        height => height,
        width => width,
        roe => roe,
        skin_onset => skin_onset,
        sr_onset => sr_onset,
        surface_rms => surface_rms,
        Ur => Ur,
        ind1 => ind1,
        ind2 => ind2,
        indmut => indmut,
        cap1 => cap1,
        cap2 => cap2,
        cap_m => cap_m,
        amp => amp,
```

```
        sections => sections + 2.0
        )
    port map(
        a_in1 => init,
        a_in2 => init,
        a_out1 => tfr(1),
        a_out2 => tfr(2),
        T_in1 => t_r_src1,
        T_in2 => t_r_src2,
        T_out1 => t1(1),
        T_out2 => t2(1),
        T_ref => ELECTRICAL_REF
        );

--MIDDLE SECTIONS GENERATION
    mid_sect : for i in 1 to (int_sections) generate
        s_rest : entity work.fdr_lw_gw_nlist
        generic map(
            res => res,
            con => con,
            gd_w => gd_w,
            length => length,
            height => height,
            width => width,
            roe => roe,
            skin_onset => skin_onset,
            sr_onset => sr_onset,
            surface_rms => surface_rms,
            Ur => Ur,
            ind1 => ind1,
            ind2 => ind2,
            indmut => indmut,
            cap1 => cap1,
            cap2 => cap2,
            cap_m => cap_m,
            amp => amp,
            sections => sections+2.0
            )
        port map(
            a_in1 => tfr((2*i)-1),
            a_in2 => tfr((2*i)),
            a_out1 => tfr((2*i)+1),
            a_out2 => tfr((2*i)+2),
            T_in1 => t1(i),
```

```
            T_in2 => t2(i),
            T_out1 => t1(i+1),
            T_out2 => t2(i+1),
            T_ref => ELECTRICAL_REF
            );
    end generate;

--LAST SECTION
    last_section : entity work.fdr_lw_gw_nlist
    generic map(
        res => res,
        con => con,
        gd_w => gd_w,
        length => length,
        height => height,
        width => width,
        roe => roe,
        skin_onset => skin_onset,
        sr_onset => sr_onset,
        surface_rms => surface_rms,
        Ur => Ur,
        ind1 => ind1,
        ind2 => ind2,
        indmut => indmut,
        cap1 => cap1,
        cap2 => cap2,
        cap_m => cap_m,
        amp => amp,
        sections => sections+2.0

        )
    port map(
        a_in1 => tfr((2*(int_sections+1))-1),
        a_in2 => tfr(2*(int_Sections+1)),
        a_out1 => tfr((2*(int_sections+1))+1),
        a_out2 => tfr((2*(int_sections+1))+2),
        T_in1 => t1(int_sections + 1),
        T_in2 => t2(int_sections + 1),
        T_out1 => tout1,
        T_out2 => tout2,
        T_ref => ELECTRICAL_REF
        );

end architecture fdr_lw_gw_gen_arch;
```

Appendix B.3

Netlist Module

```
library IEEE_proposed;
use IEEE_proposed.electrical_systems.all;

entity fdr_lw_gw_nlist is

    generic (
    res      : resistance;
    con      : real;
    gd_w     : real;
    length   : real;
    height   : real;
    width    : real;
    roe      : real;
    skin_onset   : real;
    sr_onset: real;
    surface_rms : real;
    Ur       : real;
    cap1     : capacitance;  -- capacitance (no initial value)
    cap2     : capacitance;
    ind1     : inductance;   -- inductance (no initial value)
    ind2     : inductance;
    indmut   : inductance;
    cap_m    : capacitance;  -- mutual capacitance (no initial value)
    amp      : real;
    sections: real;
    il_ic    : real := real'low
    );
 port(
    a_in1, a_in2 : in real := 0.0;
    a_out1, a_out2 : out real := 0.0;
    terminal T_out1, T_out2 :  electrical;
    terminal T_in1, T_in2 :  electrical;
    terminal T_ref : electrical
    );
end entity fdr_lw_gw_nlist;
```

```
architecture fdr_lw_gw_nlist_arch of fdr_lw_gw_nlist is

    terminal T_R_L1, T_R_L2 : electrical;

begin
-----------------------------------
--FOR TESTING NO FDR
-----------------------------------
rn1: entity work.resistor
        generic map(res => res)
        port map(p1 => T_in1, p2 => T_R_L1);
    rn2: entity work.resistor
        generic map(res => res)
        port map(p1 => T_in2, p2 => T_R_L2);
-----------------------------------------

--  fdr1 : entity work.fdr_4
--      generic map(length => length, height => height,
--          width => width, roe => roe, skin_onset => skin_onset, sr_onset =>
--sr_onset, surface_rms => surface_rms, Ur => Ur, amp => amp, sections =>
--sections )
--      port map(p1 => T_in1, p2 => T_R_L1,
--          psense_in => T_in1, a_in=> a_in1, a_out=> a_out1);
--  fdr2 : entity work.fdr_4
--      generic map(length => length, height => height,
--          width => width, roe => roe, skin_onset => skin_onset, sr_onset =>
--sr_onset, surface_rms => surface_rms, Ur => Ur, amp => amp, sections =>
--sections)
--      port map(p1 => T_in2, p2 => T_R_L2,
--          psense_in => T_in2, a_in=> a_in2, a_out=>a_out2 );
--
    l1 : entity work.inductor
        generic map(
            ind => ind1, indmut => indmut
        )
        port map(
            p1 => T_R_L1, p2 => T_out1
        );

    l2 : entity work.inductor
        generic map(
            ind => ind2, indmut => indmut
        )
```

```
        port map(
            p1 => T_R_L2, p2 => T_out2
        );

    cg1 : entity work.capacitor
        generic map(
            cap => cap1
        )
        port map(
            p1 => T_out1, p2 => ELECTRICAL_REF
        );

    cg2 : entity work.capacitor
        generic map(
            cap => cap2
        )
        port map(
            p1 => T_out2, p2 => ELECTRICAL_REF
        );

    fdg1 : entity work.gd_w
        generic map(
            con => con, gd_w => gd_w, amp => amp
        )
        port map(
            p1 => T_out1, p2 => ELECTRICAL_REF
        );

    fdg2 : entity work.gd_w
        generic map(
            con => con, gd_w => gd_w, amp => amp
        )
        port map(
            p1 => T_out2, p2 => ELECTRICAL_REF
        );

    cmut : entity work.capacitor
        generic map(
            cap => cap_m
        )
        port map(
            p1 => T_out1, p2 => T_out2
        );
```

```
end architecture fdr_lw_gw_nlist_arch;
```

Appendix B.4

Signal Dependent Resistor (SDR)

```
--Signal Dependant Resistor sdr
--include essential libraries allowing required functionality within module
library IEEE_proposed; use IEEE_proposed.electrical_systems.all;
library IEEE; use IEEE.math_real.all; use IEEE.std_logic_1164.all;
entity sdr is -- begin Signal Dependent Resistor top level description
  generic(    -- generic parameters passed to all SDR modules
    length      : real;  -- Length of the line in metres
    height      : real;  -- Thickness of the line in metres
    width       : real;  -- Width of the line in metres
    abovegnd    : real;  -- Distance to the ground plane below the line in
                         -- metres
    roe         : real;  -- Resistivity
    skin_onset  : real;  -- Frequency at which skin effect begins affecting
                         -- loss in a way that gives a recognisable amount
                         -- of loss
    sr_onset    : real;  -- Frequency at which surface roughness begins
                         -- affecting loss in a way that gives a recognisable
                         -- amount of loss
    surface_rms : real;  -- The root mean squared roughness of the surface
    BW          : real;  -- The bandwidth of the signal under test
    Ur          : real;  -- Relative constant of permeability
    sections    : real := 1.0); -- The number of sections in total
  port( terminal p1, p2,        -- Electrical physical connections of resistor
   psense_in : electrical;      -- Sense input to read voltage at input with
                                -- respect to ground
    a_in :  real := 0.0;        -- Maximum amplitude read in from previous
                                -- section
    a_out : out real := 0.0);   -- Maximum amplitude read out to next section
end entity sdr;

architecture sdr of sdr is
  quantity v across i through p1 to p2; -- define voltage across and
                                        -- current through the module
  quantity vs across psense_in to ELECTRICAL_REF;  -- sense inputs
  -- find a baseline DC resistance:
  constant rdc    : resistance := ((roe*length)/(width*height))/(sections);
```

```
  constant U0     : real := 1.2566e-6; -- Constant of permeability
  constant sigma  : real := 5.96e07;   -- Conductivity of copper
  constant dv     : real := 0.005;     -- RESOLUTION = 5mV, the module will
                                       -- only re-evaluate if the sense voltage
                                       -- changes by +/- 5mV or more
  constant d_vdot : real := skin_onset; -- RESOLUTION  in V/s, the module will
                                        -- only re-evaluate if the rate of
                                        -- change of the signal changes by the
                                        -- skin onset frequency
  signal step_check_s : real := 0.0;    -- A check to ensure a minimum time has
                                        -- elapsed before running again, takes
                                        -- the time at the end of the proces
  signal a, Am_int : real := 0.0;       -- Used to record the present and
                                        -- highest signal amplitude in the
                                        -- section
  signal s_depth_old_s : real  := SQRT((roe/(3.141569*BW*U0))); -- the last
                                        -- value of calculated skin depth
  signal r        : resistance :=       -- the present value of resistance
         ((roe*length)/(width*(SQRT((roe/(3.141569*BW*U0))))))/(sections);
  signal start, run_once, clk  : boolean := FALSE; -- Signals ensuring module
                                                   -- runs correctly,
                                                   -- accurately and
                                                   -- efficiently
  signal threshold, vdotthresh : boolean := FALSE; -- Boolean resolution
                                                      monitors whose change
                                                      activates the module
  signal v_last                : voltage := 0.0;   -- The last value of the
                                                   -- voltage across the
                                                   -- resistor
  signal vdot_last             : real    := 0.0;   -- The last value of the
                                                   -- rate of change of
                                                   -- signal in the resistor
begin
-- The 'threshold' signal changes value when the present voltage across the
-- resistor differs from the previous value from the previous time the
-- module ran either positively or negatively by the defined resolution
  threshold <= not vs'above(v_last-dv) or vs'above(v_last+dv);
-- The 'vdotthresh' signal changes when the present value of rate of change
-- of signal differs from the previous value either positively or negatively
-- by the defined resolution
  vdotthresh <= not vs'dot'above(vdot_last - d_vdot) or
                    vs'dot'above(vdot_last + d_vdot);
-- The clk signal allows the module to run with no change of signal allowing
-- a DC state after a natural amount of time to preside.
```

```
  clk <= not clk after 0.2/BW*1.0e6us;

-- Any changes in the signals 'threshold' , 'vdotthresh' or 'clk' will cause
-- the process to re-evaluate where the new skin depth and resistance are
-- calculated.

-- New process referred to as 'new_sd' for NEW_SkinDepth'
new_sd : process (threshold, vdotthresh, clk) is
  variable step : real := 0.0; -- Temporary storage to ensure time has
                               -- progressed since last iteration
  variable s_depth_new, newr_v : real := 0.0; -- Holds the newly calculated
                                              -- skin depth and resistance
  variable start_v : boolean := FALSE         -- Checks if process has run
  -- 's_depth_v' provides an initial guess for the skin depth at the
  -- highest frequency or 'BW'
  variable s_depth_v : real := SQRT((roe/(3.141569*BW*U0)));

begin
step := NOW - step_check_s; -- 'NOW' contains the current time, step receives
                            -- the present time minus the time at the end of
                            -- the last iteration
if step > 1.0e-18 then     -- If the result of the previous line is greater than
                           -- the smallest time step possible it means some time
                           -- has passed and the process may re-evaluate else it
                           -- may evaluate the same parameters twice
if start = true then       -- Check to see if the process has run before, if it
                           -- hasn't there is not point running it as the module
                           -- does not yet does have correct values to run
  if (abs(vs) > Am_int) then -- If the present value of the voltage is greater
                             -- than the internally stored one, then the
                             -- internal one takes that value to pass out to
                             -- the next section
  Am_int <= abs(vs);
  end if;
  s_depth_new_v :=  -- Calculate the new value of skin depth
       SQRT((2.0*a*roe*SQRT(abs((a**2)-((vs**2)))))/(abs(vs'dot+1.0)*U0*Ur));

  -- Check to see if the new skin depth is greater than half of the metal
  -- thickness, much like a DC condition, if yes, allocate the DC resistance
  if (s_depth_new_v > (0.5*height)) then
    newr_v := rdc;

  -- If the new skin depth is less than the DC condition and greater than
  -- the previous value, increase the skin depth at a rate equal to the
```

```
  -- extrapolated linear equation that follows then allocate new resistance
  else if s_depth_new_v > s_depth_old_s then
    s_depth_v := s_depth_old_s + 4000.0*step;
    newr_v :=
    (((roe*length)/(s_depth_v*width))/(sections))*(1.0+(width/(6.0*abovegnd)));

  -- If the skin depth is less than the DC condition and less than the
  -- previous value, decrease the skin depth at a rate equal to the extrapolated
  -- linear equation that follows then allocate new resistance
  else if s_depth_new_v < s_depth_old_s then
    s_depth_v := s_depth_old_s - 4000.0*step;
    newr_v :=
    (((roe*length)/(s_depth_v*width))/(sections))*(1.0+(width/(6.0*abovegnd)));

  -- If the skin depth is less than the DC condition but is no different to
  -- the previous value, keep the old value and use this to calculate
  -- resistance
  else
    s_depth_v := s_depth_old_s; --no change
    newr_v :=
    (((roe*length)/(s_depth_v*width))/(sections))*(1.0+(width/(6.0*abovegnd)));
    end if; end if; end if; -- terminate all 'if' statements
  s_depth_old_s <= s_depth_v; -- The present value of skin depth becomes the
                              -- old value
  r <= newr_v;                -- The value of resistance to be used in the
                              -- governing equation is updated
end if; -- End the 'if start=true' structure

-- If the process did not have the necessary information to begin properly
-- and 'start' was not 'true' this code latches 'start' true.
if abs(vs'dot) > 0.5e6 then
  start <= true;
  start_v := true;
end if;

-- Once the process has run once, 'run_once' is set to 'true', this prevents
-- the signal amplitude from changing and having adverse effects on skin
-- depth and observed loss, and hence on the signal shape
if ( (start_v = true) and (run_once = false) ) then
  if a_in > 0.1 then
    a <= a_in;
    run_once <= TRUE;
  end if;
end if;
```

```
v_last <= vs; vdot_last <= vs'dot; -- The signals are updated
end if;  -- End the 'if step' clause
step_check_s <= NOW; -- Update the time elapsed signal with the current time
end process new_sd;  -- End the process

-- The maximum amplitude achieved is passed out to the next section
a_out <= Am_int;
-- The governing equation is evaluated with the new values of resistance
v==(i*rdc)+ (i*r);
end architecture sdr;
```

Appendix B.5

Signal Dependent Conductance (SDC)

```
--Use proposed IEEE natures and packages
library IEEE_proposed;
use IEEE_proposed.electrical_systems.all;
library IEEE;
use IEEE.math_real.all;
entity gd_w is

  generic (
    con     : real; --DC leakage current
    gd_w    : real; --conductance with no frequency component
    amp     : voltage
    );
  port (
    terminal p1, p2 : electrical);

end entity gd_w;

-------------------------------------------------------------------------------
-- Ideal Architecture (v=i*1/R)
-------------------------------------------------------------------------------
architecture freq_depedant_gd of gd_w is

    quantity v across i through p1 to ELECTRICAL_REF;

    signal threshold        : boolean;
    signal vdotthresh       : boolean;
    signal v_last           : voltage := 0.0;
    signal vdot_last        : real := 0.0;
    signal a                : real := 0.6+amp;
    signal gd_f             : real := 1.0/con;

    constant delta_v        : real := 0.005;      -- RESOLUTION = 0.8mv
    constant delta_vdot     : real := 43000000.0; -- RESOLUTION = 43MV/s

begin
```

```
--  threshold <= not v'above(v_last-delta_v) or v'above(v_last+delta_v);
--  vdotthresh <= not v'dot'above(vdot_last - delta_vdot) or
     v'dot'above(vdot_last + delta_vdot);

gdw_p1: process(threshold, vdotthresh) is
begin

    if (abs(v'dot) > 43.0e6) then

        gd_f <= 6.28*gd_w*((abs(v'dot))/ SQRT(abs(a**2 -
        ((v**2)+0.00000000000001) ) ) );
        v_last <= v;
        vdot_last <= v'dot;
    else
        gd_f <= 1.0/con;
        v_last <= v;
        vdot_last <= v'dot;
end if;

end process gdw_p1;

--change the 'f' to a 'w' for the constant frequency case
i == (v/con);-- + (gd_w*v) ;

end architecture freq_depedant_gd;
```

Appendix B.6

Standard Resistor, Capacitor and Inductor in VHDL-AMS

```
-------------------------------------------------
CAPACITOR
-------------------------------------------------
-- File       : capacitor.vhd
-- Use proposed IEEE natures and packages
library IEEE_proposed;
use IEEE_proposed.electrical_systems.all;

entity capacitor is
  generic (
    cap      : capacitance;        -- Capacitance [F]
    v_ic     : real := real'low);  -- Initial voltage (activated by
                                   -- IF statement below)
  port (
    terminal p1, p2 : electrical);
end entity capacitor;

architecture ideal of capacitor is

  quantity v across i through p1 to p2;

begin
    i   == (cap) * v'dot;          -- Fundamental equation
end architecture ideal;

-------------------------------------------
RESISTOR
-------------------------------------------
-- Use proposed IEEE natures and packages
library IEEE_proposed;
use IEEE_proposed.electrical_systems.all;

entity resistor is
  generic (
    res : resistance);    -- resistance (no initial value)
  port (
    terminal p1, p2 : electrical);
end entity resistor;
```

```
-----------------------------------
-- Ideal Architecture (V = I*R)
-----------------------------------
architecture ideal of resistor is

  quantity v across i through p1 to p2;
begin

-- Characteristic equation
  v == i*res;
end architecture ideal;


-------------------------------------------
INDUCTOR
-------------------------------------------
-- File       : inductor.vhd

-- Use proposed IEEE natures and packages
library IEEE_proposed;
use IEEE_proposed.electrical_systems.all;

entity inductor is

  generic (
    ind  : inductance;      -- Nominal inductance
    indmut : inductance;    -- mutual inductance
    i_ic : real := real'low); -- Initial current (use IF statement below
                              -- to activate)
  port (
    terminal p1, p2 : electrical);

end entity inductor;

-------------------------------------------
-- Ideal Architecture (V = L * di/dt)
-- Includes initial condition
architecture ideal of inductor is

-- Declare Branch Quantities
  quantity v across i through p1 to p2;

begin
  if domain = quiescent_domain and i_ic /= real'low use
```

```
    i == i_ic;
  else       --indmut is added because it is given a '-' in testbench
     v   == ((ind * i'dot) - (indmut*i'dot));  -- Fundamental equation
  end use;
end architecture ideal;
```